

NORTHWESTERN UNIVERSITY

On Engineering the Microstructure of High-Performance Concretes
to Improve Strength, Rheology, Toughness, and Frangibility

A DISSERTATION

SUBMITTED TO THE GRADUATE SCHOOL
IN PARTIAL FULFILLMENT OF THE REQUIREMENTS

for the degree

DOCTOR OF PHILOSOPHY

Field of Civil Engineering

By

Edward Francis O'Neil, III

EVANSTON, ILLINOIS

December 2008

© Copyright by Edward Francis O'Neil 2008
All Rights Reserved

ABSTRACT

On Engineering the Microstructure of High-Performance Concretes to Improve Strength, Rheology, Toughness, and Frangibility

Edward Francis O'Neil, III

The research reported in this dissertation covers the development of two high-performance concrete materials, Very-High-Strength Concrete (VHSC) and Frangible Concrete, and the philosophy of engineering the microstructure of these materials to produce their specific beneficial traits. The underlying problem addressed was how to optimize their design to maximize their desirable properties and minimize their detrimental ones. VHSC is a concrete material that has been engineered to produce very-high strength and good ductility or toughness while maintaining rheological properties suitable for normal construction practices. Research was conducted to enhance and optimize its compressive strength by studying and varying its component materials of cement, sand, and silica fume; by researching high-range water-reducing admixtures to maintain useable plasticity in the fresh state; and by employing toughening mechanisms to combat the undesirable traits of brittleness. Specific toughening mechanisms included: types of aggregate, distributed steel fibers, and micro-inclusions of wollastonite microfibers and high-strength ceramic microspheres. Results showed that by choosing component materials that enhance strength and toughness, it was possible to reliably increase the compressive strength of VHSC to 266 MPa.

Frangible Concrete lies at the other end of the high-performance material spectrum and is believed to be a new category of material that possesses adequate structural strength yet is

designed to break into small, non-lethal fragments under dynamic blast pressures. Research was conducted to engineer the properties of slag-based cement pastes to develop a system of pre-induced microcracks that would weaken but not cripple the static load bearing capacity of the material. However, under dynamic load the fracture process would continue, producing tiny fragments much like automotive safety-glass. Laboratory and field blast tests results are presented and show that when small-diameter, mono-sized aggregate particles are coated with the pre-engineered slag paste in a no-fines-concrete approach, the Frangible Concrete material achieves its goal.

ACKNOWLEDGEMENTS

I would like to thank and gratefully acknowledge my advisor, Professor H. M. Jennings, for his wise and thoughtful guidance throughout my journey as his graduate student. I would also like to thank Professor J. R. Weertman, Research Associate Professor J. J. Thomas, and Professor R. J. Krizek for participating on the committee reviewing this work and for their helpful suggestions. Thanks are also due Ms. J. S. Soule for keeping me on track.

A great debt of gratitude belongs to the U.S. Army Engineer Research and Development Center for funding and supporting the research contained herein and the many engineers, scientists, and technicians who provided technical contributions and support to this work. Primarily among these people are: Dr. B. Mather, Mr. T. K. Cummins, Ms. P. H. Kinnebrew, Dr. T. R. Slawson, Mr. B. P. Durst, Dr. C. A. Weiss, Jr., Dr. R. L. Mosher, Dr. P. F. Mlakar, Dr. T. S. Poole, Mr. B. D. Neeley, Mr. D. E. Wilson, Mr. G. S. Wong, Mr. J. G. Tom, Mr. M. C. Sykes, Ms. S. E. Johnson, and Mr. R. X. Torres. Many more too numerous to mention are thanked as well.

I am blessed to be a partner with and eternally indebted to Dr. L. Jean O'Neil for her many contributions to this dissertation and her support of my efforts in this pursuit for greater than 12 years. Without her guidance and support both technically and domestically I would not be at this juncture today. It is to her that I dedicate this dissertation.

TABLE OF CONTENTS

Abstract.....	3
Acknowledgements.....	5
List of Tables.....	12
List of Figures.....	14
Glossary.....	16
Chapter 1 INTRODUCTION	18
1.1 Versatility of concrete.....	18
1.2 Pertinent definitions.....	20
1.2.1 High strength.....	20
1.2.2 ACI minimum criteria.....	21
1.2.3 Academic definition of high strength	22
1.2.4 Flow table and flow number	23
1.2.5 Fracture toughness	24
1.2.6 Frangibility and frangibility index	24
1.2.7 Oil-well cement.....	25
1.3 Organization of the dissertation.....	25
Chapter 2 PROBLEM STATEMENT.....	28
2.1 Concrete as a high-performance material	28
2.2 The engineering process	28
2.3 Statement of the problem.....	30
Chapter 3 BACKGROUND AND LITERATURE REVIEW I: PATH TO HIGH STRENGTH CONCRETE	32
3.1 Typical uses of concrete.....	32
3.1.1 Structural uses.....	32
3.1.2 Material uses	33
3.2 Types of strength.....	33
3.2.1 Compressive strength.....	33
3.2.2 Tensile or flexural strength	34
3.2.3 Bond strength	36
3.2.4 Fracture toughness	36
3.3 Historical efforts to describe concrete strength	37
3.4 Component materials in high-strength concrete	38
3.4.1 Cement	39
3.4.2 Aggregate.....	39
3.4.3 Pozzolans, admixtures, and additives	40
3.4.4 Fiber reinforcement.....	41
3.5 Recent advancements in high-strength concrete.....	42
3.5.1 DSP cement.....	42
3.5.2 MDF cement	42

3.5.3	Reactive Powder Concrete	44
3.6	Movement toward ceramic-like behavior	45
3.7	Summary	46
Chapter 4	BACKGROUND AND LITERATURE REVIEW II: FOR HIGH STRENGTH	47
4.1	Early development of VHSC	47
4.2	Early components of VHSC.....	48
4.3	Philosophy of VHSC.....	51
4.4	Principles underlying the philosophy of VHSC.....	51
4.4.1	Minimization of flaws in the matrix	52
4.4.2	Improvement of matrix homogeneity	55
4.4.3	Maximization of the silica content for conversion to C-S-H.....	56
4.4.4	Maximization of the density of the matrix.....	57
4.4.5	Improvement of the microstructure	59
4.4.6	Enhancement of the matrix ductility.....	60
4.5	Summary	61
Chapter 5	EXPERIMENTAL WORK ON STRENGTH	62
5.1	General experimental procedures	62
5.1.1	Background	62
5.1.2	Bench-top mixing procedures	63
5.1.3	Flow number measurement procedures	64
5.1.4	Procedures for casting compression samples.....	65
5.1.5	Procedures for curing cube and cylinder specimens.....	66
5.1.6	Preparation for compression testing.....	66
5.1.7	Compression testing procedure.....	67
5.2	Experiments with cements to improve compressive strength of VHSC.....	67
5.2.1	Background	67
5.2.2	Preferred specifications.....	68
5.2.3	Experimental procedure	68
5.2.4	Results and discussion	70
5.3	Effects of component materials on the strength of VHSC.....	71
5.3.1	Background	71
5.3.2	Purpose of the experiments.....	72
5.3.3	Experimental procedure	73
5.3.4	Experimental results.....	73
5.3.4.1	Mixture 1 – cement, silica fume, HRWRA, and water	74
5.3.4.2	Mixture 2 – cement, sand, silica fume, HRWRA, and water.....	75
5.3.4.3	Mixture 3 – cement, sand, silica fume, silica flour, HRWRA, and water	76
5.3.4.4	Mixture 4 – cement, sand, silica fume, silica flour, microfibers, HRWRA, and water.....	77
5.3.4.5	Mixture 5 – cement, silica fume, silica flour, microfibers, HRWRA, and water .	79
5.3.5	Discussion.....	80

5.3.5.1	Component strength considerations.....	80
5.3.5.2	Component rheological considerations.....	82
5.4	Experiments with HRWRAs to improve the strength of VHSC.....	83
5.4.1	Background.....	83
5.4.2	Experimental procedure.....	85
5.4.3	Results.....	87
5.4.4	Discussion.....	87
5.4.4.1	Rheology Experiments.....	87
5.4.4.2	Strength experiments.....	91
5.5	Effects of ambient temperature water curing to improve the strength of VHSC.....	93
5.5.1	Background.....	93
5.5.2	Experimental procedure.....	94
5.5.3	Results.....	94
5.5.4	Discussion.....	94
5.6	Experiments with micro-inclusions to increase strength.....	96
5.6.1	Microfibers.....	96
5.6.1.1	Background.....	96
5.6.1.2	Microfiber experimental procedures.....	97
5.6.1.3	Results.....	98
5.6.1.4	Discussion.....	98
5.6.2	Microspheres.....	100
5.6.2.1	Background.....	100
5.6.2.2	Microsphere experimental procedures.....	100
5.6.2.3	Results.....	102
5.6.2.4	Discussion.....	103
5.7	Summary.....	106
5.8	Conclusions.....	107
5.8.1	Cement study conclusions.....	107
5.8.2	HRWRA study conclusions.....	107
5.8.3	Curing study conclusions.....	108
5.8.4	Microfiber study conclusions.....	109
5.8.5	Microsphere study conclusions.....	110
5.8.6	Component materials study conclusions.....	111
Chapter 6	BACKGROUND AND LITERATURE REVIEW III: TOUGHNESS OF VERY-HIGH-STRENGTH CONCRETE	113
6.1	Background.....	113
6.1.1	Toughening mechanisms in concrete.....	114
6.1.2	Microcrack shielding mechanisms in the microcracking zone.....	116
6.1.3	Mechanisms occurring at the crack tip.....	119
6.1.3.1	Crack deflection.....	120
6.1.3.2	Crack trapping.....	121
6.1.3.3	Crack tip blunting.....	122
6.1.4	Mechanisms occurring in the crack wake zone.....	122

6.1.4.1	Crack-face pinning.....	123
6.1.4.2	Crack branching.....	123
6.1.4.3	Aggregate bridging and rupture.....	124
6.1.4.4	Fiber pull-out and rupture.....	124
6.2	Fracture toughness experiments.....	126
6.2.1	Fracture toughness of unreinforced VHSC.....	126
6.2.1.1	Experimental procedure.....	126
6.2.1.2	Results of unreinforced VHSC fracture toughness tests.....	127
6.2.1.3	Discussion of unreinforced VHSC fracture toughness properties.....	128
6.2.2	Fracture toughness of steel macrofiber reinforced VHSC.....	130
6.2.2.1	Experimental procedures.....	130
6.2.2.2	Results.....	131
6.2.2.3	Discussion of the fracture toughness results.....	134
6.2.2.4	Discussion of toughness indices results.....	138
6.2.3	Fracture toughness of VHSC with microspheres.....	144
6.2.3.1	Experimental Procedures.....	144
6.2.3.2	Results for the microsphere toughness studies.....	145
6.2.3.3	Discussion.....	145
6.3	Summary.....	148
6.4	Conclusions.....	149
6.4.1	Unreinforced VHSC toughness conclusions.....	149
6.4.2	Steel-fiber-reinforced VHSC toughness conclusions.....	150
6.4.3	VHSC with microspheres toughness conclusions.....	153
Chapter 7	FRANGIBLE CONCRETE.....	154
7.1	Introduction.....	154
7.2	Statement of problem and challenge.....	154
7.3	Background, and first series of experiments.....	155
7.3.1	Laboratory experimental development – phase 1.....	156
7.3.2	Results from laboratory development – phase 1.....	157
7.3.3	Laboratory experimental development - phase 2.....	157
7.4	ERDC preliminary blast-load studies on the 18 mixtures of phase 2.....	158
7.4.1	Background.....	158
7.4.2	Experimental procedures.....	159
7.4.3	Blast environment.....	160
7.4.4	Blast chamber results.....	160
7.4.5	Blast load analysis.....	161
7.4.6	Discussion.....	162
7.5	Laboratory experimental development - Phase 3.....	165
7.6	2004 field blast test of Frangible Concrete.....	166
7.6.1	Description of the Frangible Concrete block mixture.....	166
7.6.2	Fabrication of the walls.....	167
7.6.3	Post-blast data collection and analysis.....	168
7.6.4	Discussion of 2004 wall blast results.....	169

7.7	A new approach - description of no-fines concrete	171
7.8	Laboratory experimental development of no-fines Frangible Concrete	172
7.8.1	Laboratory impact test modifications	174
7.9	Analysis of 2007 Frangible Concrete wall field blast test	175
7.9.1	Description of the Frangible Concrete wall test set-up.....	175
7.9.2	Post-blast collection of data and analysis	176
7.10	Summary	180
7.11	Conclusions.....	180
7.11.1	Phase 1 conclusions	180
7.11.2	Phase 2 conclusions	181
7.11.3	Conclusions from the ERDC preliminary blast-load studies.....	181
7.11.4	Phase 3 conclusions	182
7.11.5	2004 field blast test conclusions	183
7.11.6	2007 field blast test conclusions	183
7.11.7	Chapter conclusions	184
Chapter 8	GENERAL CONCLUSIONS AND FUTURE WORK	187
8.1	Engineering high-performance materials.....	187
8.2	Overall conclusions on VHSC	188
8.2.1	Strength considerations	188
8.2.2	Rheology considerations	188
8.2.3	Toughness considerations	189
8.2.4	Areas for future VHSC work	190
8.3	Overall conclusions on Frangible Concrete.....	190
8.3.1	A new high-performance material	190
8.3.2	Areas for future Frangible Concrete work	191
REFERENCES	193
APPENDIX A:	204
MASS STUDY OF THE HYDRATION PRODUCTS OF VHSC		204
A.1	Background and assumptions.....	204
A.2	Component materials	206
A.3	Calculation of percent hydration under very-low w/c conditions.....	207
A.4	Mass calculations of reactants and products for the VHSC model.....	209
A.5	Chemical reactions	210
A.6	Tricalcium aluminate phase	211
A.7	The silicate phases	212
A.8	The effect of silica fume	214
A.9	The tetracalcium aluminoferrite phase.....	215
A.10	Summary of reactions	216

APPENDIX B:	219
DESCRIPTION OF THE PHYSICAL TRANSFORMATION OF DRY CEMENTITIOUS POWDER COMPONENTS INTO FRESH VHSC PASTE WHEN WETTED WITH WATER AND HIGH-RANGE WATER-REDUCING ADMIXTURES	219
B.1 Introduction and time-line format	219
B.2 Appearance of the wetted powders during mixing.....	220
APPENDIX C:	222
SAMPLE CALCULATIONS USED FOR FRACTURE TOUGHNESS IN CHAPTER 6.....	222
C.1 Background and assumptions.....	222
C.2 Set-up of experiment and dimension calculations.....	222
C.3 Analysis of fracture toughness data	223
C.3.1 Models.....	223
C.3.2 Fracture toughness calculations	224
C.3.3 Fracture energy.....	228

LIST OF TABLES

Table 1.1 Examples of high performance concrete	20
Table 1.2 Strength classifications of concrete	22
Table 3.1 Relationship of tensile strength to compressive strength	35
Table 3.2 Physical properties of some of the high-performance cement materials	45
Table 4.1 Component materials and mass proportions of early VHSC	48
Table 4.2 Summary of principles underlying the philosophy of VHSC.....	52
Table 5.1 Preferred cement characteristics	68
Table 5.2 Mill test report summaries for suitable cements.....	69
Table 5.3 Materials used in the VHSC component study	72
Table 5.4 Order of the mixtures and the component materials in each	73
Table 5.5 Compressive strength of experiments in component study	73
Table 5.6 Percent change in compressive strength and flow in component study	81
Table 5.7 Proportions for strength and rheology experiments with polycarboxylate HRWRAs .	87
Table 5.8 Strength results of baseline VHSC for four HRWRAs at high and low dosages	89
Table 5.9 Comparative proportions of VHSC and a HSC based on mass of cement	90
Table 5.10 Mixture proportions for the length of ambient temperature curing experiment	94
Table 5.11 Wollastonite chemical composition.....	98
Table 5.12 Effect on compressive strength of VHSC from addition of microfibers	98
Table 5.13 Physical properties of 3M Zeospheres™	101
Table 6.1 Fracture toughness properties of unreinforced baseline VHSC.....	127
Table 6.2 FRC VHSC f'_c , MPa.....	131
Table 6.3 Fracture toughness results for individual FRC VHSC beams	132
Table 6.4 Toughness Indices for the fiber-reinforced VHSC	134
Table 6.5 Heat cured compressive strength for microsphere toughness experiments	145
Table 6.6 Beam property calculations for VHSC microsphere toughness studies	145
Table 6.7 Fracture toughness calculations for VHSC with microspheres	146
Table 7.1 Type and levels of the variables in the phase 1 experiments.....	157
Table 7.2 Experimental design for matrix 2	159
Table 7.3 Comparative results of blast experiment and impact experiment.....	164
Table 7.4 Frangible Concrete mixture design used to make block for the 2004 blast test	167
Table 7.5 A summary of fragment data collected from block wall blast analysis.....	168
Table 7.6 Variables and levels in the experimental design.....	173
Table 7.7 Blast pressures	176
Table 7.8 A summary of fragment data collected from July 2007 block-wall blast.....	178
Table A.1 Densities and molar volumes of cementitious compounds.....	205
Table A.2 Stoichiometry of chemical reactions available to the model.....	205
Table A.3 Component materials in baseline VHSC.....	206

Table A.4 Mill test data.....	206
Table A.5 Masses of reacted compounds.....	210
Table A.6 Example table of consumed and produced compounds using equation A.8.....	210
Table A.7 Consumed and produced compounds of the C ₃ A phase using equation A.5.....	213
Table A.8 Consumed and produced compounds of the C ₃ S phase using equation A.1.....	213
Table A.9 Consumed and produced compounds of the C ₂ S phase using equation A.2.....	214
Table A.10 Consumed and produced compounds of the S reaction using equation A.3.....	215
Table A.11 Consumed and produced compounds of the C ₄ AF phase using equation A.7.....	216
Table A.12 Summation of compounds consumed and produced given in grams.....	218
Table C.1 Beam measurements.....	223

LIST OF FIGURES

Figure 4.1 Influence of porosity on relative strength of various materials	53
Figure 4.2 VHSC σ - ϵ curve.....	60
Figure 5.1 Flow table.....	65
Figure 5.2 Compressive strength for 28-day limewater curing	69
Figure 5.3 Compressive strength for heat curing.....	69
Figure 5.4 Flow numbers for the four cements.....	71
Figure 5.5 Compressive strength results of the five mixtures in the VHSC component study	74
Figure 5.6 Comparison of capillary space in fresh paste with and without silica fume	76
Figure 5.7 Wollastonite fibers.....	78
Figure 5.8 Theoretical increase in strength resulting from addition of microfibers.	80
Figure 5.9 Compressive strength versus type of HRWRA.....	84
Figure 5.10 Results of flow number and time-to-paste (TTP) experiments for baseline VHSC with four polycarboxylate HRWRAs.....	88
Figure 5.11 Compressive strength results for ambient temperature curing experiments	95
Figure 5.12 Compressive strength versus percent G-800 microspheres.....	103
Figure 5.13 Compressive strength comparison of the G-800 and G-200 microspheres.....	103
Figure 5.14 (a) General view of fracture surface of the lime pozzolan specimen and (b) Detail in center showing hydration products	105
Figure 6.1 Diagrammatic breakdown of crack-toughening mechanisms based on location of crack.....	115
Figure 6.2 Fracture toughness of unreinforced baseline mixture of VHSC	128
Figure 6.3 Plastic fracture zone, effective elastic crack, and.....	130
Figure 6.4 Load-CMOD curves for mixture 1	133
Figure 6.5 Load-CMOD curves for mixture 2.....	133
Figure 6.6 Peak load vs no. of fibers crossing the 1 st quadrant in fiber-reinforced VHSC	136
Figure 6.7 Comparison of the average Load-CMOD curves across mixtures.....	138
Figure 6.8 FRC VHSC Load-CMOD curves.....	141
Figure 6.9 Comparison of work done for unreinforced and FRC VHSC.....	143
Figure 6.10 Compressive strength of current microsphere mixtures compared to previous results	147
Figure 6.11 Fracture properties of VHSC with G 800 microspheres.	147
Figure 6.12 1 st round G-800 flow numbers.....	148
Figure 7.1 1.22-m blast chamber.....	158
Figure 7.2 Specimen housing frame.....	160
Figure 7.3 Condition of the specimens after the blast....	161
Figure 7.4 Gradation curves of the 11 mixtures that fractured and could be analyzed	162
Figure 7.5 Frangible Concrete block dimensions	166
Figure 7.6 Test walls ready for blast	167
Figure 7.7 Small fragments not recorded, Frangible wall left, Conventional wall right..	169
Figure 7.8 Modified impact tower	174

Figure 7.9 Layout of the blast field and stand-off distances to each experiment	175
Figure 7.10 Block walls ready for testing	176
Figure 7.11 Actual pressure vs range data plotted on theoretical incident and reflected pressure curves calculated using USACE ConWep.....	177
Figure 7.12 Photograph of the 70 pieces collected from the blast.....	178
Figure 7.13 Detail of Figure 12	179
Figure C.1 Beam dimensions and test setup.....	222
Figure C.2 Load-CMOD curve for beam 1 of unreinforced baseline VHSC.....	225

GLOSSARY

The definitions given in this glossary are either composed by the author or taken from [3].

Blaine surface area	The surface area of fine powders such as cement measured with the Blaine apparatus and expressed as a surface area per unit mass
Bond strength	Resistance to the separation of mortar and concrete from reinforcing and other materials with which it is in contact
Calcium-Silicate-Hydrate	Any of the various reaction products of calcium silicate and water
Crack-mouth-opening dimension	The width of a crack under stress measured at the mouth or surface of the crack on the face of the specimen
Crack-tip-opening dimension	The width of a fictitious crack measured at the tip of the actual crack it replaces. The fictitious crack is a crack (longer than the actual crack) whose extra length is based on the length of the plastic fracture zone in front of the actual crack
Distributed fiber reinforcement	Concrete reinforcement consisting of short fibers discretely distributed throughout the concrete matrix
Flexural strength	The property of a material that indicates its ability to resist failure in bending
Frangibility index	A measure of the ability of a material to fracture into small pieces from a blast or impact force. It is the ratio of the mass of fragments from an impacted specimen passing the #4 sieve (4.75 mm) to the total mass of the original specimen
Ground granulated blast-furnace slag	A slag that has been finely ground and is a hydraulic cement
High-range water-reducing admixture	A water-reducing admixture capable of producing large water reduction or great flowability without causing undue set retardation or entrainment of air in mortar or concrete
Modulus of rupture	A measure of the load-carrying capacity of a beam and sometimes referred to as rupture modulus or rupture strength; it is calculated for apparent tensile stress in the extreme fiber of a transverse test specimen under the load that produces rupture

Mortar	A mixture of cement, water, and fine aggregate
Silica fume	Very fine noncrystalline silica produced in electric arc furnaces as a byproduct of the production of elemental silicon or alloys containing silicon
Splitting tensile strength	Tensile strength of concrete determined by a splitting tensile test
Torsional strength	The tensile strength of concrete determined by a pure twisting or torsional loading
VHSC	A mixture of cement, water, sand, silica flour, silica fume, and high-range water reducing admixture that with heat curing is able to reach compressive strength of 267 MPa
Work of fracture	A measure of the work done in advancing the fracture of a specimen. It is defined as the area beneath the load-displacement curve of a specimen under tensile loading

Chapter 1 INTRODUCTION

1.1 Versatility of concrete

It has been stated that concrete is the most used building material in the world [1]. The statement reflects the material's versatility and its capability as a primary resource of the building community. Its importance to the building public lies in its economic competitiveness with other construction materials, its versatility of form, and its multiplicity of function including designated strengths.

Concrete has a number of economic advantages over other building materials when considered on a life-cycle basis including its cost and sustainability. When considering costs for a typical commercial frame building, studies have shown concrete can be more economical than steel frame and has a material lead time that is only one-third that for steel [2]. Life-cycle maintenance costs are significantly less expensive for concrete than steel. Steel requires painting on a periodic basis to protect against corrosion, whereas a low-permeability concrete can survive its entire life cycle without such maintenance.

Versatility of form means that concrete can take any shape for which formwork can be constructed. Other building materials are somewhat limited in this area. Thus a concrete structure can have the airy beauty of a Pier Luigi Nervi hanger or the bold mass of a LeCorbusier cathedral.

Perhaps the trait that makes concrete most different from other building materials is its multiplicity of function or its ability to be re-formulated to perform different tasks. Concrete can be made to be lightweight or heavyweight by using foam pellets or steel shot respectively for the aggregate. The formal name for this capability is high-performance concrete and is defined as "Concrete that meets special performance and uniformity requirements that cannot always be

achieved by using conventional materials and normal curing practices.” [3] High-performance concretes have been used in a number of studies concerning material properties. Zuber et al. [4] conducted freezing and thawing experiments using very low water-to-cement ratio (w/c) concretes, Punkki et al. [5] used lightweight aggregate concrete in experiments to explain composite strength. Both research efforts were dealing with concrete material properties, but one chose very-low w/c to study the effects of very-low permeability on the frost resistance of concrete and the other used light-weight aggregate to explain the role the aggregate plays in determining composite strength. Whatever the material property need, concrete proportions and components can be modified to support that need.

Listed in Table 1.1 are some of the forms of concrete that fall into the category of high-performance concrete including two that are the subject of this dissertation: Very-high-strength concrete (VHSC) and Frangible Concrete. These two materials are at the extreme ends of the high-performance spectrum. At one end is a material that is pushing the boundaries of high strength and searching for ways to expand that realm. Three materials that have revolutionized the advancement of high strength and fracture toughness of concrete are; silica fume; high-range, water-reducing admixtures (HRWRAs); and distributed fiber reinforcement. All three play a critical role in the strength of VHSC. The silica fume is primarily responsible for the strength gains, but because it has such a large surface area there is a great water demand placed on the limited amount of water available in VHSC. As related by Nawy [6], Khayat and Aitcin [7] showed that using 16% silica fume by weight of cement increases the demand for water by as much as 40% requiring HRWRAs to be used to replace the lost fluidity. The reduction of porosity caused by the silica fume increases both strength and brittleness and distributed fibers are necessary to replace the ductility [8].

Table 1.1 Examples of high performance concrete

High-workability concrete	Self-leveling concrete
Foamed concrete	Very-high-strength concrete
Lightweight concrete	Heavyweight concrete
Frangible Concrete	Pumped concrete
Autoclaved concrete	Roller-compacted concrete

At the other end of the spectrum is Frangible Concrete, a material that requires strength and weakness at the same time and is believed to be a new form of high-performance concrete material and first presented in this dissertation. To develop this material two elements were critical. First, use of alternative forms of cementitious materials were necessary to achieve the level of drying shrinkage necessary to produce the right level of microcracks, and second, a strong understanding of the microstructure of both portland cement and ground, granulated blast-furnace slag (GGBFS). While particle packing and high density are critical to proper development of VHSC, creation of a substantial system of voids within the macrostructure and a pre-engineered system of microcracks distributed throughout the microstructure are critical to Frangible Concrete.

1.2 Pertinent definitions

1.2.1 High strength

The definition of high strength in concrete is, in itself, a difficult entity to assess. There is no one world body that has been given the authority to set defining levels on the subject, and there are a number of well-respected experts who have taken it upon themselves to publish their definition of the level, further adding to the diversity of the definition. Among other reasons for care in defining such an entity is the aspect of change in definition with time. It can easily be said that what was suitable for high-strength yesterday is not appropriate for the same definition today, and what is considered high strength today will be normal strength tomorrow.

Further consideration is embedded in the question “What is meant by high strength?” Compressive strength is most often chosen as the norm, however it could be defined in terms of tensile, flexural or shear strength; and in some instances, particularly in ceramic materials; high-strength is defined in terms of fracture toughness. The vast majority of published data on high strength involves reference to the ultimate compressive strength, f'_c , as the bellwether of material properties; however as concrete compressive strength goes up it gets more brittle and issues of fracture resistance or toughness become significant. For purposes of this dissertation, the focus will remain on compressive strength and fracture toughness and rather than complicate the situation with an attempt to define high strength, the definitions from respected entities dedicated to concrete research will be related.

1.2.2 ACI minimum criteria

Perhaps the most trusted professional organization dedicated to the advancement of concrete research is the American Concrete Institute (ACI). With over 200 technical committees ranging from the study of admixtures to under-water concrete, the institute can claim the largest number of technical experts in the world. Committee 116 [3] is responsible for the authoritative glossary of cement and concrete terminology within the industry. Their definition of high-strength concrete is as follows:

***concrete, high-strength** – Concrete that has a specified compressive strength for design of 6000 psi (41 MPa) or greater.*

This definition was adopted by the ACI in 1984 when the level of technology was much less developed than it is today. In that timeframe, 41 Megapascals (MPa) was much more prominent a level of strength. It should be pointed out that this definition prescribes the lower end of high-

strength concrete and makes no reference to an upper limit to the category. Nor does it address any other categories to which a definition of the lower limit of strength would be an asset.

1.2.3 Academic definition of high strength

While the ACI chose to define the lower bounds of high-strength concrete, Professor J. Francis Young, at the University of Illinois, provided a strength classification system that encompasses all classes of concrete. It is shown in Table 1.2 [9]. Professor Young's efforts are notable because he has incorporated results from high-strength concrete research that had taken place in the 1980's that had developed compressive strengths significantly higher than 41 MPa.

Table 1.2 Strength classifications of concrete [9]

Characteristic	Conventional concrete	High-strength concrete	Very-high-strength concrete	Ultra-high-strength concrete
Strength, MPa	< 50	50 – 100	100 – 150	> 150
Water-cement ratio	> 0.45	0.45 – 0.30	0.30 – 0.25	< 0.25
Chemical admixtures	Not necessary	WRA/HRWR*	HRWR	HRWR
Mineral admixtures	Not necessary	Fly ash	Silica fume**	Silica fume**
Permeability coefficient (cm/s)	> 10 ⁻¹⁰	10 ⁻¹¹	10 ⁻¹²	10 ⁻¹³
Freeze-thaw protection	Needs air entraining	Needs air entraining	Needs air entraining	No freezable water

* WRA = water reducing admixture; HRWR = High-range water reducer

** Also may contain fly ash

Professor Young's classification convention divides strength classes into 50 MPa segments such that the lower end of the high-strength concrete realm begins at 50 MPa rather than the lower value adopted by ACI. It further subdivides the high-strength realm into three subclasses: high, very-high, and ultra-high, in which high and very-high reflect the limits of field placeable strengths and ultra-high reflects the strength achievements that were being realized in the laboratory. This classification system also provided some insight into the composition and properties of the concrete contained in each subclass. As strength increases, the w/c decreases

and the necessity for mineral and chemical admixtures becomes important. Most notable is the necessity for silica fume and HRWRAs in the very-high and ultra-high strength subclasses.

It should be pointed out that Professor Young's name for the subclass with strength between 100 MPa and 150 MPa, very-high-strength concrete, is the same name as the concrete material described in this dissertation. The VHSC described here has a compressive strength between 220 MPa and 266 MPa and should not be linked with his subclass.

1.2.4 Flow table and flow number

The flow table is a device for measuring the flow of cement paste and hydraulic cement mortars [10]. It measures the spread of a sample of fresh cement paste or mortar that has been molded in the shape of a truncated frustum of a cone. The sample is demolded on a table that can be raised and dropped through a distance of 12.7 mm by a cam device attached to the table. The table is dropped 25 times and the sample is spread by the impact force of the drops. The diameter of the sample is then measured at four locations 45° apart, using a caliper provided with the drop table, and the four measurements summed to give the flow number.

In standard flow measurements of fresh cement paste, the flow number is a percentage of the flow number of a standard calibrated material. As used in this work, the flow number is not calibrated to a standard material but is used as a number representing the relative flow of one sample compared to all others in the work. The flow number can be converted to an average diameter of the spread sample through equation 1.1 where d_{avg} is the diameter of the spread sample in mm and d_i is the reading from the measuring caliper. The caliper is divided into 40 segments, each 4 mm in length and measures 101.6 mm when fully closed.

$$d_{avg} = \frac{\sum_{i=1}^4 (101.6 + 4d_i)}{4} \quad (1.1)$$

1.2.5 Fracture toughness

Fracture toughness is a property that describes the ability of a material containing a crack or initiating a crack to resist further growth of that crack. It is a measure of the material's resistance to brittle fracture. Primarily used as a bellwether for strength in the ceramics industry, in recent years it has gained respect within the concrete community as concrete strength has advanced and the material has become more brittle. Any component in a material that resists the advance of cracks or causes the consumption of extra energy in allowing the advancement of the crack can be called a fracture toughening mechanism. Chapter 6 in this work is devoted to fracture toughness and explores the many types of fracture toughening mechanisms and efforts to augment the microstructure of VHSC to improve its fracture toughness qualities.

1.2.6 Frangibility and frangibility index

Frangibility, in terms of a material property, is the ability of that material to be readily or easily broken. As it relates to the materials described in chapter 7 of this dissertation, the term refers to how well the material breaks up when subjected to a dynamic blast force. The frangibility index is a term that is used to describe how well a blast-fractured material meets the frangibility requirement set forth to classify a material's frangible nature. In technical terms it is the ratio of the mass of fragments from a blast experiment that passes the #4 sieve to the mass of the entire sample. The higher the frangibility index the greater the frangibility of the material. However it will be shown that a high frangibility index is not the only criterion necessary to make a good-quality frangible material.

1.2.7 Oil-well cement

Oil-well cement is a high-performance material of the cement community. It is primarily used in the oil-drilling industry and is specially formulated to pump in the annulus around drill pipe and the drill hole to set up zonal isolation in keeping gasses and liquids in the ground from migrating from their respective layers to other layers. Because oil drilling goes many thousands of feet into the ground, the drilling grout must be able to stand up to very-high temperatures without setting too soon. To do this the cement chemistry is manipulated to keep the cement to solids ratio (C/S) very low to help keep the cement from setting too quickly. Also, the cement is purposefully ground coarsely to minimize the reactive surface area of the cement grains to further reduce generated heat. For a number of different reasons this cement is ideal for use in VHSC.

1.3 Organization of the dissertation

This dissertation describes the research work that took place over a period of 13 years to engineer the physical and material properties of two high-performance concretes: Very-high-strength concrete and Frangible Concrete.

Chapter 1 is introductory and sets the stage by defining critical terms used throughout the rest of the dissertation. Chapter 2 discusses the role concrete plays as a high-performance material, describes what is meant by engineering a material, and issues challenges to be addressed in the quest to further improve the material properties of the two specialty concretes that are the subject of this work.

Chapter 3 gives the background and historical significance of the role concrete plays in the field of engineering construction and provides literature review I concerning the historical research efforts to lead concrete on the path to high strength. Historical accounts of early

attempts to mathematically describe concrete compressive strength are reviewed in this chapter along with the pioneering work in the 1980's to begin to engineer concrete for very-high strength.

Chapters 4 and 5 discuss engineering concrete for very-high strength. Chapter 4 contains literature review II encompassing aspects of strength-giving properties of concrete. Chapter 4 details the early development of VHSC, the philosophy of VHSC, and the underlying engineering principles that guided its development, and a review and discussion of the early components of the material. Chapter 5 covers the recent research efforts to increase the strength of VHSC including research on choosing cements, component materials, admixtures, additives, and curing research.

Chapter 6 is devoted to exploring efforts to improve the toughness of VHSC. Literature review III on toughness mechanisms and fracture toughness research is located here along with segments covering the experiments on toughening VHSC with distributed steel fibers, wollastonite microfibers, and silica-ceramic microspheres. Properties of fracture toughness, Crack-mouth-opening dimension (CMOD), Crack-tip-opening dimension (CTOD), Work of Fracture (WoF), and the critical fracture energy are calculated in this chapter and used to quantify the success or failure of the experimental efforts to toughen VHSC.

Chapter 7 shifts attention from engineering for very-high strength to engineering a high-performance material for the proper balance between strength and frangibility. This chapter provides a detailed look at the military research and development program to engineer a concrete material that has adequate structural strength for use as defensive perimeter walls and will be frangible enough to break into non-lethal-size fragments when exposed to a blast force.

Chapter 8 summarizes the overall results from the experimental work in this dissertation, draws conclusions, and presents directions for future work to further engineer these two specialty, concrete materials.

Chapter 2 PROBLEM STATEMENT

2.1 Concrete as a high-performance material

As defined in the introduction, high-performance concrete is “concrete that meets special performance and uniformity requirements that cannot always be achieved by using conventional materials and normal curing practices.” This definition falls short of fulfilling the expectations of a high-performance concrete that has been engineered to exceed minimum requirements and to maximize the performance of a special need. A more appropriate definition of a high-performance concrete is “a concrete that has been formulated to optimize its material properties to maximize the performance and uniformity requirements of the special need for which it is being designed.”

By virtue of its composite nature, concrete is well suited to its role as a high-performance material. Its core components of cement, water, and aggregates can be augmented by a number of additives, admixtures, and fillers and it will still harden to a material that is capable of carrying load. How these additives, admixtures, and fillers are used will make the difference between an ordinary concrete and one that has been engineered for optimum effect.

2.2 The engineering process

Engineering, as used in the context of this dissertation, is an optimization process in which materials are chosen for use in the design mixture based on knowledge of how they will benefit the resulting mixture. Engineering a material means to manipulate or design it through a process of understanding the cement microstructure and the changing effect a component material will have on the microstructure.

There are many tools to use in implementing this process. Some are more efficient than others and often the most efficient is not the most convenient to use. The basic question to ask is:

“Knowing the desired results from the cement microstructure, what material or materials will best accomplish these goals?” Simple trial mixes is one technique, although this technique is inefficient when large numbers of mixes are involved or there are many variables to consider. Because confusing complications can arise when multiple materials are simultaneously tried as new additions, it is recommended that new additions be made separately when simple trial mixtures are involved. It is more efficient to use some sort of methodical design to test hypotheses. With small data sets, full-factorial designs yield information on all areas of the design space but they are less efficient than experimental design techniques.

Use of statistical tools such as experimental design optimization techniques for choosing the experiments to run can dramatically reduce the necessary work load. They minimize the number of experiments needed to achieve the desired results at the same time seeing that the experiments chosen adequately represent the whole design space. Beneficial interactions between two materials can be linear or non-linear. Because of this, it is important to conduct enough experiments of the chosen materials over a comprehensive domain to be sure all possible outcomes, linear and non-linear, are addressed.

Material interactions with time/environment variables are important as well. Valuable optimization information can be overlooked if the data are collected under too narrow a time or environment domain. For example, studying the effects of fly ash additions to a cementitious mixture at 1-, 3-, and 7-days age will miss the greatest strength gain from the material because the time domain is too narrow. Data to at least 28 days age and longer are necessary for detecting higher strength.

The engineering process culminates with the analysis of the trial data. The effectiveness of the added material will be based primarily on the enhancement of the material property to be

optimized. However, effects caused by interactions with other component materials can be missed with simple analysis methods. Multiple regression analysis tools are helpful in this respect to identify linear and non-linear interactions that have major effects on the main study property.

Secondary benefits are often gained with the primary material addition. Consider, for example, the addition of silica fume to a mixture for the primary benefit of improving strength. Research shows that addition of silica fume also improves durability because of reduced permeability of the resulting mixture [11-15]. This secondary effect, in most cases, is considered a benefit that has been achieved because of engineering the property of strength. However, not all secondary effects are always beneficial in an engineered material.

A detrimental secondary effect can, in the worst case, nullify the benefits of the primary enhancement. It is the further goal of the engineering process to minimize detrimental effects without impacting the effectiveness of the beneficial effects or requiring too large a compromise to the primary benefit.

The foregoing description of the engineering process covers many of the tools and techniques that can be employed. They are not always used whether for lack of understanding of the technique or constraints of time, money or other resources. They were not always used in the development of VHSC as will be seen in coming chapters, but are described to address their benefits and efficiencies.

2.3 Statement of the problem

As described in paragraph 2.1, the revised definition of a high-performance concrete strives to maximize the performance requirements of the special need being engineered.

Maximizing the performance entails enhancing the beneficial effects of additives, admixtures, and fillers. Maximizing the performance also encompasses minimizing the detrimental effects.

In the course of developing VHSC and Frangible Concrete, each material exhibited detrimental secondary properties as a function of enhancing the primary material property. Enhancing the strength of VHSC decreased both its ductility and flow properties as well as impacting its ultimate toughness. In the case of Frangible Concrete, designing the material for optimum frangibility severely limited its static strength and designing it for superior strength negated its frangible properties. The problem to be addressed in both of these cases is how to minimize the detrimental secondary effects without affecting the primary benefits. In different words, how can one restore ductility, decent flow characteristics, and toughness to a high-performance concrete without compromising the strength, and for a Frangible Concrete how can one design for strength and frangibility in the same material? This requires designing the materials using a structured process based on an understanding of how microstructure will be affected by the components and their quality and quantity used in each mixture.

Chapter 3 BACKGROUND AND LITERATURE REVIEW I: PATH TO HIGH STRENGTH CONCRETE

3.1 Typical uses of concrete

3.1.1 Structural uses

Because concrete is primarily a building material, the vast majority of examples of its use are structural in nature. Among the most obvious are: frame structures, bridges, concrete pavements, and hydraulic structures. These examples are common uses of structural concrete. But still under the category of structural uses are some of the more exotic forms of concrete building types, for example, the shell and the dome. As concrete gets stronger, the military is becoming increasingly interested in its use for blast and penetration resistant cladding as an inexpensive alternative to ceramic armor [16].

Most of these structural types are bending moment structures meaning that some of the members experience both tension and compression forces and reinforcement is needed in the tensile areas. If they are not bending moment structures then the structure experiences only compressive forces and tensile reinforcement is unnecessary. The arch structure, the gravity dam, roller compacted dam, and the arch dam are all designed so that the forces in the structure are all compressive. The concrete is well suited to the compressive forces but where there are tensile forces the concrete will fail at roughly 6 – 10 % of the compressive failure force [17, 18] and reinforcing steel must be included to carry the tensile load the concrete is no longer capable of carrying. The tensile strength of concrete and how it changes with increasing compressive strength will be discussed later in this chapter.

3.1.2 Material uses

There are a number of situations where concrete is not used primarily for its strength or structure, but for one of its high-performance materials capabilities. Concrete used for radiation shielding is a use of the materials density to attenuate radioactivity [19, 20]. Oil-well cement or grout is used primarily to create a barrier between the outer face of the well pipe and the wall of the drill hole to achieve zonal isolation of gasses in the ground [21]. Many concrete repair materials, meant to fill in a spall or replace broken concrete corners, are being used for sealing tasks or cosmetic repair rather than a structural repair. In all cases, whether the usage task is materials or structural in nature the concrete is expected to be strong.

3.2 Types of strength

Strength in concrete is defined in many ways depending on the particular type of loading the structure is being asked to carry. The two most recorded properties of concrete are the compressive and tensile strength. Two other types that are important to VHSC will be introduced here: the bond strength and the fracture toughness.

3.2.1 Compressive strength

The compressive strength of concrete is the most widely used benchmark for determining its adequacy because most structures are designed to carry compressive loads. The compressive strength test is a very simple test. Two forms of specimen are commonly used, the cylinder and the cube. Because it is so universally accepted, the compressive strength is often used as part of the calculations to determine other material properties, and the strength of many component materials used in concrete is expressed by their compressive strength.

Concrete used in construction practice today has a wide range of compressive strengths from a low around 14 MPa to a high of approximately 131 MPa [22, 23]. This covers a range of

materials from lightweight concrete to high-strength concrete. However, there are higher strength concrete materials that have been and are currently being developed with compressive strengths up to 250 MPa [9].

3.2.2 Tensile or flexural strength

The tensile strength of concrete is an indicator of its fracture-resisting capacity [24, 25]. This is an important property because all failures of concrete are related to fracture of the matrix. Tensile strength is usually taken as the critical structural property in members subjected to bending or torsion.

Direct tensile strength is a difficult property to measure because stress concentrations that develop when attempting to load the specimen affect the results. There are several different methods used to measure tensile strength. Three alternatives to direct tensile strength testing, flexural, splitting tensile, and torsional, are used. In experiments to measure the effects of type of curing on the tensile strength of medium- to high-strength concrete, Conroy-Jones and Barr [26] used these three as a means of comparing strength tests. They concluded that flexural and torsional strengths were higher than splitting tensile strengths in comparisons of similar concretes. Marzouk and Chen [27] conducted direct tensile tests on notched beams of high-strength concrete that were loaded under strain-rate control. At the same time they loaded companion compressive-strength specimens, split-tension cylinders, and modulus of rupture prisms. They observed that splitting-tensile strengths were approximately 40% greater than direct-tension tests and that modulus of rupture tests were approximately twice that of direct-tension tests.

Because the compressive and tensile strengths of the material are both functions of fracture of the concrete, it is fair to assume that there is a relationship between the two strengths.

Such a relationship does exist, but there is no direct proportionality between the two. Rather, the ratio of the two strengths, f_c and f_t , is dependent on the strength of the concrete. As the compressive strength increases the tensile strength also increases but at a decreasing rate [17]. Table 3.1 illustrates this with tension/compression data taken from Price [18]. As the compressive strength increases from 6.9 MPa to 62 MPa, the ratio of the tensile strength to the compressive strength decreases from 0.11 to 0.07. These data, published over 55 years ago, show that the rule of thumb setting the tensile strength of concrete at approximately 10% of the compressive strength is only true for a small range of the data.

Table 3.1 Relationship of tensile strength to compressive strength [18]

Compressive strength of cylinders, MPa	Tensile strength, MPa	Ratio of tensile strength to compressive strength
6.9	0.76	0.110
13.8	1.38	0.100
20.7	1.90	0.092
27.6	2.35	0.085
34.5	2.76	0.080
41.4	3.17	0.077
48.2	3.59	0.074
55.1	4.00	0.073
62.0	4.35	0.070

The tensile capacity of low strength concrete is nearly a negligible quantity, on the order of 0.7 MPa to 1.4 MPa. When considering VHSC with a compressive strength of 267 MPa, even if the tensile to compressive ratio drops to the 7% indicated by Price, the resulting tensile strength would still be approximately 19 MPa which is a significant amount of tensile load carrying capacity. This level of tensile strength in the concrete coupled with the toughening effects of steel fibers distributed throughout the matrix can effectively be applied towards reducing the need for secondary shear reinforcement in flexural members.

3.2.3 Bond strength

The strength developed between the cement paste and an included element in the concrete is referred to as bond strength. There are two important elements that have an effect on the strength of the concrete through the capacity of their bond strength, namely the aggregate and any reinforcing steel. Consider the case of a mode I crack approaching a piece of aggregate. As the crack reaches the piece of aggregate, the action of the crack opening will place a tensile force on the paste-aggregate system. If the bond strength between the paste and aggregate is poor compared to the tensile strength of the aggregate, then the crack will propagate around the aggregate at the paste/aggregate interface and the aggregate will have played a role of a filler material. On the other hand, if the bond between the paste and aggregate is stronger than the tensile strength of the aggregate, then the fracture surface will be through the aggregate rather than at its interface with the paste. This makes the strength of the aggregate part of the concrete strength and an integral part of the overall composite strength. This is a crucial component of VHSC.

In the case of the reinforcement, a strong bond between the steel and the paste will maximize the tensile load the concrete can transfer to the steel before the steel/paste interface fails and the steel begins to slip.

3.2.4 Fracture toughness

One way of defining fracture toughness in concrete is “the energy absorbed by the concrete per unit area of crack developed” [28]. Said in other words, for a given amount of energy absorbed, the smaller the area of crack developed the greater is the fracture toughness of the concrete. Fracture in the cement paste occurs at the tip of a crack or in the area directly in front of the crack tip commonly referred to as the fracture process zone [29-31]. Resistance to

development of a crack is a function of the inherent tensile strength of the material plus any energy-absorbing mechanism that may be in front of, at, or directly behind the crack tip. Thus any effort to slow crack growth or increase the energy required to promote it is a toughening agent. Chapter 6 of this work is devoted to engineering VHSC to improve fracture toughness. Much more detail on fracture toughening mechanisms can be found there.

3.3 Historical efforts to describe concrete strength

From the beginning of the nineteenth century, when there was a resurgence of interest in concrete construction, to the present, concrete researchers have been interested in improving the strength of concrete and documenting the relationships that govern strength behavior. Two of the first published attempts to define the relationship among cement, water, and strength came from René Féret in 1896 [17] and Duff Abrams in 1918 [32]. Féret offered the relationship:

$$f_c = K \left(\frac{c}{c + w + a} \right)^2 \quad (3.1)$$

in which f_c is the strength of the concrete, c , w , and a are volumetric proportions of cement, water, and air, and K is a constant. Féret's equation indirectly relates strength to the w/c through a power relationship of the volumetric ratio of the cement to the paste. It should be pointed out that Féret included the volume of air in the mixture in the denominator of his power function, indicating that compaction of the mixture (i.e., the volume of air in the mixture) affects the strength. Whether he completely understood the relationship between porosity and strength is not known. However, he was the first to acknowledge that strength is inversely related to the volume of pores.

Abrams offered the first direct relationship between strength and w/c in what has become known as Abrams' Law but in reality is more a rule:

$$f_c = \frac{A}{B^{w/c}} \quad (3.2)$$

in which f_c is the strength of the concrete, A and B are constants, and w/c is the water-to-cement ratio. These two relationships are notable among the first attempts to relate the strength to the volume of cement and water.

Popovics pointed out that the difficulty with Abrams' equation was that a different set of constants was needed for each case [32]. His generalized version of Abrams' rule is given in equation 3.3:

$$f_{co} = \frac{A}{B^{w/c}} \sqrt{\frac{S_s}{S_o}} \frac{1 - pe^{-b_1 t} - (1-p)e^{-b_2 t}}{1 - pe^{-90b_1} - (1-p)e^{-90b_2}} \quad (3.3)$$

where S_s and S_o = the specific surface of the cement in question and that of a type I cement respectively, the coefficient $A=107$ MPa, $B = 6.4$, p = the C_3S and C_3A content of the cement, t = the test age in days, and b_1 and b_2 are rate parameters. Popovics justified this model on simplicity, the need for only two independent variables (the C_3S and C_3A contents) and the two rate parameters b_1 and b_2 .

3.4 Component materials in high-strength concrete

The components of normal strength concrete are low-cost, available materials that are easily mixed and produce a concrete with a compressive strength of around 27 MPa. These components generally include: type I or type I/II cement, clean well graded coarse and fine aggregate, and potable water. The w/c is kept as low as possible to reduce excess water that forms capillary channels, yet high enough to allow all components to mix well and to flow with sufficient ease to be placed in formwork. This ratio is generally from 0.4 to 0.5 by mass. The component materials for VHSC are not significantly different. Cement, aggregate, and water are

the main components. To these are added silica fume and silica flour, a HRWRA, and distributed fibers.

3.4.1 Cement

The cement used in VHSC can be the same as is used for normal strength concrete. Type I or type I/II will work adequately but will have lower strength than cement that has been chosen for its best chemistry. A more beneficial cement would be one with a high silica content (a high C_3S content and a $C/S < 3.1$) that has been coarse ground with a low Blaine specific surface such as is found in class H oil-well cement. The coarseness of class H cement assures that the cement grains will be large. If a low w/c is used then there will not be enough water to totally hydrate the large cement grains and there will be a core of unhydrated clinker remaining surrounded by a shell of high-density calcium silicate hydrate (C-S-H). The unhydrated core of clinker acts as a strong aggregate surrounded by a high quality cement paste that has an almost perfect interface transition zone (ITZ) formed by diffusion as water diffused into the cement grain. This combination allows the clinker, which is stronger than the cement paste, to act as part of the composite and lend its strength to the equation. The water added to the cement is kept at a very low mass for two reasons: to be certain that all the water is used in the hydration process, insuring none is left behind to form capillary spaces, and to take advantage of the increase in strength that accompanies a reduction in w/c.

3.4.2 Aggregate

Attention to the aggregate in concrete is important if only because it occupies such a large volume percentage of the whole. In normal strength concrete the volume of the aggregate can be as high as 75 % by mass. Prior to the 1960's aggregate was mainly considered a filler material that was maximized in the mixture to minimize the much more expensive cement. In

that era it was a common practice to add a little water to the mixture to lubricate the paste and make it easier to place. While adding excess water certainly increased lubrication, it also caused the excess water to collect at the surface of aggregates diluting the cement paste around the aggregate [33] and weakening the paste-to-aggregate bond. The advent of silica fume and water-reducing admixtures made it possible to make a mixture with a paste-to-aggregate bond strong enough to fracture the aggregate rather than have the fracture follow the surface of the aggregate and debond from the paste. As a result of this development, the compressive strength of concrete mixtures began to increase because the strength of the aggregate was now a factor in developing the strength of the composite.

The strength of the aggregate itself is important in VHSC. Since the interface transition zone (ITZ) between the paste and aggregate is strong enough to force a fracture through the aggregate, the stronger the aggregate the stronger the concrete.

3.4.3 Pozzolans, admixtures, and additives

The distinction among pozzolans, admixtures, and additives is often subtle. ACI Committee 116 [3] defines a pozzolan as:

“A siliceous or siliceous and aluminous material that in itself possesses little or no cementitious value but that will, in finely divided form and in the presence of moisture, chemically react with calcium hydroxide at ordinary temperatures to form compounds having cementitious properties”

while admixtures and additives are materials added to either the cement (as an agent) or the concrete (as an admixture). They list fly ash, silica flour, and silica fume as pozzolans; releasing, retarding, bonding, surface-acting, and wetting materials as agents; and accelerating, air-entraining, retarding, water-reducing and high-range water-reducing materials as admixtures.

As mentioned above, silica fume and HRWRA's have dramatically expanded the scope of high-strength and high-performance concrete. These materials, along with other pozzolans, admixtures, and additives in use by the concrete industry, have improved many physical and chemical properties of the concrete including: strength, toughness, durability, density, rheology, and many aspects of the composition of the microstructure. The pozzolans and admixtures used in the VHSC described in this dissertation are: silica flour, silica fume, HRWRA's and distributed fibers, both macro and microfibers.

3.4.4 Fiber reinforcement

Since its first introduction into concrete in the mid-nineteen sixties, distributed-fiber reinforcement has been an effective means of evenly distributing stresses throughout the concrete, minimizing the opening of cracks, and acting as a toughening mechanism by resisting pull-out of the fiber. There are a number of different kinds of fibers available: steel, glass, synthetic (nylon, polypropylene etc), and natural (grasses and other organic fibers) [34]. Steel fibers generally have high tensile strength and Young's modulus. Their physical properties are unaffected by the alkaline environment of cement paste and, in fact, that environment helps protect the steel from corroding. Steel fibers are fabricated in a number of configurations (straight, ribbed, dog-bone, crimped and hooked end) designed to enhance their pull-out resistance. Glass and synthetic are more difficult to fabricate with deformations, are generally made from some pultrusion method, and are chopped to the proper length. Any bond enhancement they may have is a function of roughing their surface.

Glass and synthetic fibers are weaker than the steel and have a lower Young's modulus [34]. Unlike steel fibers, the alkaline environment of the cement paste affects glass fibers. Borosilicate and soda-lime-silica glass fibers tend to degrade and lose their strength in the

cement paste. A resistant glass has been developed but also shows long-term degradation. In terms of strength and durability, natural fibers are not contenders in the high-performance field. Their fiber strength is limited and they have durability issues related to water swelling.

3.5 Recent advancements in high-strength concrete

3.5.1 DSP cement

In June of 1981, H. H. Bache published an article [35] on densifying cement pastes by using very small particles of silica fume and crushed quartz. He was the first to make use of particle packing principles to fill the spaces between grains of cement thus reducing the porosity of the cement paste [36]. Powers [37] and Birchall [38] both noted that strength increases with decreasing porosity and with systems containing smaller pore sizes. Because Bache used silica fume (average particle size approximately 0.1 μm) as the particle packing medium, he was filling voids in the paste with solid particles and was in effect densifying the material and reducing the number of sites where cracking could begin. The technique and the material went on to be known by the phrase “densified with small particles” or DSP cement. The component materials in DSP include cement, a high volume of silica fume, aggregate, a HRWRA, and water. By using large volumes of silica fume and a HRWRA, the material can be mixed with a very low water-to-solids ratio, as low as 0.15 [39]. It can also be cured at ambient or elevated temperatures, with increased strength being realized at elevated temperatures.

3.5.2 MDF cement

At about the same time Bache published his work, Birchall and colleagues published a paper discussing the reason for low flexural strength in hydraulic cements. Their contention was that large pores in the cement were the cause of low flexural strength and claimed that the removal of such macro-defects would yield flexural strengths up to 70 MPa [38]. As evidence of

their claims they presented data comparing their new formulation against a 0.22 standard w/c paste. Because the increases in compressive and flexural strength were claimed to be a function of the absence of the large voids they called their new material macro defect free cement or MDF cement. Details of its manufacture were not discussed in the paper other than to say that "...the size of large included voids was reduced by a combination of rheological control and efficient mixing."

Subsequent to publishing this paper, several contributors [40, 41] wrote letters questioning the probability that the strength increase achieved could come from only eliminating macro flaws. Chatterji conjectured that the level of improved strength was consistent with altering the nature of the paste with polymers. In their closure letter, Birchall et al. held that the high flexural strength was due to the elimination of macro pores in the matrix. Without ever acknowledging the presence of polymers, they defended their original conclusions and closed the letter.

In future publications they would disclose the composition of the MDF cement as being a combination of hydraulic cement and a water soluble polymer used as a processing aid. The mixture they settled on consisted of a calcium aluminate cement, water, glycerine, and a hydrolyzed polyvinyl-alcohol/acetate copolymer (PVA) [42]. The mixture also required specialized processing. A process of three intensities of shear mixing was necessary to fully distribute the polymer around the cement grains and affect packing density. The process also requires pressing between platens of an hydraulic press at 5.2 MPa pressure and 80 °C temperature.

This processing produced high compressive and flexural strengths but also made the material brittle. To combat the brittleness and increase the toughness, fibers were incorporated

into the mixture. MDF is not without problems. In addition to its difficult shear mixing process, MDF cements also have a degradation problem when exposed to water or high humidity. Water is absorbed by the polymer, plasticizing it and changing its response to that of a weak, rubbery solid with excessive viscoelastic behavior. This has a major effect on its strength.

3.5.3 Reactive Powder Concrete

On the heels of the announcement of DSP and MDF cements, scientists in the research and development division of the French construction giant, Bouygues¹, initiated a long-term research program to optimize the quality and quantity of the components of an hydraulic cement composite with the end goal of achieving ultra-high strength and ductility in the material. Under the direction of Bouygues scientists Pierre Richard and Marcel Cheyrezy, a family of hydraulic-cement concretes that fell under the name reactive powder concrete (RPC) were developed. The material at the lower end of their spectrum was called RPC 200 because of its 200 MPa compressive strength. It is a field-castable material that requires no application of pressure and only heat curing to 90 °C to achieve 200-MPa strength. At the upper end of the spectrum was their RPC 800 material which required high temperature (240 – 400 °C) and high pressure (variable) during curing to yields a material with 600 – 800 MPa compressive strength. The high-end material is described by its inventors “...to be used only for small or medium size prefabricated elements.” [43] Because it can not be placed in the field, RPC 800 will not be discussed further.

RPC 200 consists of portland cement, fine sand, silica fume, precipitated silica, HRWRA, water, and steel fibers. Like DSP, MDF, and VHSC, RPC 200 is technically a mortar because of the absence of any coarse aggregate. However, all these mortars are used as concrete and

¹The phonetic pronunciation of the word Bouygues is Bwēēg

therefore take on the visage of concrete. The term “powder” in reactive powder concrete refers to the fine particle sizes of the dry ingredients, they are essentially powders. And the reactive nature of the cement and silica fume accounts for the word reactive in the name. Table 3.2 gives a comparison of some of the physical properties of the high-strength concretes that have evolved since the beginning of the 1980’s. Properties of VHSC are included in this table but have not been discussed here as they are the primary subject of this dissertation and will be discussed in the remaining chapters.

Table 3.2 Physical properties of some of the high-performance cement materials [9, 42]

Property	DSP	MDF	RPC 200	VHSC
Compressive strength, MPa	200-300	300	170-230	180-266
Flexural strength, MPa	20-30	150	30-60	17.5
Modulus of elasticity, GPa	30-50	45	54-60	51
Fracture toughness, MPa·√m	0.5	3	5.4 – 11.3*	1.1
Density, Kg·m ⁻³	2800	2400	2230	2350

* Steel-fiber reinforced

3.6 Movement toward ceramic-like behavior

In each of the materials described in section 3.5 there was an effort to make the cement paste matrix denser by packing smaller particles into the spaces between the cement grains. Silica flour and silica fume are the two materials primarily responsible for accomplishing this task. Normally ground cement particles are typically between 10 μm and 100 μm in diameter. Coarsely ground cement can be even larger. Silica flour particles range from 5 μm to 40 μm[44] and silica fume particles are generally in the range of 30 to 300 nm [17]. As these particles fill the spaces between cement grains they displace water and create C-S-H, making the matrix stronger by eliminating some of the porosity. As will be discussed in chapter 4, the strength of a material increases as its porosity decreases. As a cementitious material becomes less porous,

denser, and more homogeneous it begins to behave more like a ceramic material. Ceramics are very strong but also very brittle [29, 45, 46]. One of the characteristics of a brittle material is a linear or near-linear stress-strain curve right up to the point of failure. This is non-characteristic of a normal strength concrete. The stress-strain curve will be linear to approximately 50% of ultimate stress but will become non-linear above that level exhibiting increasingly greater strain per unit of stress until failure. This nonlinear behavior is a sign that microcracking is taking place in the material prior to failure. These microcracks began to propagate at pores in the cement paste. The stress-strain curve of VHSC, on the other hand, remains relatively linear right up to failure. It is able to maintain this linear characteristic because there are very few pores in the matrix and as a result, no sites for the initiation of microcracks.

3.7 Summary

Chapter 3 introduced the discussion on concrete's path to high strength. Topics addressed at the outset included the typical uses of concrete and the types of strength that concrete brings to these uses. The chapter continued by relating the engineer's historical attempts to describe the strength of concrete mathematically, for the first time tying concrete's strength to the amount of water in the mixture. Being a composite material, concrete's components have an effect on its strength and the chapter continued with discussion on component contributions to strength. The chapter concluded with discussion of the late 20th century advances in strength development that were afforded by new concrete admixtures and additives that dramatically changed the microstructure of the cement and dramatically increased the strength.

Chapter 4 BACKGROUND AND LITERATURE REVIEW II: FOR HIGH STRENGTH

4.1 Early development of VHSC

The Corps of Engineers' early effort to develop a very-high-strength concrete was conducted under the Department of the Army's Hardened Structures Research Program by research engineers at the Corps' Waterways Experiment Station (WES) in Vicksburg, MS. Under a work unit initiated in 1989 to develop cementitious material systems, concretes, procedures, and construction technology to enhance the survivability of the Army's hardened facilities, the research team was tasked to develop a concrete with the highest strength possible. Previously under this work unit the research team developed a number of special concretes with the highest compressive strength in the vicinity of 103 MPa. With this new task their goal was to maximize the properties of the concrete, to meet or exceed properties of the advanced research concretes published in the literature.

Working independently from other researchers at the WES and starting from papers in the open literature by Richard and Cheyrezy describing RPC [43], research engineers Neeley and Walley developed a concrete material they named Very-High-Strength Concrete (VHSC) that used different component materials from RPC, was considerably cheaper, and still had comparable compressive strength.

The entire archive of research notes kept by Neeley and Walley remain unpublished today and as such are unavailable for scientific study. They published one article on VHSC [47] in which they described component materials used. These are given in Table 4.1.

Table 4.1 Component materials and mass proportions of early VHSC [47]

Component	Mass proportion	Description
Cement	1.00	Type V OPC
Sand	1.20	Siliceous natural sand
Silica fume	0.24	A low-carbon silica fume
Silica flour	0.34	Finely crushed quartz
w/cm	0.20	w/c = 0.25
HRWRA	0.04	Unspecified
Steel Fibers	0.31	Cold-drawn fiber, 30 mm long and 0.5 mm in diameter

4.2 Early components of VHSC

Early on, the cement used in Neeley and Walley's VHSC was type V cement as defined by ASTM C 150 [48] because of the limit of C_3A content specified by ASTM. A low C_3A and low combination of $C_3A + C_4AF$ perform better because low percentages of these components generally mean higher percentages of C_3S and C_2S which are primarily responsible for the development of C-S-H. Another aspect of the choice of this type cement was its fineness. Type V cement has a moderate Blaine fineness. Cements that are ground to a very small particle size have much larger surface areas and thus create a higher adsorbed water demand. With the very small amount of water used in VHSC this becomes a critical matter.

Because the aggregate makes up a large percentage of the volume of any concrete mixture, how it is chosen is particularly important. Neeley and Walley experimented with numerous kinds of aggregate getting the best results from well-graded calcined bauxite. Despite the superiority of this aggregate it was too costly and they ultimately chose a siliceous natural sand for the aggregate in VHSC to reflect a combination of cost and performance. They remarked that the hardness or strength of the aggregate is particularly important especially in cases where the paste has a strong bond to the aggregate. They also noted that the grading of the aggregate had an equally important role, here referring to the packing aspect of the particles in

the mixture. The aggregate they ultimately chose was a chert sand with particle sizes ranging from 200 μm to 6.4 mm. Chert is a hard siliceous aggregate that when combined with a paste that produces good bond will add considerable strength to the composite. When compared to RPC, the particle packing contribution of this sand was not as optimal as that of the uniformly graded 300- μm quartz sand used in RPC. However, when combined with the particle sizes and volumes of silica fume and silica flour Neeley and Walley used, the performance was adequately approximated while costing only a fraction of the cost of the finely graded quartz sand.

Neeley and Walley studied the effects of different silica fumes on the rheology of the fresh paste and the strength of the hardened paste. They found that the higher the silica content the greater the strength afforded the VHSC. It was their observation that the highest strength came from the silica fume produced as a by-product in making zirconium because it had the highest SiO_2 content and the fewest impurities. They observed that the higher the carbon content in the fume the stiffer the fresh paste, reasoning that the carbon in the silica fume had a high water demand which reduced the amount of water available to fluidize the paste.

As early as 1995 Neeley and Walley recognized the benefits of adding silica flour to their mixture design to improve the strength and durability. They saw the particle packing benefit of having a range of silica particles of different diameters such that smaller ones would fit in spaces made between larger ones. They stated that the hardness of the aggregate was important to strength, but also recognized the important role the grading of the aggregate occupied [47]. They referred to the silica flour as an aggregate in their writing but implied it provided a pozzolanic effect in the presence of moderate heat, referring to the practice of curing VHSC at 90 °C. There is evidence in the literature of pozzolanic benefit from silica flour, but these references are for oil-well cements cured at much higher temperatures (230 °C) [49, 50].

Neeley and Walley reported using a water-to-cementitious-material ratio (w/cm) of 0.20 in VHSC. Although it was not specified in their paper, it is assumed that the cementitious materials included the cement and silica fume, since both materials contribute to the production of C-S-H. Their w/cm is considerably higher than that published by Bouygues for RPC (w/cm = 0.129) [43]. Much of what was done for VHSC was done to make the material user-friendly without compromising the strength and ductility. It is thought that Neeley and Walley chose a higher w/cm to make the mixture more mixable and placeable. Their aggregate gradation was not developed for optimum particle packing, rather for some level of particle packing balanced against cost and workability.

As with the silica fume, Neeley and Walley experimented with a number of HRWRAs before settling on one that was inexpensive and provided the level of rheology needed for the VHSC to be workable. While the type of high-range water reducer they used was not specified in their published literature, it has been determined from personal correspondence that they used the powder form of a poly-naphthalene sulfonate sodium salt that is produced by Handy Chemical Company and sold under the trade name Disal™. Disal™ is marketed in powder and liquid form. The liquid form is 41% solids and 59% water. The powder form was used in VHSC to avoid having to account for the water in the liquid form as part of the w/cm.

Because VHSC and RPC have such a dense, homogeneous matrix, they are characteristically more brittle than conventional concrete. Some form of distributed reinforcement was needed to help restore some of the ductility and fracture toughness to the matrix. The RPC engineers studied many different types of distributed reinforcement including glass, aramid, carbon, and steel wire. The material that performed the best was a straight, brass-coated-steel fiber 13-mm long by 0.16-mm in diameter. Neeley and Walley also studied a range

of distributed reinforcement and came to the same conclusion as the RPC engineers. However, because the fibers chosen for RPC were very expensive and difficult to procure, they chose an alternative steel fiber 30-mm long and 0.5-mm in diameter that performed reasonably well and was significantly cheaper than the wire chosen for RPC.

Neeley and Walley used the metric of compressive strength to judge their progress. The best results they reported [47] were compressive strength of 239 MPa from VHSC cured at 83 °C for 56 days and 216 MPa from VHSC cured at 83 °C for 3 days.

4.3 Philosophy of VHSC

The current philosophy of VHSC is as much a part of its high strength as the materials comprised in its make-up. It embodies what can be done if maximization of the beneficial properties and minimization of the detrimental properties of concrete are pursued as the primary considerations tempered by cost considerations in extreme situations. The philosophy is rooted in the belief that choosing the right materials, the best quality and the right quantities of those materials, and only considering cost on an as needed basis, will produce a vastly superior concrete that can often be cost competitive with less-expensive concrete on a dollar-per-MPa basis. The philosophy is further based on the principle of applying sound engineering thinking to the choice of materials and methods of combining those materials to optimize strength, density, rheology, toughness, homogeneity of the microstructure, and ductility of the resulting concrete.

4.4 Principles underlying the philosophy of VHSC

Many positive steps can be taken to improve the strength and durability of any particular concrete mixture. The ones that were pursued to improve the material properties of VHSC are summarized in table 4.2. These are the properties that contribute the most to maximizing strength and durability and minimizing conditions that promote weakness and premature crack growth.

Table 4.2 Summary of principles underlying the philosophy of VHSC

Minimization of flaws in the matrix
Improvement of matrix homogeneity
Maximization of the silica content for conversion to C-S-H
Maximization of the density of the matrix
Improvement of the microstructure
Enhancement of matrix ductility

4.4.1 Minimization of flaws in the matrix

Because of its composite nature, concrete is an inherently flawed material. Flaws can be actual voids or weak material in the paste that will initiate cracking more readily than the surrounding material. Flaws come from such sources as high porosity, excessive capillarity from high w/c pastes, entrained or entrapped air voids, and zones of weakness in the paste often occurring at the paste/aggregate interface where the chemistry of the paste is different from that in the bulk paste [51-55]. Physically, flaws are the sites for the initiation and development of microcracks that grow into macrocracks under the application of stress. The fewer flaws that exist initially, the fewer sites for crack development and the greater the likelihood that the matrix will be able to withstand a higher level of ultimate stress before cracking. This is not to say that fewer flaws will prevent cracking of the concrete. Concrete will crack when the tensile strain capacity of the material has been exceeded. However, it is fair to say that the tensile strain capacity of a concrete will be higher if there are fewer flaws in the paste than if there are many.

Perhaps the greatest source of flaws in the cement paste is from the porosity. The strength of many materials is a function of the volume of voids they contain. This is illustrated in the normalized graph shown in Figure 4.1. The deterioration of strength in all these materials is a function of the percentage of porosity they contain. A change in the porosity from 0% to 10% results in a 60% drop in the ultimate strength, illustrating the importance of the strength-porosity

relationship. To describe the relationship as it applies to cement a number of semi-empirical equations have been proposed [56]. Balshin proposed a power function

$$\sigma = \sigma_o(1 - P)^A \quad (4.1)$$

in which the strength is a function of the strength at zero porosity times the solid volume of the paste raised to the power A. Ryshkewich [57] used an exponential function

$$\sigma = \sigma_o e^{-BP} \quad (4.2)$$

in which the strength is a function of the strength at zero porosity times the exponential of the negative power of the porosity.

Both of these relationships relate the strength at a given porosity to the strength at zero porosity, a value difficult to measure for want of flawless material. Beaudoin and Ramachandran [58] did work on strength versus porosity of pastes made from pure cement phases. They discovered that the data in a semi-log plot of strength versus porosity fell on a straight line. The data for the silicates (C_2S and C_3S) and the aluminoferrite (C_4AF) fell on one line and the data for the aluminate (C_3A) fell on a different line. However, when extrapolated back to zero porosity, both these lines converged on the same strength, 400 MPa, implying that this was perhaps a high-end threshold for cast, cementitious systems unenhanced by pressure or high temperature. Roy and Gouda, as reported by Neville [17], studied porosity and strength of

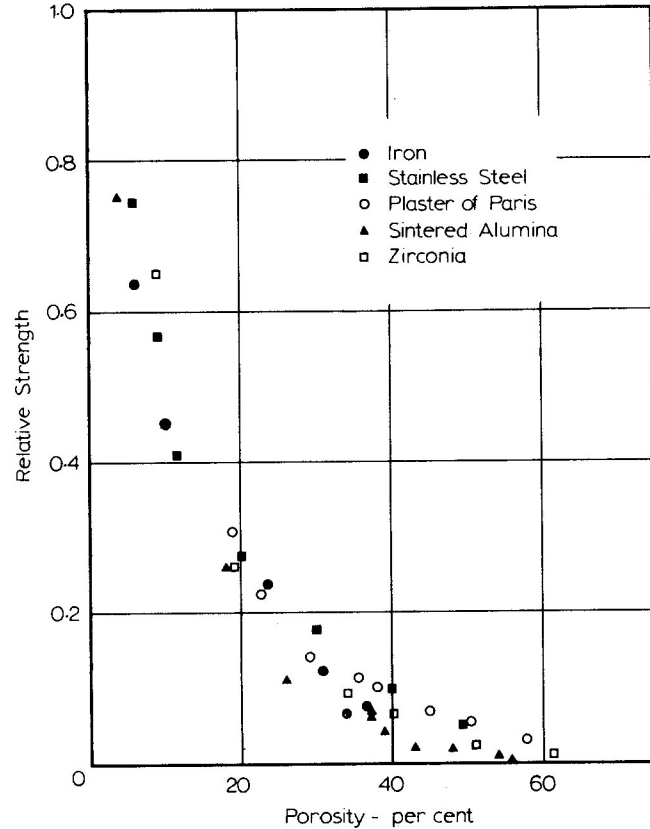


Figure 4.1 Influence of porosity on relative strength of various materials [17]

cement paste compacts cast under various pressures and temperatures and reported compressive strength as high as 650 MPa at approximately 2% porosity. Richard and Cheyrezy [59] reported a compressive strength of 810 MPa from a compact of RPC containing fine, steel aggregate and compressed under 60 MPa pressure during curing and heat treatment to 400 °C. To date, portland cement mixtures cast without the advantage of either heat or pressure have yet to achieve a compressive strength near 400 MPa.

Pores in hardened cement are generated from sources of liquids and gasses, the obvious liquid being water and the most prominent gas being air. Powers and Brownyard [37] divided the water in a mixture into non-evaporable and evaporable water. The former they referred to as combined water or water of crystallization and the latter as adsorbed water (gel water) and capillary water. Combined water is chemically tied to the hydrates and is impossible to remove short of driving it from the structure with high temperature. Gel pores and capillary pores are generated from evaporable water in the paste and constitute the body of porosity from water. The portion that is gel water is derived from Brunauer-Emmet-Teller (B.E.T.) theory and according to Powers is that quantity of evaporable water that can be adsorbed into the densest possible paste under saturation conditions. Any additional water is considered capillary water. This distinction is important because capillary water is water that is not adsorbed into the gel and ultimately forms into channels in the cement paste creating capillary pores that remain in the paste as flaws. Without pressure to squeeze the capillary water channels from the mixture, these flaws remain making it difficult to achieve zero porosity. The w/cm in VHSC is kept so low as to guarantee that all the evaporable water will be adsorbed as gel water and there will not be any available to form capillary pores.

Porosity derived from entrained air and entrapped air come from chemical admixtures such as air-entraining agents and mixing techniques respectively. Air-entraining agents are never used with VHSC and internal and external vibration of the fresh mortar is used to remove as much entrapped air as possible. Other gasses can be responsible for increasing the porosity of the paste. For example, bubbles of hydrogen [17] can be liberated into the paste from the reaction of aluminum powder with the alkalis in cement paste. Inadvertently this happens when aggregate has been transported in aluminum-body trucks. Short of applying high pressure to the fresh paste these voids may remain as flaws.

4.4.2 Improvement of matrix homogeneity

The basic philosophy behind improving the homogeneity of the matrix is to produce a composite, composed of many different materials, that behaves as if all the materials were similar in properties. The previous section stressed reducing porosity as a means of improving strength. If porosity cannot be completely eliminated then a solution to reducing the porosity is to fill the pores with materials having similar properties to the surrounding material. This has the potential for reducing microcracking by bringing the elastic properties of all the components closer together. Spaces between cement particles filled with small particles of silica-rich material such as silica fume or silica flour behave more homogeneously than spaces filled with water or air. This is the major principal behind DSP cements. A void filled by a material similar in properties to the surrounding material will resist differential movement between the void and its surroundings better than one filled with material having dissimilar properties or not filled at all.

This concept applies at all levels of the matrix be it in the microstructure or the macrostructure. In a conventional concrete the modulus of the paste can be much weaker than that of the coarse aggregate. Haecker et al. [60] reported 22.4 GPa for a modulus of C-S-H while

empirical estimates of rock mass moduli, based on the Geological Strength Index, range from 20 to 90 GPa [61]. In a mixture with a low paste modulus and a high aggregate modulus, when stress is applied to the composite, the strain in the paste will be larger than that in the aggregate. Where these two materials come together, at the paste/aggregate interface, the differential strain is likely to produce a tensile stress greater than the tensile capacity of the interface and microcracks will develop. Efforts to bring the moduli of all the component materials closer together will reduce the differential tensile strain and the development of microcracking will be delayed to a higher stress level.

Homogeneity in VHSC is further improved by eliminating the coarse aggregate. VHSC contains only fine aggregate. The size of the microcracks developed under a given stress is a function of the size of the aggregate and related to the size of the zone under stress [59]. Reducing the size of aggregate reduces the size of microcracks. In the case of VHSC, the diameter of the largest aggregate is 6.4 mm while in conventional concrete it is generally three times that diameter. Since the zone under stress is related to the surface area of the aggregate, the surface of the largest aggregate in conventional concrete is approximately 900% greater than that of VHSC encouraging larger microcrack formation.

4.4.3 Maximization of the silica content for conversion to C-S-H

Reactive forms of silica can be beneficial to the strength of the cement paste matrix by forming additional amounts of C-S-H, filling voids between the particles in the larger classes of materials, and adding a lubricating effect to the rheology of the paste [62, 52]. The primary objective of these additions is to use the silica to react with available water and CH to produce additional C-S-H, but the benefit goes beyond producing additional C-S-H to include: (a) consumption of the CH that often produces weak material in the vicinity of the paste/aggregate

interface [63, 64]; (b) providing heterogeneous, nucleation sites in the matrix for deposition of hydration product [65]; and (c), filling otherwise water-filled space with solid particles that densify the matrix. These forms of silica can be incorporated into the matrix from a number of different sources. Use of silica-rich, dry components in the mixture such as silica fume, silica flour and fly ash will maximize the volume of silica capable of producing C-S-H. The volume of silica fume used in VHSC is purposefully large to take advantage of all the above benefits. Mass calculations of the products of hydration of VHSC given in Appendix A reveal that less than 11% of the silica fume used in the mixture consumes all the CH produced by the silicates and produces 53% additional pozzolanic C-S-H to compliment the conventional C-S-H. The remaining 89% acts to provide sites for C-S-H growth and fill void spaces with a near-pure-silica based filler enhancing the density and homogeneity of the paste.

The choice of type of cement used to make VHSC makes a difference in its resulting properties. While any of the standard portland cement types are suitable, some are more efficient than others. It is beneficial to have high silica content, a low C_3A content, and a low C/S ratio to maximize the volume of silica. VHSC is made using class H oil-well cement that reflects these properties. The mill specification report given in Table A.4 of Appendix A reveals that the cement has a high C_3S plus C_2S content, a very low C_3A content and a 2.95 C/S ratio, all properties that maximize the silica content.

4.4.4 Maximization of the density of the matrix

An ideal cementitious matrix would be a highly dense matrix that contained no flaws or voids. As was previously discussed, this is a nearly impossible condition to achieve. One strategy for moving in this direction would be to strive to minimize the voids and maximize the solid volume of the matrix. A cement paste with a high density will have fewer voids than a similar

paste, of equal volume with a lower density, simply because a given volume of cement has greater mass than an equal volume of water and air. Thus a high density paste will have fewer voids in the volume, and fewer sites for the initiation of microcracking.

A number of things can be done to achieve this goal. Using particle packing methods will increase the solid volume of the matrix. Calculating the appropriate volumes of cementitious powders of several particle sizes will insure that the spaces between larger diameter particles will be filled with particles of smaller diameters rather than becoming air- or water-filled spaces. Filling the spaces between large cement particles with smaller particles of silica fume, fly ash or, for that matter, even an inert filler, will increase the strength of the matrix by creating a solid structure where a flaw had previously been.

In terms of increasing the durability of the matrix, a highly dense microstructure will impede the passage of liquids and gasses through the matrix making it difficult for these materials to penetrate and cause damage. If cement particles of only one diameter range are used, the spaces between particles will potentially become a network of connected pathways that can become a passage into the concrete for harmful materials. If, however, the system of voids between cement grains is now filled with smaller solid particles there will no longer be a path for liquids and gasses to travel through the paste and thus the durability will be improved.

High w/cm's are also damaging to the permeability of the matrix. If all the water added to the mixture is not consumed as combined or gel water, the unused portion will remain in the paste forming channels or capillary spaces through which liquids and gases can travel. By adopting a practice of using a very low w/cm, it can be assured that all the water provided to the mixture is consumed in the hydration process and none will be left to form capillary channels.

4.4.5 Improvement of the microstructure

The microstructure of C-S-H is very complex. Among the components present are: C-S-H, both low and high density [66]; CH; unhydrated cement grains; voids ranging from a few nanometers to several millimeters; water; and a number of other compounds both beneficial and detrimental to the strength and durability of the material. Improvement of the microstructure can be affected in a number of ways, among them are techniques to: create more C-S-H; improve the quality of the C-S-H; and improve the bond between paste and aggregate at the microstructure level. Creation of more C-S-H is achieved through supplementing the portland cement with pozzolans and natural cements. These materials not only create more C-S-H, they can consume compounds that weaken the paste. Improvement of the quality of the C-S-H is achieved by increasing the density of the paste through particle packing techniques and through heat curing the hardened concrete. Heat curing is believed to accelerate the pozzolanic reaction and modify the microstructure of the C-S-H. Richard and Cheyrezy [59] point out that heating the curing concrete to 90 °C significantly accelerates the reaction of the C-S-H and modifies the structure of the hydrates that have formed. At this temperature, the C-S-H remains an amorphous structure. With the further application of heat, the amorphous structure of C-S-H can be transformed into a crystalline structure. The crystalline compound xonotlite has been found on heating the concrete to temperatures above 240 °C [95].

The coarseness of the ground cement is also a consideration. Cement that is finely ground is unacceptable because of its high surface area and the high demand for water that accompanies it. Coarsely ground cement has a lower surface area and a higher volume-to-surface-area ratio. The lower surface area demands less water allowing the limited amount of water available to better fluidize the mixture. The larger grains of cement benefit the mixture because at the very

low w/c of VHSC the core of the cement grain will remain unhydrated and act as a strong aggregate in the composite mixture.

In the development of VHSC, all these techniques short of heating to 240 °C have been employed to improve the microstructure. The two techniques that have been particularly useful are strengthening of the C-S-H through the use of heat treatment and densification of the microstructure through the use of micro and nano-size particles.

4.4.6 Enhancement of the matrix ductility

All of the aforementioned techniques have been employed to enhance the strength and durability of the VHSC material. While the optimization of the mixture design of VHSC has been very successful in improving the strength and durability of the material it has also made it very brittle. A graph of a typical stress vs. strain curve is nearly linear from start to failure (Figure 4.2). However, to make VHSC useful as a construction material, some level of ductility must be returned to the matrix. One method of restoring this ductility is achieved

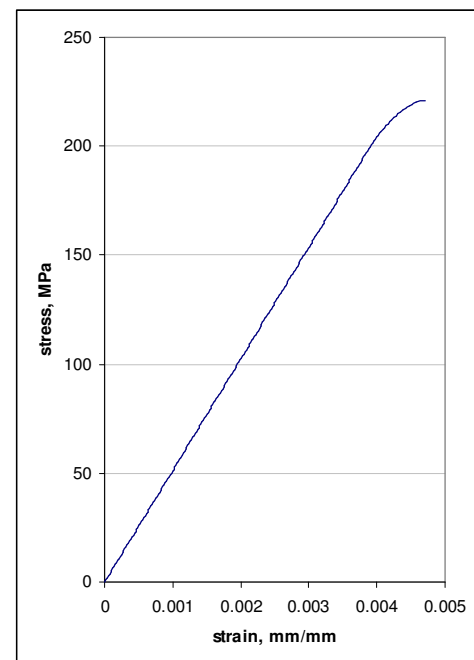


Figure 4.2 VHSC σ - ϵ curve

by mixing distributed fibers into the fresh paste. When the matrix hardens, the fibers are available to act as crack arresters when fracture of the matrix occurs. After the paste has fractured, for the fracture faces to open and the crack to propagate, input of additional energy is required to break the bonds between fiber and paste and to overcome the friction needed to pull the fiber from one face of the crack.

To optimize the ductility enhancing benefits of fiber reinforcement, much research has been conducted to identify the optimum type, length, volume and aspect ratio of fiber [8, 29, 34, 67-70]. In addition, research has been conducted to identify the potential benefits of adding microfibers to the matrix to address arresting of microcracks, and inclusion of microspheres to act as microcrack-blunting mechanisms and stress relievers to further slow the progress of microcracks [71-74].

4.5 Summary

Chapter 4 introduced the reader to VHSC, the first of the two high-performance materials whose engineering is the subject of this dissertation. The first topic was a description of the early work involved in developing VHSC and a description of its components. Following this, the philosophy of VHSC was discussed and the engineering principles behind the philosophy were related. This chapter set the stage for chapters 5 and 6 which relate the research work conducted to improve the strength, rheology, and toughness of VHSC beyond the levels described at the outset of the chapter.

Chapter 5 EXPERIMENTAL WORK ON STRENGTH

5.1 General experimental procedures

5.1.1 Background

The development of VHSC was started in 1989 by Neeley and Walley. Their materials and proportions were given in Table 4.1. Their work was continued by O'Neil and co-workers in 1994 and continues into the present. As the military continues to have a strong interest in its development it will no doubt continue into future years. To cover all the experimental work that took place over the span of the past 20 years would be impossible to document and is far beyond the scope of this dissertation. The problem statement to this dissertation focuses on developmental research that maximizes beneficial properties and minimizes detrimental ones. In the case of VHSC, how to engineer high strength but still maintain desired ductility, flow, and toughness is emphasized. In the case of Frangible Concrete, how to achieve a workable balance between strength and frangibility is the crucial asset. Research and discussion on these topics will be the ones explored here.

The baseline proportions of VHSC under the current research are somewhat changed from those used by Neeley and Walley to better reflect the philosophy of maximizing beneficial properties and minimizing detrimental ones. The proportioning of aggregates was reduced to allow a larger volume of smaller particles and provide better packing arrangement. The aggregates, sand and silica flour, were reduced from mass ratios of 1.2 and 0.34 based on mass of cement to 0.97 and 0.28 respectively. The silica fume was increased from a mass ratio of 0.24 to 0.39 to increase the mass of pozzolanic material and provide a larger volume of very-small particles. The w/c was reduced from 0.25 to 0.22 to help increase the strength. The proportions

given in Table A.3 of Appendix A reflect these changes and became the baseline proportions of VHSC in the current research.

The vast majority of experimental work done to enhance the properties of the baseline VHSC was done through bench-top experimental mixtures. As in any large experimental program, small-scale experiments were conducted to explore possibilities before larger ones were done to confirm results. The general experimental procedure for small-scale, bench-top experiments was the same throughout the developmental program. Rather than repeating the details of these experimental steps with each topic discussed, they will be given here once and referred to throughout the dissertation.

5.1.2 Bench-top mixing procedures

Bench-top experiments were conducted to produce fresh and hardened VHSC materials to document: mixing time, time-to-paste, flow as measured by a flow-table, and compressive strength at various ages after having been cured in a 100% humidity room (fog room) for the first 24 hours and then either in limewater to testing age or under a heat-treating procedure that will be referred to as heat curing.

Mixtures were proportioned by mass, weighing component materials to a mass ratio based on the mass of cement in the experiment. For example, if the mass ratio of silica flour was 0.28, and the mass of cement in the experiment was set at 500g, then the mass of silica flour was weighed to 140.00 ± 0.05 g. Materials were mixed in Hobart™, food-processing mixers meeting the standards of ASTM C-305 [75] and using a standard beaver-tail paddle for mixing. Two different size bench-top mixers were used depending on the volume of the mixture being made. For small size experiments, a 4.78 l mixer was used and for medium size experiments, a 9.56 l mixer was used. Large experiments were mixed in a floor-mounted, 28.92 l mixer.

The dry materials were placed in the bowl of the mixer in the order of smallest to largest diameter of particle and dry mixed on the lowest mixer speed for 5 minutes. This order was chosen so that the largest diameter particles, the sand, would form a cap over the smaller particles and prevent the lighter material from being ejected from the bowl when the mixer was started. Liquids consisted of the mixing water and liquid HRWRA if one was used. Any liquid HRWRA was added to the water and thoroughly mixed before the liquids were added to the dry components. As the liquids were being added to the bowl, the time was marked and the time it took the materials to become a paste (time-to-paste) was recorded. During the time before the wetted materials became a paste, the mixer was stopped once and the sides and bottom of the bowl were scraped with a rubber spatula to incorporate those materials clinging to the sides or bottom beneath the influence of the mixing paddle into the wetted mix. When it was determined that the materials had become a paste, a subjective observation, time was again marked and the paste mixed for an additional 5 minutes.

5.1.3 Flow number measurement procedures

Each experiment was sampled and tested immediately after mixing to determine its flow number in accordance with the provisions of paragraph 10.3 of ASTM C-109 [76]. The flow number is a relative measurement that represents the percent increase over the original diameter of the mortar specimen after being dropped 25 times through a distance of 13 mm on a standard flow table (Figure 5.1). Because VHSC is often very sticky, the inside surface of the cone used to form the fresh paste is coated with light coat of oil before the sample material is placed in the cone to insure the entire mass of the sample remains intact when the cone is removed. The sampled material is tamped into the truncated cone and screeded level with the top of the cone, the cone is removed, and the dropping sequence started. After the sample has spread, its diameter

is measured four times using a specially calibrated measuring instrument. The sum of the four measurements is the flow number. Flow numbers range from 0, indicating that the dropping sequence did not change the diameter of the sample, to 142, the largest diameter of the dropped sample before it begins to fall off the table. A flow number greater than 142 represents a rheology that is nearly a self-leveling material. Throughout the development of VHSC the flow number has been used as a relative number to judge the rheology of one mixture relative to another.



Figure 5.1 Flow table

5.1.4 Procedures for casting compression samples

Because of the high compressive strength involved, the standard compression testing specimen used throughout the developmental program was the 50.8-mm cube. This specimen type was chosen because the cube can be tested without any grinding preparation before testing. If cylinder specimens were needed they were cast in 76.2- by 152.4-mm plastic cylinder molds.

Immediately after completing the flow number test, cube specimens were made. Three-specimen, steel or brass, 50.8-mm cube molds were coated with a release agent and assembled for casting compressive strength specimens. One, three-specimen mold was cast for small experiments and three, three-specimen molds were cast for medium and large experiments. External vibration was used to help consolidate specimens from all experiments. Specimen molds were placed on a vibrating table and filled with the VHSC in two layers, tamping each layer with a prismatic rubber rod. When the molds were filled, the mortar was brought level with the top surface of the mold by screeding with the edge of a small hand trowel. The filled molds were then vibrated until air bubbles no longer appeared on the surface of the VHSC paste. The

filled molds were then placed in a 100%-humidity room for the first 24 hours. At the end of 24 hours the specimens were checked to see if they were hardened. If they were, the molds were broken open, the cubes removed, given an identification number, and placed in limewater. If the specimens were still soft at 24 hours, a condition that would occasionally happen when the mixture had been given a dose of HRWRA outside the limits of the manufacturer's recommended dose, the specimens were left in the molds for an additional 24 hours and demolded at 2-days age.

5.1.5 Procedures for curing cube and cylinder specimens

VHSC cube and cylinder specimens generally received either limewater curing or a heat treatment régime. Specimens that only received ambient-temperature curing were kept in limewater until the testing age, generally 1-, 3-, 7-, or 28-days age. The heat-curing procedure consisted of 100%-humidity curing for the first 7 days, in which the specimens were stored in limewater after demolding. After 7 days of ambient-temperature water curing, the specimens were transferred to hot water that was kept at 90 °C for the next 4 days. After hot-water curing the specimens were put in an oven and heat dried at 90 °C for an additional 2 days before they were ready for testing.

5.1.6 Preparation for compression testing

The vast majority of compression testing specimens were 50.8-mm cubes. These specimens were either removed from the limewater on the day of testing and allowed to dry to surface-dry conditions or in the case of heat curing they were already dry. The edges of the cubes were inspected for any burrs and were lightly filed with a fine-toothed file to remove any mortar that could produce stress concentrations when tested. Because of the strength of the mortar, cylinder specimens could not be capped with sulfur compound to bring the ends parallel. Instead

they had to have their ends ground parallel to each other and perpendicular to the side of the specimen before they were ready for testing.

5.1.7 Compression testing procedure

Cubes were tested in accordance with the provisions of ASTM C 109 [76]. The compression testing machine was either a 1.95 MN Baldwin compression/tension testing machine or a 4.44 MN Satec compression testing machine. Each cube was centered on a 76.2-mm-diameter swivel and the swivel centered between the top and bottom platens of the loading machine. Because the cubes were cast in forms that had 5 finished steel faces and one open face, the cubes were placed on the swivel with the rougher, open face of the cube oriented parallel to the axis of loading. Cubes were loaded at a rate of between 900 and 1800 N/s. Cylindrical specimens were tested in accordance with the provisions of ASTM C 39 [77] using one of the two testing machines described above and tested at the specified rate of between 13 and 30 N/s.

5.2 Experiments with cements to improve compressive strength of VHSC

5.2.1 Background

VHSC as developed by Neeley and Walley used type V cement because of its low C_3A content. Under the current work to improve the compressive strength of the material, an effort was undertaken to identify which type of cement would work the best. A series of bench-top compressive strength experiments was conducted where only the type of cement was varied and all other materials kept constant. All types of cement were considered for these experiments but preference was given to those that had specifications that met requirements for high silica content and low surface area.

5.2.2 Preferred specifications

The preferred characteristics of a good cement for VHSC are given in Table 5.1. The CaO/SiO₂ ratio less than 3.1 favors a cement with a higher silica content. The requirement for high C₃S favors cements that provide early strength gain. The specification for low C₃A and combined C₃A and C₄AF is to limit the amount of compound that does not add to the C-S-H formation and allow for higher quantities of silicates. The Blaine specific surface is kept small to limit the adsorbed water demand and to keep cement particles large so that some percentage of the grain does not hydrate but remains as clinker. Mill test reports were requested from a number of cement manufacturers. The list of suitable cements found is given in Table 5.2 and the cements selected for study from those submitted are highlighted gray.

Table 5.1 Preferred cement characteristics

CaO/SiO ₂ < 3.1
C ₃ A < 7%
C ₃ S > 55%
C ₃ A + C ₄ AF < 20%
Blaine specific surface 260-350 m ² /Kg

5.2.3 Experimental procedure

Four cements were selected for the study and for each cement mixtures were made at three water-to-cement ratios (0.21, 0.23, and 0.25). Each mixture contained the cement being evaluated; a high-purity, crushed, silica sand from Unimin Corporation with particle sizes ranging between 500 and 150 μm; a low-carbon silica fume from Elkem Corporation; and a poly-naphthalene-sulfonate, sodium-salt HRWRA in liquid form from Handy Chemical Corporation. Mixing and casting were done as outlined in paragraphs 5.1.2 through 5.1.7. Compressive strength cube specimens were made for curing in limewater for 28 days and for receiving heat curing.

Table 5.2 Mill test report summaries for suitable cements

Manufacturer	Plant	Cement type	CaO (%)	SiO ₂ (%)	CaO / SiO ₂ (%)	C ₃ S (%)	C ₂ S (%)	C ₃ A (%)	C ₄ AF (%)	C ₃ A + C ₄ AF	Blaine m ² /kg
Holnam	Ada, OK	V	65.00	22.00	2.95	58.00	20.00	4.00	13.00	17.00	354.10
Holnam	Ada, OK	Class H	64.00	22.00	2.91	58.00	19.00	2.00	12.00	14.00	280.60
Southwestern	Odessa, TX	V	64.30	20.86	3.08	63.40	11.90	0.00	11.93	11.93	222.00
Lafarge Corp.	Canada	Class G	62.50	21.55	2.90	56.70	N/A	1.80	13.00	14.80	328.00
Lafarge Corp.	Joppa, IL	Class H	63.70	21.60	2.95	62.00	15.15	0.20	13.39	13.59	305.00
Kaiser Cement	Cupertino, CA	V	66.05	22.16	2.98	64.50	N/A	3.10	11.80	14.90	339.00
Kaiser Cement	Cupertino, CA	I, II	64.32	21.59	2.98	55.80	N/A	3.10	11.80	14.90	328.00
Kaiser Cement	Cupertino, CA	V low alkali	65.50	22.08	2.97	61.60	N/A	3.50	12.00	15.50	319.00
Lone Star	Sweetwater, TX	II high heat	65.30	23.09	2.83	66.00	N/A	6.00	8.00	14.00	300.00
North Texas	Midlothian, TX	II	N/A	20.87	N/A	63.90	N/A	6.90	N/A	N/A	313.00
Cal Portland	Mojave, CA	Class G	64.76	22.18	2.92	56.00	N/A	4.00	N/A	N/A	324.00

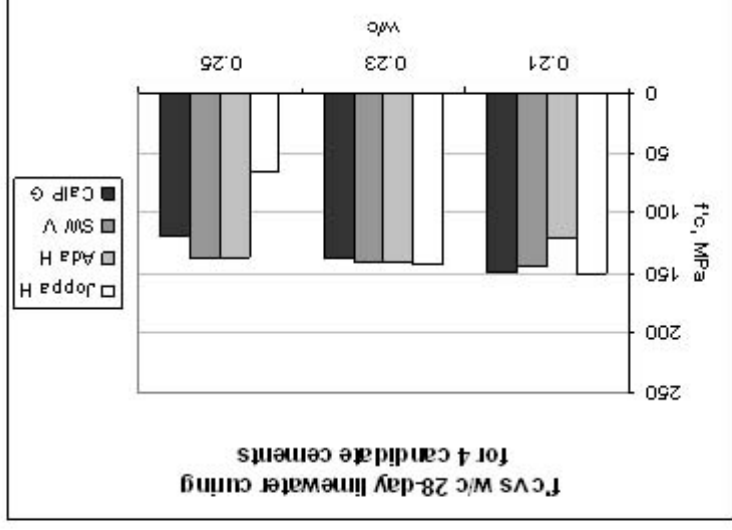


Figure 5.2 Compressive strength for 28-day lime water curing

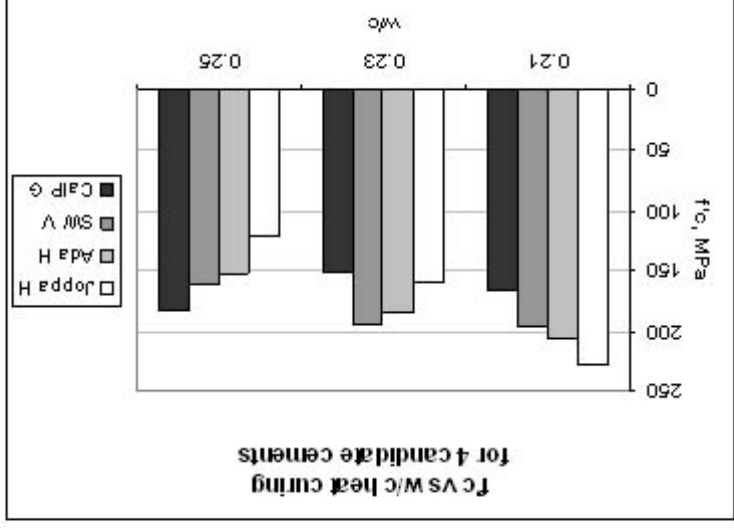


Figure 5.3 Compressive strength for heat curing

5.2.4 Results and discussion

Figures 5.2 and 5.3 show the compressive strength results versus w/c for 28-day limewater curing and heat curing, respectively. For all cements, the strength under heat curing was higher than the counterpart experiment cured in limewater for 28 days, ranging from 110% for California Portland class G oil well cement (CalP G) at 0.23 w/c, to as high as 183% for Lafarge Joppa class H oil well cement (Joppa H) at 0.25 w/c. The strength generally decreases as the w/c increases for both 28-day limewater and heat curing, but the effect was more pronounced for the heat curing experiments. The exceptions to this result were 28-day, limewater-cured, Holnam Ada class H oil well cement (Ada H) and heat cured CalP G. For both limewater cured and heat cured experiments, the Joppa H cement produced the highest compressive strength of the four candidates at 0.21 w/c and the lowest strength at 0.25 w/c.

The flow numbers for these experiments were also recorded. They are shown in Figure 5.4. With the exception of the CalP G cement at 0.21 w/c, all cements had very high flow numbers at all three w/c's. The dotted line at flow number 142 represents the largest flow number measurable. A sample that would have a larger %-increase would flow off the edges of the table. Those bars that have a magnitude of 160 have been artificially set to 160 because a flow number for them could not be measured. These experiments showed that the Lafarge class H oil well cement from the Joppa plant produced the strongest VHSC material and had the highest workability at all w/c studied. The magnitudes of the strengths in the heat-cured group were higher than those in the limewater-cured group and the differences in strength among the four cements were also more pronounced in the heat-cured group. This implies that heat curing

not only increased the strength of the mixtures over ambient-temperature curing, but also affected the strengths of the mixtures differently for different cements.

5.3 Effects of component materials on the strength of VHSC

5.3.1 Background

Concrete can truly be classified as a composite material. It exhibits characteristics of a composite on at least three different levels from the macrostructure to the microstructure. At the macrostructure level, the concrete itself is a composite consisting of coarse aggregate embedded in mortar. The mortar component as well can be classified as a composite material consisting of sand embedded in cement paste. Further following this direction of thought, at the microstructure level the cement paste can be considered a composite consisting of C-S-H, CH, secondary hydration materials, unhydrated clinker, void space, and water. Because of the nature of a composite material, each of its components, in some way or other, affects the material properties the composite exhibits.

VHSC is a composite material with excellent compressive and tensile strength carrying capacity which it derives from the materials and proportions of those materials chosen for its composition. All of the component materials in VHSC have been chosen to enhance the strength of the composite making every effort to eliminate or minimize any component that would have an adverse effect on strength.

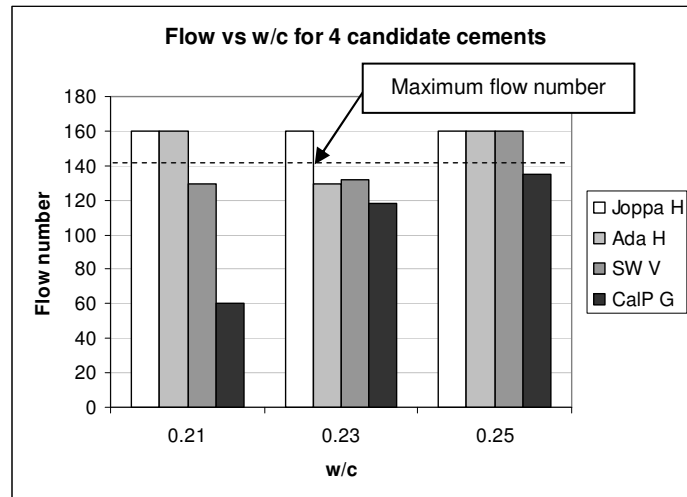


Figure 5.4 Flow numbers for the four cements

5.3.2 Purpose of the experiments

To better understand the contribution made by each component of VHSC, a series of experiments was designed and conducted to show the strength contribution and effect on rheology of each component. This section will describe experiments in which the components of VHSC were systematically added to and subtracted from a baseline cementitious paste, with documentation of the resulting change in strength and rheology.

The components of the VHSC formulation for this series of experiments are given in Table 5.3. The mixtures made for the series of experiments described in this section ranged from a cement-silica fume-HRWRA paste up to a mixture containing the full set of component materials used in VHSC with the addition of wollastonite microfibers. These experiments were performed solely for strength and rheology comparisons, and as such, only the fresh material property of flow and the hardened property of compressive strength from 50.8-mm cubes were collected. Macrofibers, which are normally hooked- end, steel fibers 30 mm long, were not used in the cubes because the potential for non-random orientation of the fibers in the small cubes could affect the strength results. When larger specimens are cast in which the dimensions of the specimens would be large enough to allow the fibers to naturally orient themselves in a random fashion, the steel fibers are included.

Table 5.3 Materials used in the VHSC component study

Component	Comment
Cement	Class H oil-well cement
Sand	River sand
Silica fume	> 95% amorphous SiO ₂
Silica flour	Finely crushed quartz
Microfibers/inclusions	Wollastonite fibers
Macro fibers	Not used in these experiments
HRWRA	Liquid high-range, 45% solids content
Water	w/c used was 0.22

5.3.3 Experimental procedure

Table 5.4 presents the five mixtures produced in this series and the order in which they were made. Components that were always present were cement, silica fume, water and HRWRA. Components that were added to or subtracted from the previous mixture were sand, silica flour, and wollastonite. All mixtures were small mixtures batched as described in paragraphs 5.1.2 through 5.1.7. After mixing was completed the flow number was measured and a set of three 50.8 mm cubes was cast to receive heat curing before testing.

Table 5.4 Order of the mixtures and the component materials in each

Order	Component materials
1 st	C SF HR W
2 nd	C S SF HR W
3 rd	C S SF SFI HR W
4 th	C S SF SFI WOL HR W
5 th	C SF SFI WOL HR W

C=cement, S=sand, SF=silica fume, SFI=silica flour, WOL=wollastonite, HR=high range, W=water

5.3.4 Experimental results

The results of the hardened cube compressive strength tests of the mixtures in this series are presented in Table 5.5 and graphically depicted in Figure 5.5.

Table 5.5 Compressive strength of experiments in component study

Component mixture	Compressive strength, MPa
C SF HR W	162
C S SF HR W	209
C S SF SFI HR W	236
C S SF SFI WOL HR W	267
C SF SFI WOL HR W	156

C=cement, S=sand, SF=silica fume, SFI=silica flour, WOL=wollastonite, HR=high range, W=water

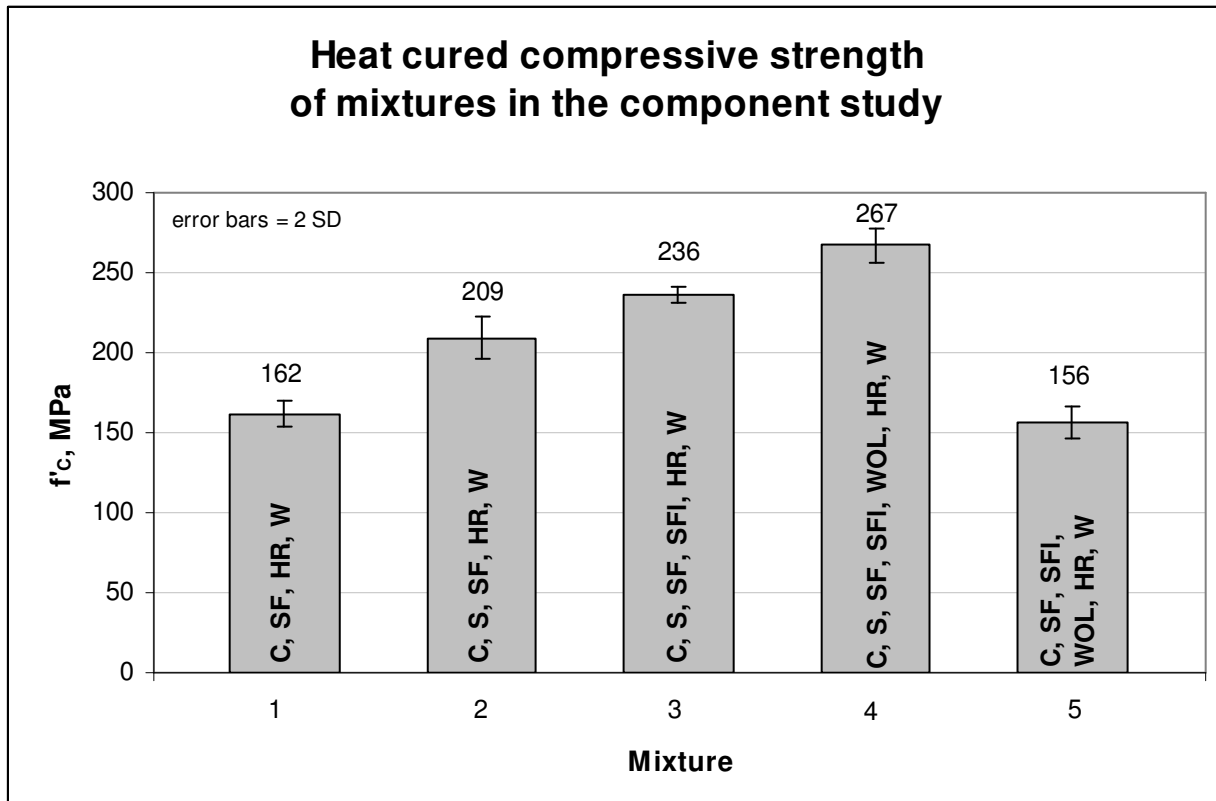


Figure 5.5 Compressive strength results of the five mixtures in the VHSC component study

5.3.4.1 Mixture 1 – cement, silica fume, HRWRA, and water

While the most basic component mixture to study would be just cement and water, the first mixture cast and tested contained cement, water and silica fume with HRWRA to aid rheology. In conventional terms, the strength of this mixture is considerably above the average for high strength concrete and is still among the weakest mixtures in the study. Silica fume and the HRWRA are the only component materials in this mixture that are out of the norm for a standard cement paste. Two traits of the silica fume make it an attractive asset to this mixture: its pozzolanic nature and its small particle size. Silica fume will consume CH and produce a pozzolanic C-S-H as long as CH and water are available. This coupled with the fact that it has such a small particle size compared to a cement grain means that it can fill space that would

otherwise be left as a void or filled with water. This provides for a higher density paste with fewer voids and significantly higher compressive strength than conventional high strength concrete.

5.3.4.2 Mixture 2 – cement, sand, silica fume, HRWRA, and water

Sand was the next component added to the mixture. This increased the compressive strength 29 percent to 209 MPa. The sand used in these experiments was a rounded river sand of maximum diameter approximately 6.4 mm from Prescott, Arkansas. Mineralogically, it is predominantly a chert aggregate. The water-to-solids ratio (w/s) of mixture 1 (**C SF HR W**) was 0.157. The addition of sand in mixture 2 (**C S SF HR W**) decreased w/s to 0.093. The overall effect of this reduction in is to make the mixture stiffer because there is now more solid surface area to wet with the existing volume of water. This, indeed, was the case as revealed in the resulting change of flow number. Mixture 1 had a flow number of 56.8 and the flow number for mixture 2 was 29.2 resulting in a 48.6 percent drop from base.

The presence of the aggregate was primarily responsible for the increased strength of mixture 2; however, the strength increase would not have been as great if the silica fume were not present. The silica fume in the mixture (Figure 5.6) provided an excess of small, pozzolanic particles that fill void spaces between cement grains at the surface of the aggregate, consume CH, and produce extra C-S-H. Silica fume promotes a strong, void-free interface that adheres well to the chert aggregate. The strong bond between the paste and the aggregate brings the strength of the aggregate into the composite increasing the overall strength.

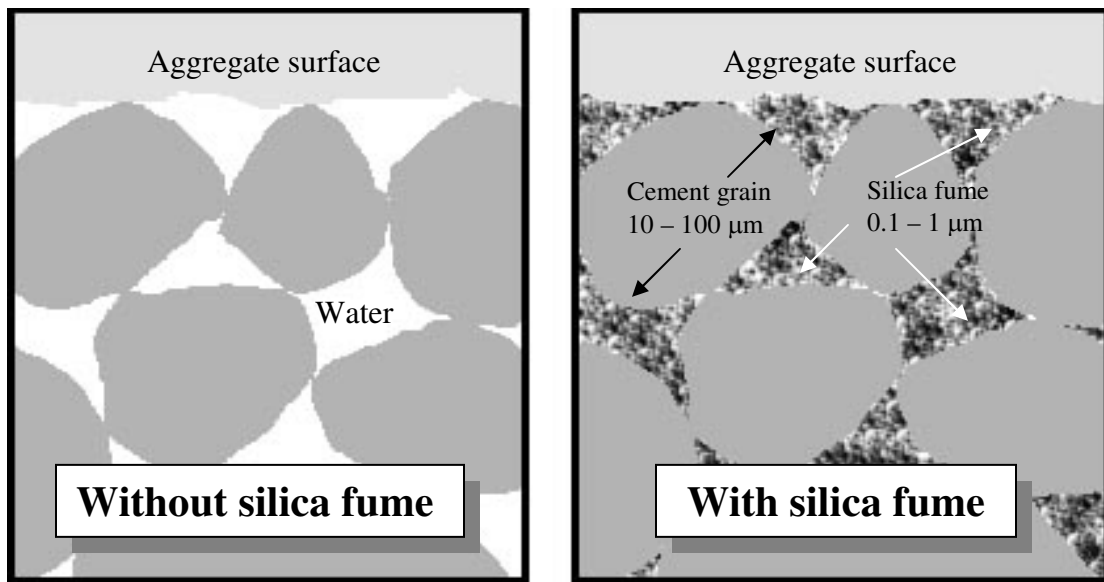


Figure 5.6 Comparison of capillary space in fresh paste with and without silica fume

5.3.4.3 Mixture 3 – cement, sand, silica fume, silica flour, HRWRA, and water

Silica flour was the component added to mixture 2 to produce mixture 3. Silica flour is powdered crystalline silica. In VHSC it is presumed to be an inert filler that acts as an additional aggregate with a particle size greater than silica fume but less than the cement. Its inclusion had the overall effect of raising the strength to 236 MPa (an increase of 46 percent above base and a relative change of 13 percent above mixture 2) and increasing the flow number to 71.5, an increase of 26 percent above base. Because it is another dry powder added to the mixture, it lowered the w/s to 0.083. Being pure quartz and angular in nature, it also bonds well with the cement paste adding another strong aggregate to the composite.

The increase in compressive strength can be attributed to two factors. First, the silica flour itself is stronger than the C-S-H, and with excellent bond between the paste/silica-flour ITZ, the composite would benefit from the extra strength. Secondly, the decrease in the w/s implies a smaller fraction of available water for hydration of the cement. With a smaller volume

of water for hydration, the hydration process will stop sooner leaving a larger core of cement clinker which is stronger than the C-S-H.

The increase in flow number from 29.2 for mixture 2 to 71.5 for mixture 3 is likely due to a lubricating effect from the silica flour and silica fume. While the silica flour is an angular particle, its small size and cuboid shape would allow the individual particles to slide over one another providing the lubricating effect.

5.3.4.4 Mixture 4 – cement, sand, silica fume, silica flour, microfibers, HRWRA, and water

Wollastonite microfibers were the newly added component in mixture 4. This addition had the effect of again raising the compressive strength from 236 MPa in mixture 3 to 267 MPa, (an increase of 65 percent over base and a 13 percent increase relative to mixture 3). This addition lowered the w/s to 0.080 and dropped the flow number to 48.9 (a drop of 14 percent below the base value and down 32 percent relative to 71.5 in mixture 3). While interest in this additive as a reinforcing element in concrete has not been strong, several researchers have reported increases in compressive and flexural strength as well as increases in flexural toughness with use of microfibers. Low and Beaudoin [74] reported increases in flexural strength from 10 to 20 MPa in cement-silica fume beams when the volume percentage of wollastonite microfibers, 25 to 40 μm in diameter and 500 to 600 μm in length, was increased from 0 to 12.5 %. They also found increases in flexural toughness by a factor of 2 in cement-wollastonite composite systems when compared to plain cement matrices [72, 73]. Beaudoin et al. [78] experimented with high-aspect-ratio aragonite microfibers in volume fractions up to 20 % as micro-reinforcement in cement-silica fume paste beams and found mixed results in providing increased ductility and toughness depending upon the fiber loading and distribution of fibers within the paste matrix.

The wollastonite microfibers, shown in Figure 5.7, contribute to the strength and toughness of the matrix by acting as microcrack arresters in much the same way as macro reinforcement acts to arrest macrocracks. In VHSC, as the porosity decreases the strength increases, the matrix becomes more brittle, and its resistance to crack propagation decreases.

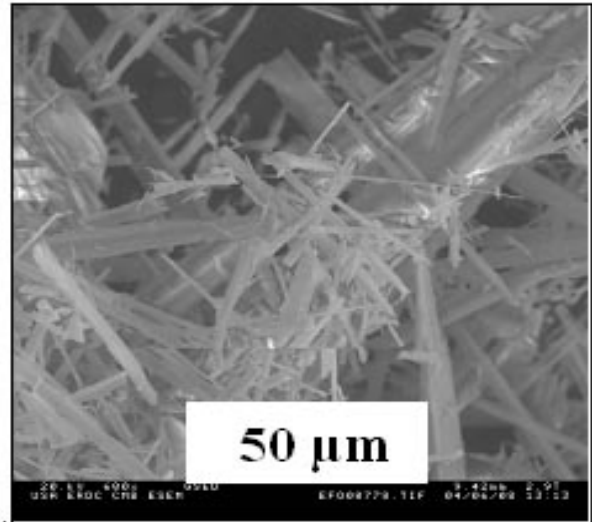


Figure 5.7 Wollastonite fibers

This occurs because of the low w/c, and the action of the silica fume and other micro-particles that fill otherwise water-filled space. The increase in cementitious material and the decrease in void space increase the homogeneity of the matrix and the material begins to behave more like a ceramic material than a conventional concrete. In a homogeneous, high-strength, quasi-brittle material there are few mechanisms for arresting crack growth. Because of this, the materials' fracture properties (energy release rate and fracture resistance) approach conditions where the fracture becomes unstable under an increase in load and cracking will grow in an uncontrolled manner until conditions are again stable.

To increase the resistance to crack propagation, additional crack arresting mechanisms must be employed. One such method used to combat the propagation of macro cracks is the addition of distributed macro fibers to the mixture. In VHSC, 30-mm-long, hooked-ended, steel fibers are the preferred fiber for arresting crack propagation and increasing strength and toughness. These steel fibers are mixed into the fresh concrete and distribute themselves randomly throughout the matrix. When the concrete has hardened and is put under stress, before the concrete cracks, the fibers act mainly to distribute the stresses more evenly within the matrix.

After a major crack has traversed the concrete and its path crosses many fibers, more external work must be done before the faces of the crack can open. The extra energy is needed to break the paste-to-steel bond stresses of any fiber crossing the crack and further frictional energy must be consumed in pulling the fiber from one side of the crack before the crack can open.

The crack arresting mechanism described above for macrocracks is believed to apply where microfibers cross microcracks adding a strengthening and toughening mechanism that works when microcracking begins. Because microcracks occur chiefly during the last quarter of the rising portion of the load-deflection curve, it is expected that any benefit arising from increased resistance to microcrack propagation will manifest itself as increased load and possibly extended deflection in the last quarter of the rising portion of the curve and the first half of the strain-softening portion. This theoretical benefit, conceived in this dissertation, is depicted graphically in Figure 5.8.

5.3.4.5 Mixture 5 – cement, silica fume, silica flour, microfibers, HRWRA, and water

The final mixture in this component study was designed to see the effect of removing the sand from mixture 4 which contained all the other components and, in this investigation, was also the mixture with the highest compressive strength. The results are given in Table 5.5 and Figure 5.5. The removal of the sand caused a drop in the compressive strength to 156 MPa (a drop of 41 percent below mixture 4 and to a level 3 percent below the base strength) and a large increase in the flow from 48.9 for mixture 4 to 90.2 for mixture 5. The strength of mixture 5 is approximately equivalent to that of mixture 1 containing the components cement, silica fume, water, and HRWRA and lower than the strengths in all other mixtures in the component study.

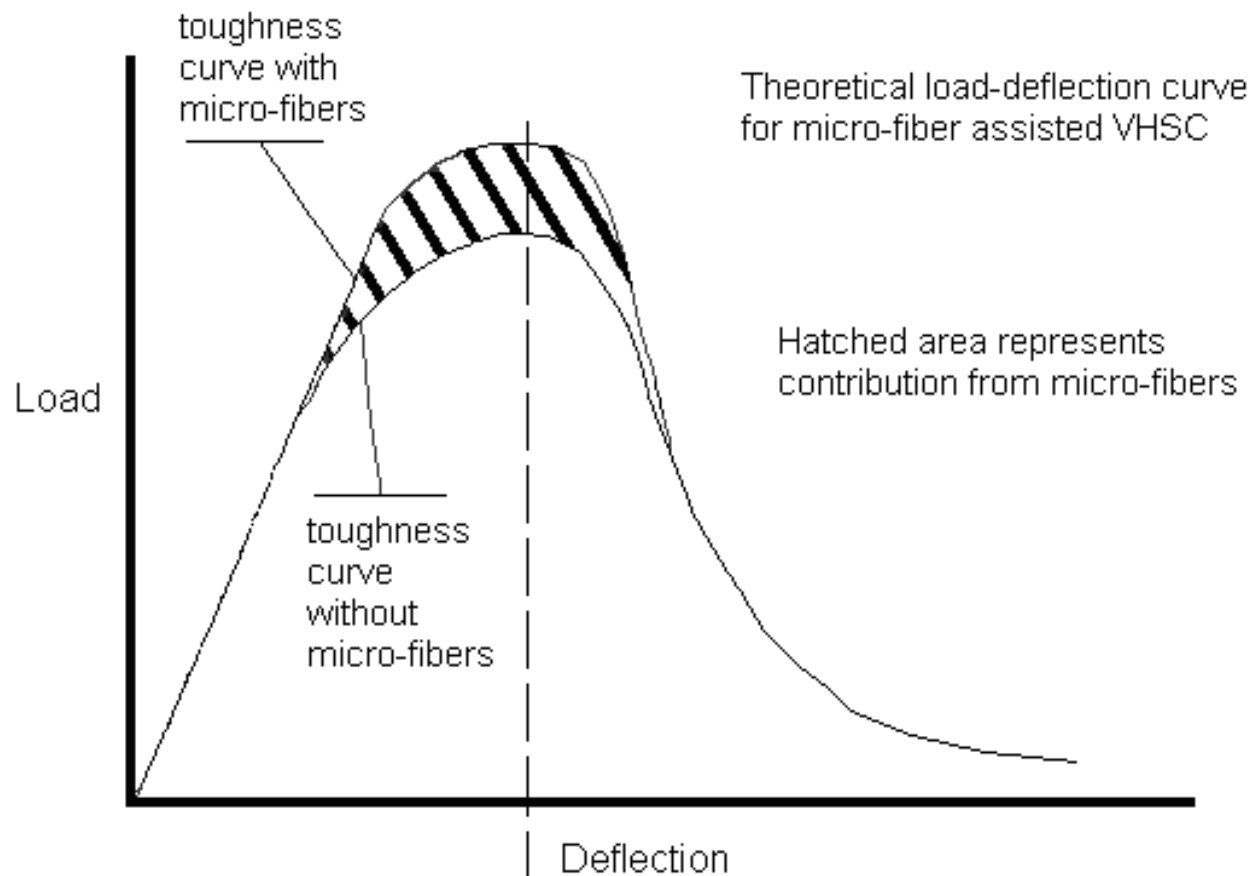


Figure 5.8 Theoretical increase in strength resulting from addition of microfibers.

5.3.5 Discussion

5.3.5.1 Component strength considerations

The effect of adding one component at the time to the mixture containing the minimum cementitious material provides a good means of assessing the contribution of each component to the overall strength and rheological properties of the VHSC. Table 5.6 summarizes the compressive strengths and flow characteristics for each mixture as well as the percent change of the strength and flow number properties from those of the base mixture.

While there is not one component that is responsible for all the changes in strength in the five mixtures, the addition and removal of the sand gave rise to the greatest relative percent

Table 5.6 Percent change in compressive strength and flow in component study

Component mixture	Compressive strength, MPa	Percent change	Flow number – (w/s)	% Change of Flow number
Cementitious only	162	0 (base)	56.8 – (0.157)	0 (base)
Sand added	209	29	29.2 – (0.093)	-48.6
Silica flour added	236	46	71.5 – (0.083)	26
Wollastonite added	267	65	48.9 – (0.080)	-14
Sand removed	156	-3	90.2 – (0.123)	58.8

change in compressive strength (29.4% from base) of all the component materials, followed by the wollastonite and the silica flour in that order. One might not immediately consider the aggregate to be the most beneficial component in the mixture; however, the strength changes reflect this reality. Strength rose 29 percent when sand was added to the components of mixture 1 and dropped to 3 percent below the base for a change of 68 percent below mixture 4 when it was removed. This left the strength after the sand was removed about the same as the base mixture before the sand was first incorporated. This implies that the strength of the aggregate is important to the strength of any mixture provided that the aggregate functions as part of the composite matrix and is not just filler.

On closer study of the component materials and how they interact with one another, it becomes apparent that three component materials interact to cause this large change in compressive strength from 162 to 267 MPa. The aggregate enhanced the change in compressive strength the most, however the cement, silica fume, and water were responsible for providing the dense, strong, low-porosity environment that created the strong bond to the aggregate. Since the bond is strong, the high strength of the chert aggregate contributes to the overall strength of the composite. Without the silica fume the space between cement grains would have been filled with water and CH which only weakens the strength of the matrix. This relationship is particularly important at the paste-aggregate interface where the paste either tenaciously holds onto the

aggregate or forms a weak film that fractures under low stress [17, 64, 79]. Lastly, the cement clinker was integral in increasing the compressive strength of the matrix. In all these mixtures the w/cm was constant and extremely small (0.157). This guaranteed that there was insufficient water to completely hydrate the cement and that self-desiccation would occur at approximately 41 percent of full hydration (refer to Appendix A for calculations) leaving the core of the larger cement grains unhydrated. They then function as a strong aggregate surrounded by a high-density C-S-H shell with perhaps the best possible interface between paste and aggregate, since the high-density C-S-H is diffusion-generated, in place, from the clinker itself.

5.3.5.2 Component rheological considerations

Analyzing the effect of each component material on the rheological property of flow was more difficult. There was no clear trend in the direction of the flow number in relation to the decrease in the w/s . Rather than being a phenomenon related to the w/s , it appears to be more related to the type and shape of material being added or removed. When the sand was added to mixture 1 there was a large drop in flow (48.6 % below that of mixture 1), and when it was removed from mixture 4 there was a large increase in the flow, 58.8 % relative to mixture 4. This large a change in the rheology in both instances would be expected if the sand was a crushed aggregate; however, since it was a rounded sand the particle size distribution of the aggregate must be such that the particles pack in a way that resists flow. Additionally, the sand is a large volumetric component of VHSC and has a considerable demand on the available water in the matrix, further affecting the rheology of the matrix.

The addition of silica flour increased the overall flow of the material. Although silica flour is a crushed aggregate, its particle shape is mostly cuboid, with an aspect ratio ranging from 1.4 to 4 [80]. This shape is closer to that of a sphere or cube, which would encourage flow, than

to that of a needle-like particle which would hamper flow characteristics. The silica flour particle is so small and present in such a relatively small volume that it does not behave in an interlocking manner. Addition of silica flour to mixture 2 raised the flow number 26 percent over the base mixture. By contrast, the wollastonite fibers added in mixture 4 decreased the flow by 14 percent in relation to the baseline flow. Referring to figure 5.7, the wollastonite particles are acicular and would interlock in a manner that would resist flow.

5.4 Experiments with HRWRAs to improve the strength of VHSC

5.4.1 Background

High-range, water-reducing, admixtures can serve two roles when added to a concrete mixture. If used as a fluidifier, they allow for greater slump or workability of the mixture without adding additional water. This does not improve the strength but does improve the ease of placement of the mixture. If used as a water reducer, they allow the amount of water in a mixture to be reduced while maintaining the same slump or workability. The lower amount of water thus reduces the w/c and improves the strength. This latter approach was employed in developing the strength of VHSC.

Without addition of HRWRAs, the minimum acceptable w/c in a mixture containing cement, sand, silica fume, silica flour, and water was approximately 0.4 to 0.42. Workability of mixtures with a lower w/c was unacceptable and strength at a w/c of 0.4 or more was often around 100 MPa. Improvements in strength of early formulations of VHSC clearly necessitated experimenting with available HRWRAs to allow reduction in the w/c. When HRWRAs were included in the mixture, acceptable workability could be achieved at w/c's between 0.18 and 0.23. At the time, the state-of-the-art HRWRAs were either ligno-sulfonate based, or one of the

synthetic poly-naphthalene-formaldehyde sulfonate (NFS) or poly-melamine-formaldehyde sulfonate (MFS) based chemicals.

Example strength results from early HRWRA/strength experiments are given in Figure 5.9 to provide background for current work. In that work, all mixtures were cast and cured as described in paragraphs 5.1.2 through 5.1.7. Cement was Lafarge class H oil well from the Joppa plant, sand was Granusil 4030 from Unimin Corporation, and silica fume was E960 from Elkem Corporation. All mixtures were cast at a 0.2 w/c, contained HRWRAs at a solids content of 1.89% mass of cement, and were limewater cured for 28 days before testing. The three HRWRAs were described as follows: Durasar™ was a calcium salt of naphthalene sulfonate polymerized with formaldehyde (Ca NFS), Meladyne™ was a sodium salt of melamine sulfonate polymerized with formaldehyde (Na MFS), and both Disal™ products were sodium salts of naphthalene sulfonate polymerized with formaldehyde (Na NFS). All HRWRAs were from

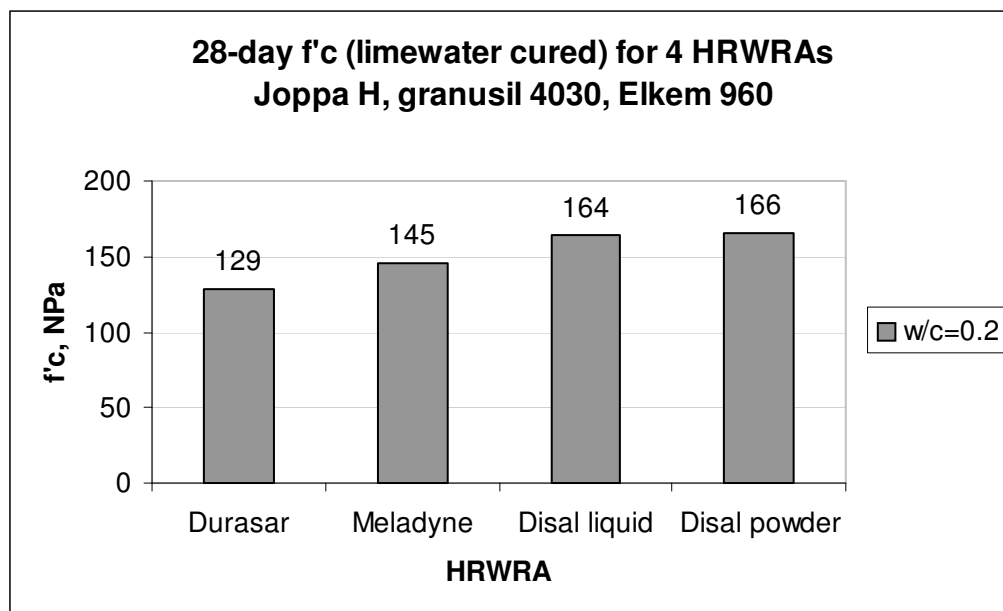


Figure 5.9 Compressive strength versus type of HRWRA

Handy Chemical Corporation. As seen in figure 5.9, the most efficient HRWRAs in terms of deflocculating the cement and producing the highest compressive strength were the Na NFS chemicals regardless of their powder or liquid form.

The current work involves rheology and strength development experiments using the most recent generation of HRWRAs, those commonly referred to as polycarboxylate or comb-type HRWRAs. This class of HRWRA differs from the conventional MFS and NFS HRWRAs because they have a lower content of ionic groups in their main chain and the presence of carboxylate and ether side chains [81, 82]. They are often referred to as comb-type HRWRAs because the side-chain groups are arranged off the main chain like the teeth of a comb. Their mechanism of action is both similar and dissimilar to the MFS and NFS HRWRAs. Like the MFS and NFS HRWRAs, they disperse the large agglomerates of cement particles in the fresh paste by the action of electrostatic repulsion of ionic groups adsorbed on the surface of the cement particles. The carboxylate side groups are said to be instrumental in the adsorption of the admixture to the cement [83, 84]. However, because of their lower content of ionic groups they are less efficient in this action than the MFS and NFS HRWRAs. They differ from the MFS and NFS HRWRAs in that the long, ether side chains produce a type of steric hindrance when the HRWRA is adsorbed onto the cement particles. Because the ether side chains are very long they are more efficient in separating the cement grains than the MFS and NFS HRWRAs [81].

5.4.2 Experimental procedure

Prior to conducting bench-top experiments on the strength properties derived from the polycarboxylate HRWRAs, a series of experiments was conducted using these HRWRAs. A range of dosages covering the mid to upper range recommended by the manufacturer was used

then dosages extended beyond manufacturer's recommended range to determine the range of useful rheological properties available with the baseline formulation of VHSC.

Four polycarboxylate HRWRAs were studied in the current VHSC development program, two from BASF Corporation (then Master Builders) and two from Grace Chemical Corporation. The BASF products were PS-1446 (a then internal Master Builders' product identifier) and Glenium 3030 NS™. The Grace products were ADVA 170™, and ADVA Cast 500™.

PS-1446 had a manufacturer-recommended dosage range of from 1.3 to 7.8 ml/kg. For this product dosages ranging from 3.47 to 24.27 ml/kg were tested. The Glenium 3030 NS™ HRWRA had a recommended range of dosages from 1.95 to 11.7 ml/kg. Here, dosages in the range of 5.2 to 35.52 ml/kg were tested. The ADVA 170™ recommended dosage range was 1.95 to 6.56 ml/kg and dosages ranging from 5.06 to 18.73 ml/kg were tested. The ADVA Cast 500™ recommended range was 1.95 to 8.77 ml/kg and actual dosages in the range of 5.30 to 26.47 ml/kg were used.

For the rheology experiments, mixtures were proportioned as given in Table 5.7 and mixed as described in paragraphs 5.1.2 through 5.1.7. The first mixture was made using the low-end of the HRWRA dosage range and flow number and time-to-paste (TTP) data were collected if the mixture turned to a paste before 30 minutes of mixing. Additional mixtures were made by increasing the dosage by an amount between 1.68 and 4.32 ml/kg until the high-end dose was reached.

Table 5.7 Proportions for strength and rheology experiments with polycarboxylate HRWRAs

Component	Mass, g
Cement	1123.78
Sand	1087.20
Silica flour	311.08
Silica fume	437.11
HRWRA	Varies by experiment
Water	Varies to make w/c = 0.22
Distributed macro fibers	None

Once the rheology experiments were complete, a subset of the rheology mixtures was re-cast for strength evaluation. The mixtures were made at the extremes of the useful range of the rheology experiments. The first mixture was made at the lowest dosage for which the rheology mixtures formed into a paste and a second mixture was made at the highest dose of the rheology experiments. These mixtures were also proportioned as Table 5.7. Each of the HRWRAs was a liquid based material so the mass of water in each of the experiments was based on the water in the HRWRA dosage and the additional mixing water necessary to make the 0.22 w/c. Compressive strength cube specimens were made for 28-day limewater curing and for heat curing.

5.4.3 Results

Figure 5.10 a-d presents the results of the flow number and time-to-paste experiments for the full range of dosages for the four polycarboxylate HRWRAs studied under the rheology developmental work. Table 5.8 presents the results of the fresh and hardened properties of the mixtures made for strength using the four polycarboxylate HRWRAs.

5.4.4 Discussion

5.4.4.1 Rheology Experiments

From the four bar charts presented in Figure 5.10 it can be seen that none of the four HRWRAs were effective at producing a mixture that formed to a paste at any dosage within the

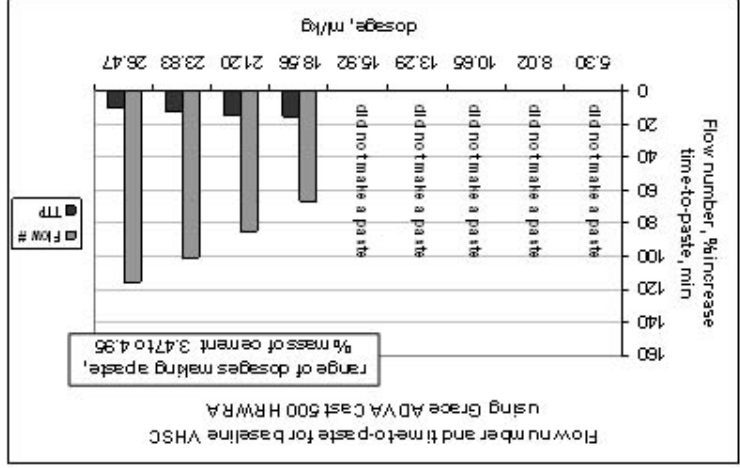
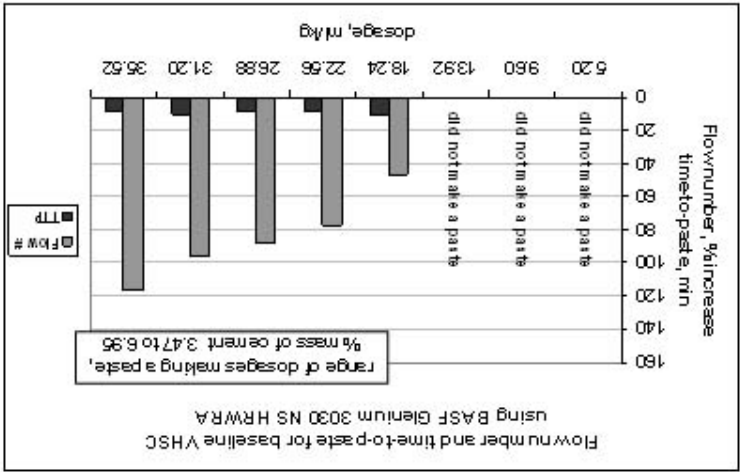
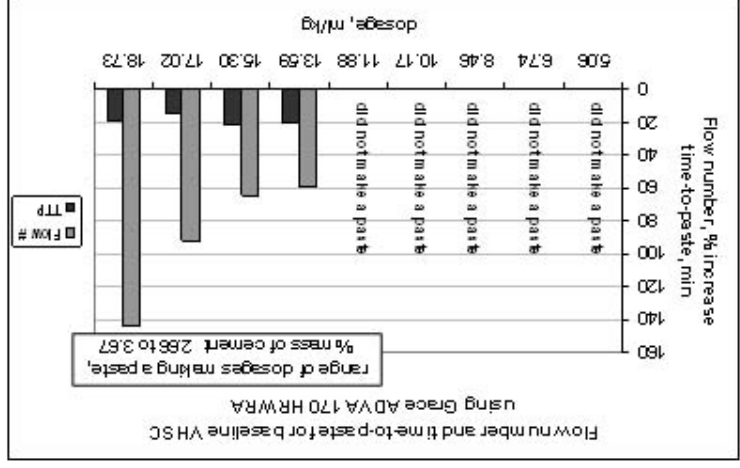
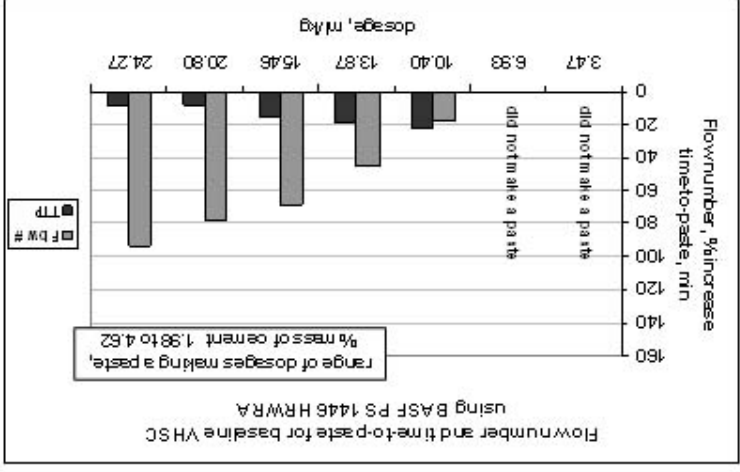


Figure 5.10 Results of flow number and time-to-paste (TTP) experiments for baseline VHSC with four polycarboxylate HRWRA

Table 5.8 Strength results of baseline VHSC for four HRWRAs at high and low dosages

HRWRA	Dosage, ml/kg	Time to paste, min:sec	Flow number	f'c 28-d limewater, MPa	f'c heat cured, MPa
PS-1446 (low)	10.40	10:00	29.8	123.7	176.1
PS-1446 (high)	24.27	4:00	102.8	149.8	133.7
Glenium 3030 NS™ (low)	18.24	8:30	56.0	179.3	242.3
Glenium 3030 NS™ (high)	35.52	6:00	128.9	143.2	225.9
ADVA 170™ (low)	13.59	7:45	61.8	177.5	210.1
ADVA 170™ (high)	18.73	6:30	122.1	165.2	246.7
ADVA Cast 500™ (low)	18.56	5:30	61.0	136.4	239.6
ADVA Cast 500™ (high)	26.47	5:00	112.2	149.2	210.7

manufacturers recommended dosage range. The concrete mixtures for which chemical companies design HRWRA dosages are significantly different from mixtures such as VHSC.

Table 5.9 compares the proportions of VHSC and an HSC used for high strength column tests [85]. For equal masses of cement and HRWRA, the VHSC contains 6.5 times the mass of silica fume, silica flour that is 28% of the mass of the cement where the HSC contains none, and a w/c that is 66.7% that of the HSC. The sand content has a surface area that is 400% greater than the HSC even though the mass of sand is only 25% of the mass of sand in the HSC (based on average particle diameters of 3.2 mm for the VHSC and 4.75 mm for the HSC). The obvious difference is that the VHSC has a significantly larger combined surface area of dry ingredients and smaller water content than the HSC. Thus, even though the low-end dosages of the HRWRAs are within manufacturers recommendations, the high surface area and low water content of the VHSC prevent the admixtures from fluidifying the powders. For all four HRWRAs, all the mixtures that turned to paste were at dosages that would be considered overdoses for more conventional concretes. For comparison, the range of dosages that formed a paste for the four HRWRAs are given in the graphs of Figure 5.10.

Table 5.9 Comparative proportions of VHSC and a HSC based on mass of cement [85]

Mixture	Cement	Aggregate	Silica fume	Silica flour	Water	HRWRA
VHSC	1	0.97	0.39	0.28	0.22	0.03
HSC	1	3.99	0.06	0	0.32	0.03

The HRWRA that caused a paste to form at the lowest dosage was the PS-1446 (Figure 5.10a). At 10.4 ml/kg it fluidified the mixture at a dosage 34% lower than the ADVA 170™ and 75% and 78% lower than either the Glenium 3030 NS™ or the ADVA Cast 500™, respectively. However its fluidifying effect at the high-end dosage was the smallest at a flow number of 93.5 compared to 115.8, 116.5, and 143.9 for ADVA Cast 500™, Glenium 3030 NS™, and ADVA 170™, respectively. From this point of cost and efficiency, the ADVA 170™ is the best source of HRWRA for use with VHSC.

Much of the literature written about the effects of the polycarboxylate class of HRWRAs focuses on the time of addition of the chemical to the rest of the cement mixture [81-83, 86]. When added with the mix water at the initial wetting, much of the HRWRA is adsorbed onto the C₃A/gypsum reactants and the product ettringite since these are the first compounds to react. This leaves less of the chemical available for adsorption onto the silicates and renders the dosage less efficient. If addition of the HRWRA is delayed for 5 to 10 minutes after initial addition of the mix water, the adsorption will be greater on the silicates and will be more efficient in fluidifying the paste.

This technique was not used in developing VHSC because at the time this research knowledge was not available. All liquids, including the water in the HRWRA, were added at the time of adding the initial mix water because of the extremely small amount of water employed and the very high volume of very-small particles in the mixture. Adding only part of the water to

the dry materials initially would only dampen the powders and severely prolong the time it took for the dry materials to make into a paste.

The TTP for all HRWRAs was less than 22 minutes and decreased as the dosage increased. The time it takes for VHSC to change from wetted powder to a fully mixed paste, and the stages it goes through in making this transition is in itself a fascinating process and one that is highly different from the normal procedure of making concrete. For the reader interested in the details of this transition, it is available as Appendix B to this dissertation.

5.4.4.2 Strength experiments

The low dosage for each of the HRWRAs in Table 5.8 was the lowest dosage that allowed the dry components of the mixture to form to a paste at a w/c of 0.22. The efficiency of the HRWRAs as described in the manufacturer's brochures was such that it would allow a 40% reduction in the amount of water necessary to make a workable mixture. As previously discussed, these recommended dosage rates are for more conventional HPC mixtures with proportions different from those described in Table 5.7. It is not surprising to find that the manufacturer's recommended range of dosages is insufficient to allow VHSC to form to a paste. If one assumes 0.4 as a w/c that will produce a workable mixture without HRWRAs then a w/c 40% lower than that would be 0.26 which is still greater than the 0.22 w/c used with VHSC. The mixtures made from the high-end dosage given in Table 5.8 are actually dosages higher than the manufacturer's recommendation by as much as 23.8 ml/kg. Where this would normally be an overdose according to the constraints of more conventional HPC, in the case of VHSC it produced mixtures with good flow and strength properties that set without retardation.

Strength data for 28-day limewater cured mixtures will be discussed first and data for heat cured mixtures will be discussed in the next section. In comparison to the limewater cured

mixtures made at a w/c of 0.20 using the MFS and NFS HRWRAs (presented in Figure 5.9), the strengths of the limewater cured mixtures made with the polycarboxylate HRWRAs are as strong as or stronger than those mixtures even at a higher w/c of 0.22 indicating the more efficient nature of the polycarboxylate admixtures. The strengths from the PS 1446 HRWRA were the lowest of the four; however, the strength of the 28-day limewater cured mixtures does not vary significantly from the low end of the useful dosage range to the highest dosage tested in all experiments. This observation has been seen in a number of studies where the w/c of a mixture has been held constant and the dosage of HRWRA varied from a low dose to a high one [82, 87]. This is not surprising because the w/cm is the same in both the low and high dosage mixtures; and in theory at least, the HRWRA is not supposed to have a major effect on strength.

In two out of four of the HRWRAs, the strength at the lower dose is slightly higher than the strength at the higher dose. While both the low and high dosage were above manufacturer's recommended dosages, the low-dosage mixtures took a longer time to turn to a paste and when they did convert, they were stiff (their flow numbers were < 62), and they required external vibration to get the paste to flow into the molds. At the other extreme, the high-dosage mixtures had high flow numbers (> 102) and were near self-leveling in rheological properties. While these strength differences are small, it is possible that the strengths are just a function of the spread in the individual breaks that make up the average. It was observed that the stiffer, low-dose mixtures presented less of an opportunity for air to be entrapped during mixing, because of their sticky thixotropic nature; whereas the thinner mixtures could entrap air bubbles much more easily because the mixing paddle had less resistance when moving through the paste. More air bubbles were removed by external vibration from the high-dose mixtures than the low-dose mixtures.

Similar results in strength difference between low and high dosages were found for the heat cured mixtures as well. They were all within 36 MPa of each other regardless of the magnitude of the dosage of HRWRA they received.

5.5 Effects of ambient temperature water curing to improve the strength of VHSC

5.5.1 Background

The experimental data presented in Table 5.8 illustrate the strength differences typically observed when specimens from a given mixture of VHSC are cured in limewater at ambient temperatures and using the heat treating methods. Strengths were increased by 34 to 75% (with the exception of the PS-1446 mixture at high dosage) when heat treating was used.

The 7-4-2 heat treating method described in paragraph 5.1.5 was taken from published literature coming from RPC research [43]. For most of the early development of VHSC it was presumed that because the curing technique had been published it was a necessary step to achieve the extra strength. It wasn't until O'Neil and co-workers began to study the material that experiments were conducted to study the effect of the heat treating method.

The majority of techniques used to accelerate the strength development of concrete generally start within the first 24 hours of casting. They include autoclaving and steam curing. After the concrete is cast, the heat is applied as soon as it is feasible to remove it from the forms. The cement paste has only a small number of hours to develop under conventional conditions before the accelerating curing begins. VHSC, on the other hand, typically allows seven days of moist curing at ambient temperatures before heat is applied. This allows for greater development of the microstructure and production of more C-S-H before thermally induced change is affected. The basic postulate for the ambient temperature water curing experiments was to find if it is

optimal to wait for seven days before start of heat treatment. Six identical experiments were conducted to find the effect of the 7-day ambient curing portion of the heat curing technique.

5.5.2 Experimental procedure

Six bench top mixtures were made with the proportions in Table 5.10. They each received six different ambient water curing times: 1, 3, 7, 14, 21, and 28 days, followed by four days in a 90 °C water bath and further cured for two days in a 90 °C oven. The seven-day mixture was considered the baseline and all others were compared to it. Compressive strength cubes were cast as discussed in paragraphs 5.1.2 through 5.1.7.

Table 5.10 Mixture proportions for the length of ambient temperature curing experiment

	Cement	Sand	Silica flour	Silica fume	HRWRA*	Water
Relative mass	1	0.97	0.28	0.39	0.03	0.22
Actual mass, g	1123.8	1090.1	314.7	438.3	33.7	247.2

*HRWRA was Disal™ powder

5.5.3 Results

Figure 5.11 shows the results of the compressive strength tests after the variable ambient strength curing and 4 days 90 °C water and 2 days 90 °C air. Two data points are shown at 21-days ambient water curing. The lower point includes all three data points (201.7, 157.5, and 83.7 MPa) while the upper point has been averaged on the upper two data points.

5.5.4 Discussion

The results of the length of ambient water curing before exposure to high temperature experiments show that it is not necessary to cure specimens for seven days to receive full benefit. Data points at 3, 7, 14, and 28 days are nearly all of the same magnitude. The data points at 1 and 21 days bear some explanation. At 1 day, the three breaks were all closely clustered (160.1, 177.0, and 197.9 MPa). Their average, 178.0 MPa, is 12.5% lower than the average of the data points for 3-, 7-, 14-, and 28-days strength and is explainable from the standpoint of immature

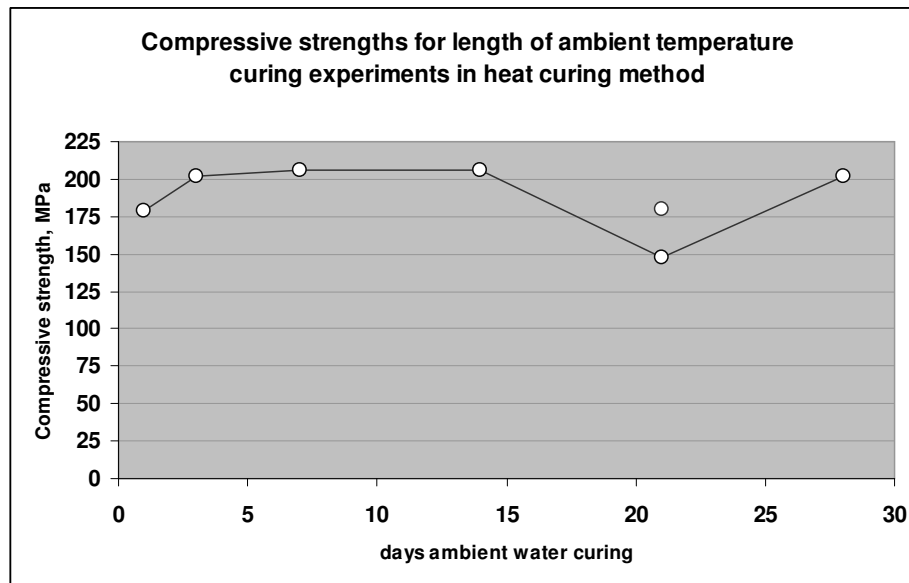


Figure 5.11 Compressive strength results for ambient temperature curing experiments

development of C-S-H. The data at 21 days are harder to explain. One would expect that if there was no significant strength change between the ages of 3, 7, and 14 days and that again at 28 days the strength was very close to the earlier-age strengths, that the data at 21-days age would also be close. The fact that they do not indicates a problem with the data at that age. Though the three data points are widely spread (201.74, 157.47, and 83.68 MPa), simple statistical practices for dealing with outliers [88] did not permit rejection of the lowest data point^{II}. In Figure 5.11, the upper data point at 21-days age is the average of the top two cube breaks. Even that average

^{II} The spread between three compressive strength cube breaks in VHSC is often wide, more so than the differences between high and low breaks for conventional concrete. This most likely is a function of the quasi-brittle nature of the material, microcracks in the paste structure, and the lack of sufficient crack arrest mechanisms to keep the change in fracture resistance greater than the change in the energy release rate of the material. Abnormalities such as entrapped air voids in the mortar, inhomogeneous distribution of aggregate in the paste, cube geometry that leaves loading faces non-parallel, stress concentration points on the surface of the specimen, or even small pieces of debris between the specimen and the loading head of the test machine can cause a break significantly below others.

Simple statistical practices for dealing with outliers such as the one-sided T test described in ASTM E 178-02 rely on large populations of data from which samples may be drawn and the use of a standard Gaussian probability curve to generate critical values of T to compare against calculated T values. In a large population of VHSC breaks, the majority of data will fall to the high side of the distribution with a smaller percentage breaking on the low side producing a skewed distribution. With the small numbers of sample observations used in the VHSC research, and the lack of a large population of data to generate a skewed distribution, it is highly difficult to meet the requirements to reject a datum point. For these reasons data points that appear suspicious and do not meet the rejection criteria of the one-sided T test will be reported as part of the data but may be noted in the discussion.

is low compared to the 3-, 7-, 14-, and 28-day data. While it is possible that there is a logical explanation for the low strength it is believed to be a result of two bad breaks in one experiment.

From these data it can be said that even at 1-day ambient temperature curing before applying heat treatment that the strength achieved is high, but still not sufficient to develop the full potential of the heat curing. The strength development at 3-day ambient temperature curing is statistically no different from those at 7-day ambient curing or longer and from a standpoint of efficiency could be substituted for the 7-day ambient temperature water curing without significant loss of strength.

5.6 Experiments with micro-inclusions to increase strength

5.6.1 Microfibers

5.6.1.1 Background

Inclusions in a concrete mixture can be an asset to the rheology, strength, and toughness properties of the material. The use of distributed steel fibers in the mixture to increase strength and toughness is one excellent example while the choice of a strong aggregate is another. These additions, on the macro scale, have been beneficial choices for many years. Only recently have researchers considered enhancing material properties through the use of micro-inclusions. Increases in flexural strength and toughness of cementitious mixtures containing some form of microfibers are the most prevalent in the literature.

In the early 1990's, Low and Beaudoin published a body of work on flexural strength and toughness of portland-cement-based binders reinforced with wollastonite fibers [72-74, 90]. They reported increases in flexural strength of up to 145% as a result of incorporating increasing volumes of wollastonite microfibers in their base mixtures. Their findings indicated that optimum results were obtained with additions of microfibers at 11.5% by volume. Beaudoin

et al. [78] studied portland-cement pastes reinforced with 3 - 20 volume % of aragonite microfibers and found similar increases in flexural strength. Banthia and Sheng [91] studied the flexural strength and toughness of cement/silica fume mixtures reinforced with carbon, steel, and polypropylene microfibers. They reported that with increasing volumes of microfibers (1 – 3% by volume), both increases in load-carrying capacity and deformability were observed when carbon fibers were used. Steel microfibers led to increases in strength of the matrix but toughness improvements were not realized. For polypropylene microfibers, no increase in strength was recorded but there was improvement of post-peak load carrying capacity (toughness). None of these studies reported on microfiber improvements in the compressive strength.

5.6.1.2 Microfiber experimental procedures

A series of basic VHSC mixtures using the 4 polycarboxylate HRWRAs described in section 5.4.2 and containing wollastonite microfibers was studied to compare the effect of the microfibers on the compressive strength of the mixtures against the strength of companion mixtures without the fibers. The mixtures followed the proportions presented in Table 5.10 with the exceptions that the Disal™ HRWRA was replaced by each of the polycarboxylate HRWRAs, and that each mixture contained the wollastonite microfibers. The wollastonite microfibers are a naturally occurring mineral fiber (Figure 5.7), acicular in nature, with diameter ranging from 5 to 15 μm and aspect ratio ranging from 5 to 20. Their chemical composition is given in Table 5.11. The fibers were introduced as an addition to the mixtures at a mass ratio of 11% of the mass of the cement. Mixtures were made according to the procedures outlined in paragraphs 5.1.2 through 5.1.7 and compressive strength cube specimens were made for 7-day, 28-day, and heat-cured testing. The mixtures were compared to companion mixtures used to study the effect of HRWRAs on strength described in section 5.4 of this chapter.

Table 5.11 Wollastonite chemical composition

Component	Weight %
CaO	46.70
SiO ₂	52.20
Fe ₂ O ₃	0.15
Al ₂ O ₃	0.25
MgO	0.20
Loss on Ignition	0.50

5.6.1.3 Results

The results of the microfiber inclusion studies are presented in Table 5.12. These results are presented for three curing conditions and four HRWRAs and are compared to similar experiments that did not include any microfibers.

Table 5.12 Effect on compressive strength of VHSC from addition of microfibers

HRWRA	Dose, ml/kg	Containing microfibers	Compressive strength, MPa		
			7-day	28-day	Heat cured
PS-1446	24.3	no	124.3	149.8	133.7
	25.2	yes	135.4	147.0	227.2
Glenium 3030 NSTM	18.2	no	122.2	179.3	242.4
	23.4	yes	153.8	153.8	267.0
ADVA 170TM	18.7	no	138.3	165.2	246.7
	19.4	yes	147.6	165.0	245.1
ADVA Cast 500TM	26.5	no	135.3	149.2	210.8
	27.5	yes	149.0	103.5	249.1

5.6.1.4 Discussion

In general, the addition of the wollastonite microfibers increased the compressive strength of the VHSC at the 7-day age and under heat treating. At the 28-day age the strength of the mixtures containing wollastonite were the same as the mixtures not containing microfibers under two of the HRWRAs and slightly lower with the other two. The increases in strength attributable to the wollastonite microfibers under either ambient or heat curing treatments were not significantly large. The exception to this result is the increase shown for the heat-cured PS-

1446 HRWRA mixtures. The data for the heat-cured specimens not containing any microfibers in this comparison are suspect since their strength is smaller than the average for the 28-day strengths. The heat-cured strength for the mixture with the microfibers is in line with the rest of the heat-cured mixtures.

The explanation for the increase in strength is not completely clear from these data. If the microfibers were acting as microcrack arresters as was discussed in paragraph 5.3.4.4, then there should be evidence of microfiber pull-out in scanning electron microscope (SEM) photomicrographs of the fractured surfaces. During the investigation, SEM attempts to view individual wollastonite fibers in fractured surface images of heat-cured VHSC specimens proved unsuccessful. No fibers were observed despite the inclusion of microfibers in the mixture at 11% by mass of cement. Low and Beaudoin [90] studied the long-term stability of cement-based binders reinforced with wollastonite microfibers cured in limewater at ambient temperatures and found microfibers in the SEM photomicrographs at 28-day and 350-day ages. Either all the microfibers fractured at the crack face because the fiber/paste interfacial bond was very high thus leaving no visual evidence of fibers, or some chemical phenomenon caused the microfibers to dissolve during the hydration and heat curing process.

Because the wollastonite fibers are composed of CaO and SiO_2 it is possible that the fibers acted as additional calcium-silicate material that was converted into C-S-H during hydration, particularly in the heat-treated specimens. If this was the case, the small increase in strength could be linked to additional C-S-H produced from the fibers. If, on the other hand, the microfibers are there but not visible on the fractured surface because they broke rather than pulled out of the matrix, there would be a small strength increase from the extra energy required

to break the microfibers in tension to allow the microcrack to open. In either case the microfibers worked to increase the compressive strength of the mixture.

5.6.2 Microspheres

5.6.2.1 Background

The class of materials that is labeled micro-inclusions contains more than just microfibers. In truth, any micro-sized particle that can be incorporated into cement paste qualifies as a micro-inclusion. The ERDC research team chose to examine microspheres as an inclusion to strengthen VHSC. A number of companies manufacture materials that can be classified as microspheres. These materials range in size from 0.1 to 500 μm in diameter, can be solid or hollow core, thin or thick walled, and made of any material compatible with the chemistry of portland cement. As a first trial, a series of experiments to replace the sand component of VHSC with hollow, thin-walled, lightweight microspheres was tried. The sand component of a basic VHSC mixture was replaced with these microspheres in proportions similar in mass and particle size gradation. The compressive strength results of this series were very disappointing. Even with heat curing the highest strength produced was less than 110 MPa. Replacing the strong chert aggregate with a much weaker material removed the contribution of the hard aggregate from the strength of the composite. Subsequent experiments were conducted with stronger microspheres as an addition rather than a replacement to the basic VHSC mixture. Two varieties of high strength microspheres were obtained from 3M Corporation for the next series of experiments.

5.6.2.2 Microsphere experimental procedures

The basic VHSC mixture described in Table A3 of Appendix A was used as the control for the series of experiments. Two varieties of 3M Zeospheres™, G-800 and G-200, were used

as microsphere inclusions. These materials are hollow, thick walled, high-strength, gray ceramic microspheres of silica-alumina ceramic composition. They are typically used in coating formulations to reduce volatile organic compound levels, increase filler loadings, improve hardness, and add abrasion resistance [92]. Their physical properties are given in Table 5.13.

Table 5.2 Physical properties of 3M Zeospheres™ [92]

Properties common to both G-200 and G-800 Zeospheres™		
Crushing strength, MPa	>413	
Hardness, Mohs scale	7	
Softening point, °C	1,020	
Individual material properties	G-200 Zeospheres™	G-800 Zeospheres™
True density, g/cm ³	2.5	2.2
Particle size, μm - 95% passing	12	200
Particle size, μm - 90% passing	9	75
Particle size, μm - 50% passing	4	18
Particle size, μm - 10% passing	1	2
Surface area, m ² /cm ³	6	3

The first series of mixtures was made using the G-800 microspheres. Small bench-top mixtures were made as described in paragraphs 5.1.2 through 5.1.7. G-800 microspheres were added in increments of 1.5% by mass of mortar, from no microspheres through 12%. For each mixture, three compressive-strength cube specimens were made and cured using the heat curing method.

The question arose as to whether the microspheres might behave in a pozzolanic manner or whether they would act as inert filler. A lime-pozzolan test was performed to determine the reactivity of the microspheres. In a lime-pozzolan test, lime, water, and the material being tested for pozzolanic activity are mixed, cast, and heat cured for 7 days. The specimens are then compression tested to determine the level of strength resulting from the mixture. If there is little

or no strength, then the material is not pozzolanic. The applicable portions of ASTM C 593 [93] were followed to proportion, mix, and cure specimens for this test.

In the first round of G-800 mixtures the w/c was held constant at 0.22. As microspheres were added to each mixture in the round of experiments, the w/s decreased and the water available for hydration decreased in each mixture based on the water demand of the microspheres. To address this situation, a second round of G-800 mixtures was made to further explore the change in compressive strength results under conditions where the w/s was held constant and the w/c allowed to vary. In the second round, mixtures were made in increments of 3% through 9% by volume of mortar and the baseline mixture (0% G-800 microspheres) had a w/c = 0.22 and a w/s = 0.0835. For all the rest of the mixtures in the second round the mass of mixing water was increased to offset the added mass of microspheres and to keep the w/s constant at 0.0835. As before, for each mixture three compressive-strength, cube specimens were made and cured under the heat curing regime.

The third round of mixtures was a companion to the second round with G-200 microspheres being used instead of G-800 microspheres to see if the diameter of the microspheres made any appreciable difference in the compressive strength. As in the second round, the w/s was held constant at 0.0835.

5.6.2.3 Results

The combined results of the first and second round of G-800 microsphere mixtures are presented in Figure 5.12 and the comparison of the second round of mixtures (G-800) with the third round of mixtures (G-200) is presented in Figure 5.13. The result of the lime-pozzolan test on the G-800 microspheres was an average compressive strength of 6.15 MPa.

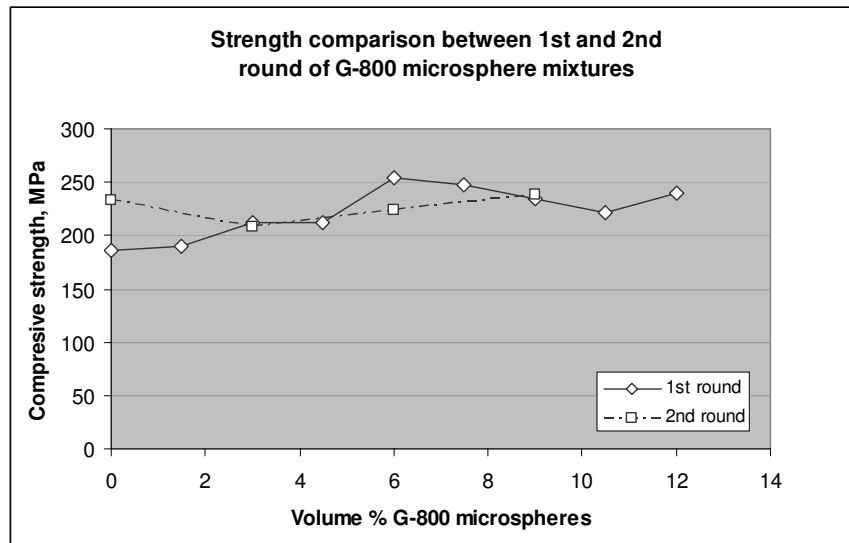


Figure 5.12 Compressive strength versus percent G-800 microspheres

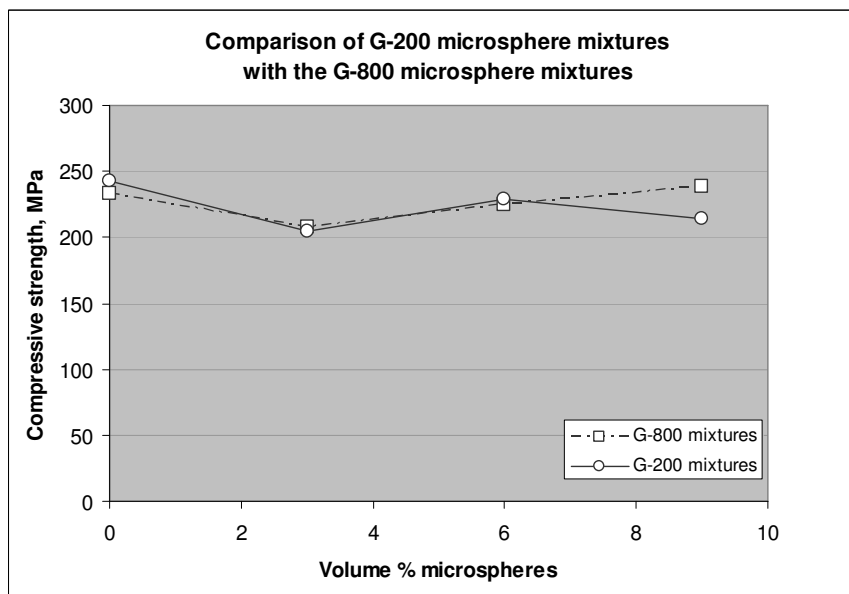


Figure 5.13 Compressive strength comparison of the G-800 and G-200 microspheres

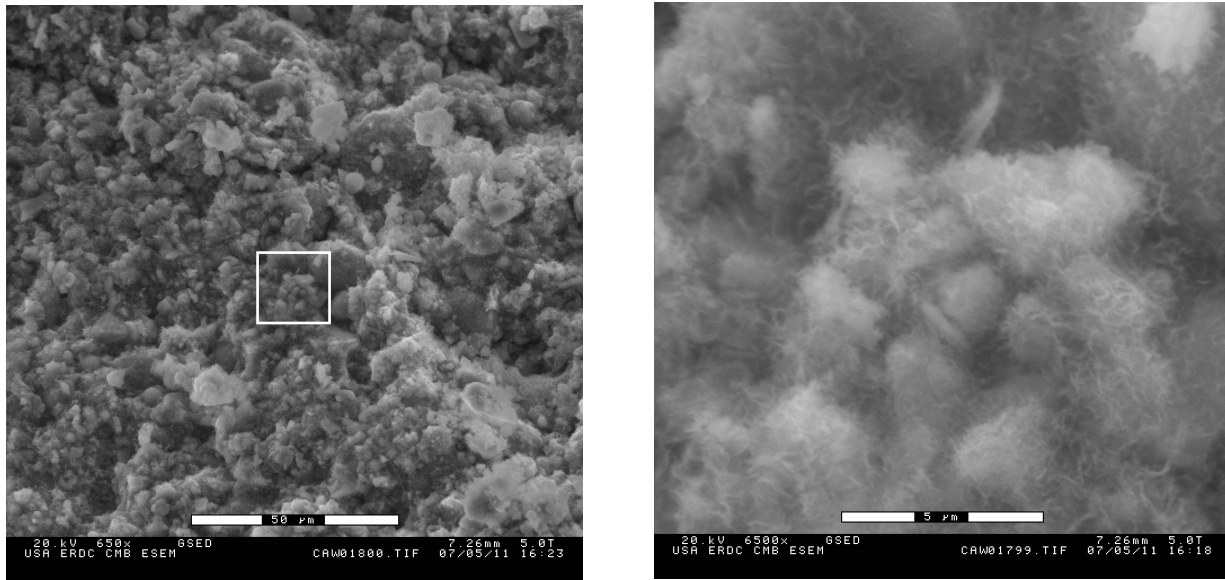
5.6.2.4 Discussion

The results from the first round of mixtures presented in Figure 5.12 show the strength increasing from 186 MPa for the control at 0% microspheres to 254 MPa for the mixture

containing 6% of microspheres and then decreasing slightly as the percentage of microspheres is increased to 12%. The increase in strength from 0 to 6% microspheres immediately leads to the supposition that the microspheres are responsible for the strength change either through their role as a very strong aggregate or through their modification of the physical characteristics of the cement paste. On further study of the data several conditions come to light that have an effect on the results. The lime-pozzolan test revealed that the microspheres are pozzolanic to a small degree. The Corps of Engineers considers a fly ash to be an acceptable pozzolanic material if the strength from the lime-pozzolan test is greater than 6.21 MPa. While the 3M microspheres are not fly ash, they did have compressive strength close to the lower limit and thus make a strength contribution through the generation of C-S-H.

Figure 5.14a shows a SEM photomicrograph of the fracture surface of the lime-pozzolan specimen after it had been failed. The detail photomicrograph in Figure 5.14b shows hydration products growing on the surface of the CH and the microspheres indicating pozzolanic activity. However, if their pozzolanic contribution were only on the order of 6 to 7 MPa, the strength gain would have been much smaller than the 36.5% increase revealed in first round mixtures.

The question of the change in the water-to-solids ratio (w/s) as microspheres are added also has a role in the strength change. As microspheres are added to the mixture (under a constant w/c), the w/s will decrease and a portion of the available water will be adsorbed onto the surface of the newly added microspheres. This will theoretically reduce the water available for hydration and effectively reduce the w/c . The decrease in w/c will increase the compressive strength of the VHSC as long as there is enough C-S-H to hold the components materials together. This critical value of w/c has been calculated by Richard and Cheyrezy [59] for RPC as



(a)

(b)

Figure 5.14 (a) General view of fracture surface of the lime pozzolan specimen and (b) Detail in center showing hydration products

0.08. This effective reduction in w/c is the more likely change responsible for the increase in strength.

In the second round of G-800 microsphere mixtures the w/c was increased with the addition of microspheres to keep the w/s constant. This increased the w/c from 0.22 to 0.24 but kept the effective w/c closer to 0.22 over the full range of the experiments. This had an effect of keeping the compressive strength more uniform over the full range of microsphere additions as is reflected in Figure 5.12.

The third round of mixtures was conducted to determine if there was any difference in strength that was a function of the size of the microspheres. The G-200 microspheres are much smaller than the G-800 variety. Figure 5.13 shows the comparison of these two sizes of microspheres. The data for the different loadings of microspheres from the two rounds of mixtures are essentially the same indicating that the different sizes of the microspheres do not have an influence on the strength of the mixtures.

5.7 Summary

Chapter 5 covered the experiments that were conducted to improve the strength of VHSC. The changes to the baseline mixture proportions of VHSC from those of Neeley and Walley [47] were discussed at the beginning of the chapter. These changes were made to bring the proportions more in line with the philosophy of VHSC. Studies of the cement that would be used for VHSC revealed that a class H oil well cement gave the highest strength. Advances in the chemistry of HRWRAs led to a set of experiments designed around the third-generation polycarboxylate water-reducers. Improvements in strength and rheology were realized just by changing the type of HRWRA.

Understanding the process of heat curing of VHSC was important and an experiment was designed to study part of this process. Varying the time that VHSC was under the ambient curing portion of the heat curing sequence identified the minimum number of curing days for full effect.

Studies on the inclusion of microfibers and microspheres in the VHSC formulation were conducted to find if these materials were beneficial additives. It was found that there was a strength relationship between the volume of micro-inclusions added and the water they demand from surface adsorption.

Finally, to help identify the contribution of individual components of VHSC to its strength and rheology, a study was conducted, starting from a high-strength cement paste, where one component was added at a time and rheology and strength data collected. The changes revealed magnitude of the contributions from each material.

5.8 Conclusions

5.8.1 Cement study conclusions

Four cements from a field of 11 that met mill report criteria beneficial to formulation of VHSC were studied. Baseline mixtures using each cement were made and rheology and strength data collected. From these studies the following conclusions were made:

- 1) The properties of strength and flow resulting from mixtures made with different cements differed significantly depending on cement composition and specific surface.
- 2) For maximizing the potential for formation of C-S-H, cements high in C3S with a low C/S are desirable. Cements with low surface area (moderate to low Blaine specific surface) are desirable because they require less water to start hydration and have a low surface-to-volume ratio that leaves a portion of the cement grain as unhydrated clinker to act as a strong microaggregate.
- 3) Based on the strength and flow results achieved in the cement studies, the Lafarge class H oil well cement from the Joppa plant was identified as the best cement.

5.8.2 HRWRA study conclusions

High-range, water-reducing admixtures have been used to improve the strength and rheology of VHSC since its inception. Through the years VHSC was being developed, great advances in the chemistry of HRWRAs took place. Over that time, a number of conclusions about HRWRAs were made:

- 1) From the early development of VHSC when HRWRAs consisted of salts of naphthalene sulphonate and melamine sulphonate polymerized with

formaldehyde, the best performing HRWRA was a powder version of a sodium salt of naphthalene sulphonate polymerized with formaldehyde.

- 2) Because of the advances in polymer chemistry, the polycarboxylate generation of HRWRAs are more efficient in deflocculating clumps of cement, and allowing the limited water in VHSC to better spread to each cement grain and promote greater hydration. The result of this is greater strength development and fluidification of the cement paste.
- 3) Based on the compressive strength produced, the flow number attained, and the small size of dose required achieving the strength and flow, the polycarboxylate HRWRA ADVA 170™ was identified as the best admixture for VHSC.

5.8.3 Curing study conclusions

Proportioned at its highest strength-giving composition, VHSC is capable of producing compressive strengths in the range of 160 to 180 MPa when cured in ambient temperature water conditions. The same mixture will produce compressive strengths in the range of 245 to 267 MPa when cured at 90 °C for a number of days. Because this material is fairly unique in the cement and concrete industry, the literature on this phenomenon is very scarce. Current attempts to shed light on the cause of this strength gain with heat curing were also disappointing because of limited resources. From the research into curing that was conducted the following can be concluded and hypothesized:

- 1) Under studies conducted on the necessary length of ambient temperature curing before being subjected to 90 °C water and air temperatures, 7 days ambient temperature curing as recommended is unnecessary. Curing for 1 day

produces elevated strength but does not provide enough time for proper cement hydration to occur. Curing in ambient water temperature conditions for 3 days or greater before application of heat produces the same compressive strength result. Therefore 3 days ambient temperature curing is the minimum required curing time.

- 2) The heat treating accelerates the reaction of the hydrates, both pozzolanic and natural, such that they achieve very-high strength in a short, accelerated curing time [59, 89].

5.8.4 Microfiber study conclusions

The following conclusions are drawn from the strength studies done with wollastonite microfibers:

- 1) The addition of wollastonite microfibers to the basic VHSC mixture proportions increased the compressive strength of the material by between 6 and 25%. It can be concluded from this result that the microfibers are strength-giving additives to the baseline VHSC formulation.
- 2) Because individual microfibers could not be detected in SEM photomicrographs of the fractured surface of the VHSC beams containing 11% wollastonite fibers, the exact cause of the strength gain is inconclusive. It can be concluded that either the bond between the paste and microfiber was so strong that all the fibers fractured at the crack face leaving the crack face free from any pulled out fibers; or that because of the CaO and SiO₂ nature of the wollastonite the fibers acted as additional calcium-silicate material that was converted into C-S-H during hydration, particularly in the presence of the heat-

curing environment. Given that there is no evidence in the literature to support the conversion of wollastonite to C-S-H, the former conclusion is favored.

5.8.5 Microsphere study conclusions

The following conclusions can be made regarding the compressive strength studies of VHSC augmented with 3M G-800 and G-200 Zeeospheres™

- 1) The results of the lime-pozzolan test showed that the calcium silicate ceramic microspheres were borderline pozzolanic and contributed some level of pozzolanic C-S-H to the mixtures. This was confirmed through SEM photomicrographs showing hydration products on the fractured surface of the specimens. However, the pozzolanic strength gain of 6.15 MPa was not sufficient to account for all the strength gained through adding microspheres to the mixture.
- 2) The round one mixtures containing up to 12 volume % of G-800 microspheres showed a 36.5% increase in compressive strength as microspheres were added up to the 6% level. This strength gain was realized while holding the w/c constant and adding solid material that caused a decrease in the w/s and an effective decrease in the w/c as a by-product of some of the hydration water being adsorbed onto the surface of the microspheres. Because of the dense microstructure of the VHSC, there was still room for an effective reduction in the w/c of the material below the actual w/c of 0.22 that would have a strength giving effect on the mixtures. From this it is concluded that the effective decreases in the w/c in first round experiments as increments of microspheres were added up to the 6% level was the chief reason for the increase in strength.

- 3) The results from the second round of G-800 microsphere mixtures, in which the w/s was held constant, dictated a small increase in the w/c over the range of 0 to 9% microsphere additions. As a result, the mixtures showed only a small change in the compressive strength across the full range of microsphere additions. Additionally, the results of the experiments on the effect of size of microspheres generated through the comparison of G-800 and G-200 microsphere mixtures in second and third rounds showed no difference in strength due to size. From this and the above results it is concluded that the addition of the microspheres contributed to the strength of VHSC in two ways. First, strength was given through the generation of pozzolanic C-S-H, and second, the physical addition of the microspheres indirectly produced a strength increase through modification of the effective w/c of the mixtures.

5.8.6 Component materials study conclusions

The following conclusions can be made as a result of the component materials experiments in VHSC:

- 1) VHSC is a composite material with strength and rheological properties dependant on the type, quantity and bonding condition of the component materials that make-up the composite.
- 2) The contribution of the aggregate to the strength of the composite mixture is highly important and strongly depends on the strength of the aggregate, and the quality of the interface between the aggregate and the paste matrix. A strong interface will allow the strength of the aggregate to play a role in the strength of the composite, whereas a weak interface will render the aggregate merely a

filler contributing no strength benefit.

- 3) Lowering the water-to-solids ratio (adding more solid materials to a constant mass of water) does not necessarily control the strength and rheology of the composite. Strength is controlled by the judicious choice of type and volume of component materials and the rheology is governed by the shape of the component particle, its packing ability, and its adsorbed water demand.

Chapter 6 BACKGROUND AND LITERATURE REVIEW III: TOUGHNESS OF VERY-HIGH-STRENGTH CONCRETE

6.1 Background

In the problem statement to this dissertation it was stated that to engineer a high-performance material it is important to optimize the material properties that are desirable and minimize those properties that are detrimental. The discussions in chapters four and five focused on those material properties that brought strength to VHSC. Many of the steps taken to improve the strength such as choosing small size aggregate, adding silica fume and silica flour to enhance particle packing, minimizing the w/c, and optimizing the type of HRWRA also increased the brittle nature of the material to the point that the ability of the VHSC to resist fracture became very small. Very-high strength is a desirable property, but obtaining it at the cost of poor fracture properties is unacceptable and must be addressed to make VHSC a useful construction material.

To counteract the brittle nature of VHSC, steps must be taken to increase the fracture resisting properties of the concrete. Doing so increases the ductility or toughness of the material. Toughness in concrete is a difficult parameter to define. Two criteria from fracture mechanics principles help quantify toughness: the critical energy release rate, G_f , referred to as the fracture energy, and the critical stress intensity factor, K_{Ic} , referred to as fracture toughness.

The fracture energy is the energy needed to create a crack of unit area, for example, the amount of energy applied to a cracked plate of unit thickness to create a new crack of unit length. The larger the amount of energy required to do this the tougher the material being fractured. Fracture energy can be determined experimentally through a load-displacement (or alternatively a load-crack-mouth-opening displacement (CMOD)) test. This test creates a load-displacement

(or CMOD) curve, the area beneath which is a measure of the work done to fracture the material and is called the work of fracture (WoF). The fracture energy can be found as:

$$G_f = \frac{WoF}{A_{lig}} \quad (6.1)$$

where A_{lig} is the area of the crack created in the specimen. It is also important to mention that the work of fracture is equal to the area under the load-displacement curve and that it is proportional to the area under the load-CMOD curve.

From a theoretical point of view, based on energy criteria, fracture toughness is defined as the critical value of the stress intensity factor, K_{Ic} , and is related to the critical energy release rate, G_f , through the relationship:

$$K_{Ic} = \sqrt{G_f E} \quad (6.2)$$

accordingly [94], a crack with an energy release rate $G < G_f$ cannot propagate and where $G > G_f$ equilibrium is not possible. Under conditions where $G = G_f$ the crack will be unstable under load control if $\partial G/\partial a > 0$ and can grow in a stable manner under load control if $\partial G/\partial a < 0$ where a is the crack length in question. In this context, fracture toughness is a critical stress level that dictates the future behavior of a crack present in the material. In the physical sense of the term, toughness is a material's ability to resist propagation of a crack by means of toughening mechanisms within the material's structure that consume energy that would otherwise be spent on furthering the growth of the crack. These toughening mechanisms are a function of the components of the material and influence energy consumption to varying degrees.

6.1.1 Toughening mechanisms in concrete

To properly discuss the toughening mechanisms that occur in the vicinity of a fracture in concrete, it is prudent to first define the crack zones and the actions occurring there. Figure 6.1

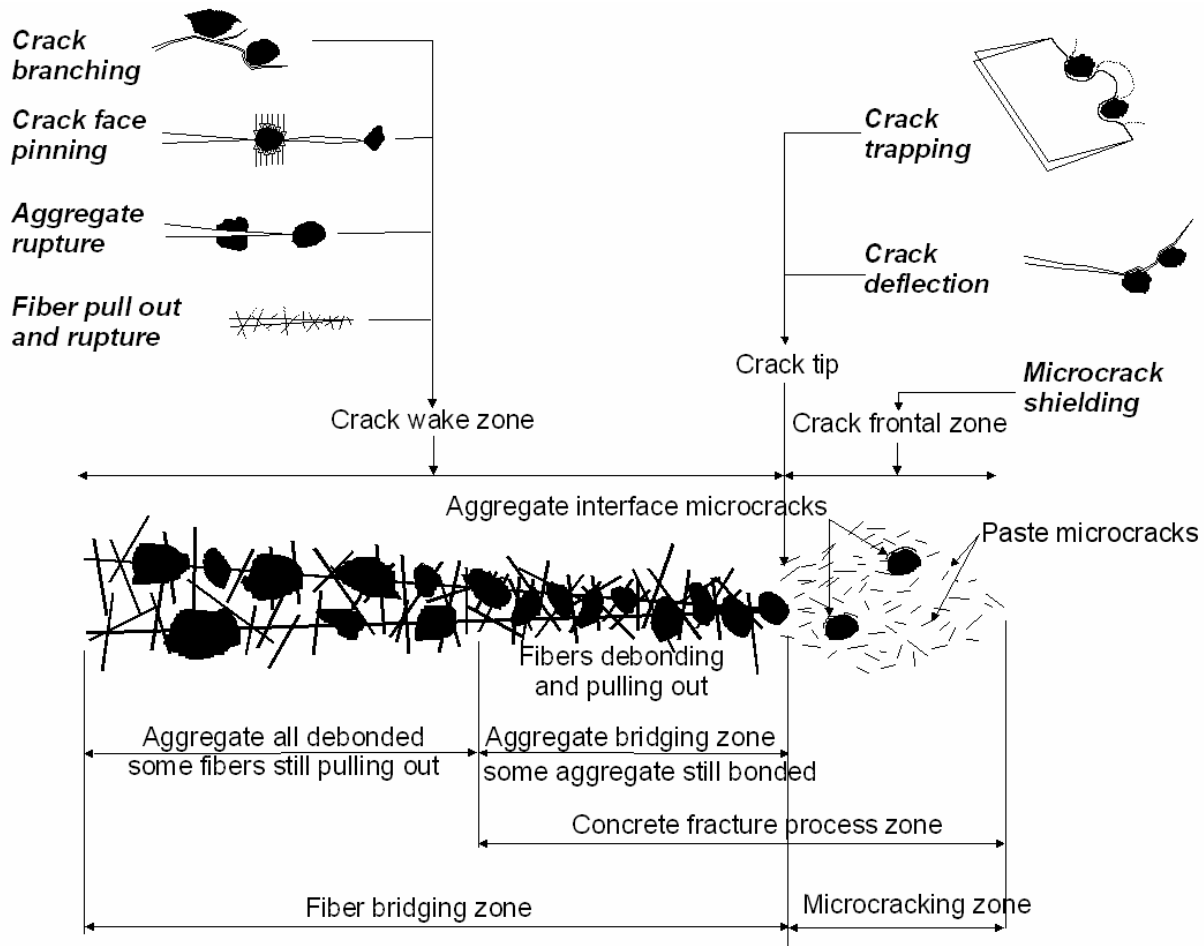


Figure 6.1 Diagrammatic breakdown of crack-toughening mechanisms based on location of crack.

shows an idealized crack with its various zones identified and a number of the fracture-toughening mechanisms associated with each zone. The discussion that follows applies to both unreinforced and fiber reinforced concrete (FRC). The fiber-related toughening mechanisms apply to both macro-fiber and microfiber-reinforced concrete.

The physical boundaries of an edge crack in concrete extend from the mouth of the crack to the crack tip as in the case of a surface crack propagating inward from the exterior face of a cracked specimen. In this case, the mouth of the crack is the opening on the surface of the specimen (the left edge of the crack in Figure 6.1) and the tip of the crack is the zero-width

location immediately in contact with the microcracking zone in front of the crack (identified as crack tip in Figure 6.1). In the case of an interior crack that propagates from both directions from an interior flaw in the matrix such as a macro pore or a shrinkage microcrack, the mouth of the crack would be the location at the widest opening of the crack (such as the mid-point between the ends of the crack) and the tip of the crack (in this case there would be two tips) is as described above. The zone composing the two opposing faces or sides of the crack running from the mouth to the tip of the crack define the crack-wake zone. Many of the most important toughening mechanisms occur in this zone.

The physical crack tip is more of a location than a zone in the two-dimensional-crack model; however, in the three-dimensional world the crack tip is a non-linear path through the depth of the specimen more easily propagating where there are no impediments and being hindered where there are toughening mechanisms encountered in its path. Lastly, in Figure 6.1, the zone in front of the crack (to the right side of the crack tip) is known as the microcracking zone. Most of the technical literature describing the zones of a crack refers to this zone plus that part of the crack-wake zone where the aggregate still influences the opening of the crack, as the fracture process zone. The extent of this region is greatly debated in the literature owing to the difficulty in measuring the processes that take place within its confines [70]. It is generally agreed that the larger this region is the greater the opportunity for encounters with toughening mechanisms and the tougher it becomes. On the other hand, the smaller this region is the more brittle and less-tough the concrete becomes.

6.1.2 Microcrack shielding mechanisms in the microcracking zone

Microcracking in concrete begins to occur at the paste/aggregate interface of larger sized aggregate particles at a stress level somewhere above the 50% level of the peak load in the

stress-strain (σ - δ) curve of the member being loaded. The microcracks begin in the weak paste around larger aggregates where bleed water has a tendency to collect and dilute the w/c of the paste. Their location and direction of propagation are relatively random early in the loading process, generally dictated by the shape and orientation of the aggregate. As the stress increases, the microcracks grow and begin to propagate at smaller paste/aggregate interfaces and also begin to link together creating longer microcracks beginning to orient in a plane perpendicular to the major tensile stress. As this happens, the microcracks increase and continue to link together in weaker areas of the material while in stronger areas the stress on the microcracks is relieved and the cracks close. The microcracks linking together in the weaker areas begin to widen as the stress continues to increase producing a non-linear response in the σ - δ curve predicated on the summation of the elastic strain of the bulk matrix plus the plastic strain produced by the widening of the microcracks. As the stress is increased, the microcracks continue to grow together forming major cracks and the σ - δ curve grows more non-linear. This process of producing microcracks is the first instance of a toughening mechanism in the concrete. Extra energy is required to create them thus starting the toughening process.

The model in Figure 6.1 can be used when a major crack is first formed. According to the principles of linear elastic fracture mechanics [28, 95] (LEFM), the tensile stress at the tip of a sharp crack becomes infinitely large. Because no material can carry an infinite stress, the largest stress that can be carried before it fails is the material's ultimate tensile stress. This singular stress presents a problem for using the theory of LEFM to analyze the fracture properties of a material.

This problem is addressed by realizing that the zone in front of the crack tip, under the influence of stresses greater than the material's tensile capacity, must be damaged to an extent to

account for this singularity. The result depends on the material being stressed. In purely brittle materials such as glass, the infinite stress at the crack tip fractures the glass and the material fails catastrophically. In ductile materials such as steel, a plastic deformation zone is formed in front of the crack tip to dissipate the singular stress down to a tolerable level and cracking can continue in a controlled manner. In materials that are between brittle and ductile, such as concrete, a damage zone in front of the crack tip is also produced. However, because concrete is a quasi-brittle material, a zone of plastic deformation like that formed in ductile materials is not possible and the damage is manifested in the form of microcracks in the matrix. This is the microcrack zone or crack frontal zone in Figure 6.1.

The size of this damage zone regulates whether LEFM theory can be applied in analyzing the fracture properties of the material. If, as in the case of purely brittle materials, the damage zone is non-existent, LEFM is properly applied. In the case of ductile materials, the damage zone is small compared to the overall dimensions of the stressed material and although not perfect, LEFM principles can still be applied. This is not true for quasi brittle materials, where the damage zone is large in comparison to the overall dimensions. In this case LEFM is not appropriate and the fracture mechanics principles must be modified to a non-linear approach.

Two forms of microcracks occur in the microcrack zone for concrete: paste microcracks (generally formed at flaws, or directly in the paste from differential shrinkage strains during curing), and paste/aggregate interface microcracks (refer to Figure 6.1). There have been many techniques used to detect microcracks in this zone as well as attempts to document the size of the zone. Jacquot and Rastogi [96] used speckle metrology and holographic interferometry to detect surface cracks and cracking in the FPZ. Further interferometry techniques were used by Castro-Montero et al. [97] (laser-holographic technique) and Cedolin et al. [98] (optical-laser

technique). A number of researchers employed acoustic emission (AE) techniques to explore the microcrack zone. Mihashi and Nomura [99] found evidence that the width of the FPZ but not its length was a function of the size of the aggregate in the concrete. Nomura et al. [100] used AE techniques to better understand the different phases of the tension-softening diagram, concluding that the beginning of the tension-softening diagram coincides with internal microcracking and the tail end concludes with aggregate bridging effects in the crack wake zone. Denarie et al. [101] used a fiber optics technique involving wavelength shift (Bragg grating technique) to measure internal concrete strains in the vicinity of a crack. Their experimental results implied that the size of the microcrack zone is approximately three times the diameter of the largest size of aggregate.

The cracks forming in the microcrack zone are both forms of the toughening mechanism referred to as microcrack shielding. As described above, this zone is formed from the high level of energy at the crack tip, and the zone's size and microcrack density is related to the amount of energy necessary to bring the crack energy into equilibrium. For the crack to continue to propagate, more microcracks must be formed and additional energy consumed in the process. The microcracks developed in this zone lower the effective elastic modulus of the material [29], thus reducing the crack tip stress intensity factor, K_I , enhancing the toughness of the material.

6.1.3 Mechanisms occurring at the crack tip

Aggregates in the path of the crack tip hinder propagation of the crack through three mechanisms that cause extra energy to be expended. Crack deflection produces a more tortuous fracture path, crack trapping inhibits cracking progress by constraining the crack face opening to zero in the vicinity of well-bonded aggregates in the crack path, and crack tip blunting reduces the stress intensity at the tip of the crack to a minimum.

6.1.3.1 Crack deflection

The more tortuous (the more non-planar) the path a crack must take in getting from one point to another in a medium, the farther that crack must travel and the greater the amount of energy it must expend in doing so. This is the main premise of the crack-deflection fracture-toughening mechanism. The path directly from one point to another covers the minimum distance a crack must travel and is also the minimum energy path it will seek provided there are no hindering particles in the way. Crack propagation through cement paste quite often produces a near-planar fracture path because there are no toughening mechanisms in the crack path to alter the direction of travel. In the other extreme, when a crack front encounters a series of tough aggregate particles in its path, the crack will deflect around the aggregate traveling through the weaker paste matrix because this path consumes less energy than that needed to fracture the aggregate and traveling the less-tortuous path through it. Even though less energy is consumed for the crack front to travel the more tortuous path around the aggregate, more energy is expended than if the crack front did not encounter any hindering inclusion and traveled a straight path through the paste. The path around the aggregate is the most common route in normal strength concrete (NSC). In HSC or VHSC where the paste/aggregate interface is much stronger than in NSC, the path of least energy consumption is often the less tortuous path through the aggregate. This is especially true in VHSC where only small diameter aggregate are used and the surface area of the fracture plane through the aggregate is so much smaller than that of large-diameter aggregate. From the above discussion, the aggregate is acting as a crack deflector of the crack front and is an effective fracture-toughening mechanism.

A thorough study of crack deflection toughening using a fracture mechanics approach was undertaken by Faber and Evans [102]. They conducted an analysis based on determination

of the initial tilt (deflection) and maximum twist (rotation) of a crack front between two particles as it encounters a randomly distributed field of a secondary hindering phase (e.g. aggregate). Their analysis was conducted for spherical-, rod-, and disc-shaped phases and they concluded that: the toughening is primarily derived from the twist of the crack front and secondarily from the tilt or deflection produced in the encounter. The toughening predictions were invariant with particle size and only dependent on particle shape; and the most effective toughening phase shape was that of a large-aspect-ratio rod with the sphere and disc being less effective in toughening.

6.1.3.2 Crack trapping

When a crack front encounters aggregate particles it can neither deflect around nor fracture through to continue its progress, then the crack front is temporarily halted at the sites of the aggregates and forced to grow past them in a bowed crack front between adjacent aggregate particles [29, 102]. This mechanism is called crack trapping and occurs when the crack is confined to zero opening displacement at discrete locations along the crack front. To continue, the crack is forced to grow in a bowed manner between the aggregate particles. The crack can only propagate if the stress intensity factor is raised to the critical value, K_{Ic} , along the bowed portion of the crack front. According to Li and Maalej [29], three conditions need to be satisfied to encounter this type of mechanism. First, the aggregate toughness needs to be stronger than the matrix toughness so that the crack does not propagate through the aggregate. Second, the bond between the aggregate and the matrix must be strong enough that aggregate debonding or crack deflection does not occur. Third, the elastic modulus of the aggregate must be equal to or greater than that of the matrix to insure that opening displacement can be suppressed at regions along the crack front.

6.1.3.3 Crack tip blunting

It has been well established in LEFM theory that the stress intensity at the tip of a sharp crack is many times higher than the far-field stress driving the sharp crack through the matrix. From basic theory of elasticity [103], the maximum stress, σ_{\max} , at the edge of an elliptical hole in an infinite plate with far-field tensile stress, σ_0 , oriented along the y-axis is:

$$\sigma_{\max} = \sigma_0 \left[1 + 2\sqrt{\frac{a}{\rho}} \right] \quad (6.3)$$

where a is the radius of the hole along the major axis and ρ is the radius of curvature. In an infinitely sharp crack (an elliptical hole with a major-axis width = $2a$ and minor-axis height ≈ 0), the radius of curvature at the x-axis crack tip is very small. This drives σ_{\max} in equation 6.3 to near infinity. At the other extreme of stress conditions, a round hole, the radius of curvature becomes equal to the radius, a , and σ_{\max} turns to the minimum value $3\sigma_0$. Thus any mechanism that causes a crack front to intercept a large number of spherical inclusions in its path would cause the high crack-tip stress-intensity factor to be reduced to a very low magnitude where it intercepted the spherical inclusions and reduce the crack-tip stress-intensity factor. To return the crack-tip stress-intensity factor to its high stress state requires input of extra energy and thus toughens the matrix. This mechanism is called crack-tip blunting and naturally occurs where a crack runs into a spherical void, such as an entrapped or entrained air void or a weakly bonded spherical aggregate, in the cement paste.

6.1.4 Mechanisms occurring in the crack wake zone

Many of the important fracture toughening mechanisms happen in the crack wake zone. Here, in the region of the crack behind the crack front where true fracture of the material has already happened, aggregates and other macro and micro inclusions are the mechanisms that

provide toughness. Many of them rely on the contribution of the aggregate in the paste matrix to provide the toughness such as crack branching, crack-face pinning, and aggregate rupture. The most well known mechanism though is pull-out and rupture of distributed fibers embedded in the matrix.

6.1.4.1 Crack-face pinning

Crack-face pinning is somewhat of a derivative of crack trapping in that it presents a follow-on condition arising out of the crack trapping mechanism. It is grouped with the crack wake zone mechanisms because by the time it delivers its toughening value, the crack front has passed and it is now in the crack wake zone. When the bowed out segments of the crack trapping mechanism grow beyond the first layer of aggregates, the crack front coalesces and continues on to the next encounter with aggregate particles, leaving in its wake a number of pinned paste/aggregate locations that are still experiencing zero crack separation. Through this process, several rows of pinned paste/aggregate locations can form in the wake of the crack. Because the crack faces are pinned together in the wake of the crack front, the full intensity of the crack driving force cannot be brought to bear on the crack tip and the crack-tip stress-intensity factor is reduced until the pinning mechanism is eliminated.

6.1.4.2 Crack branching

Crack branching refers to the condition in which secondary cracks branch off a main crack traveling through a matrix, creating multiple crack tips to which the crack driving force is distributed. The creation of secondary cracks to the side of a main crack in a heterogeneous material such as concrete can be the result of the tortuous path the crack takes in deflecting around aggregate particles or from localized weaknesses in the matrix behind the crack tip that spawn a new fracture direction. As a toughening mechanism, the creation of secondary crack tips

siphons energy from the crack driving energy being devoted to the main crack tip and ultimately requires more energy to be consumed to drive the multiple cracks.

6.1.4.3 Aggregate bridging and rupture

Several toughening mechanisms can be described under this category depending on whether the aggregate breaks free from the matrix or ruptures through itself. Aggregate or grain bridging refers to the ability of an aggregate to continue to transfer load across the faces of a crack for a period of time after the crack front has passed. If the bond between the paste and aggregate on one face of the crack has failed, that aggregate will pull out of its paste socket as the crack opens. However, due to frictional forces between the aggregate and paste as well as interlock between closely spaced aggregate particles during this pull out process, additional energy must be expended to open the crack. Shah et al. [28] describe this as one of the more important toughening processes in concrete. Aggregate bridging, along with the mechanism of fiber pull out which will be discussed in paragraph 6.1.4.5, are believed to be the mechanisms responsible for the strain-softening behavior of concrete [29].

If the bond between the paste and aggregate is very strong, as is the case in the crack-pinning mechanism, then for the crack faces to open sufficient energy must be expended to fracture the aggregate. This is often the case in HSC and VHSC where low w/c, silica fume, and HRWRAs provide for a very strong paste/aggregate interface that forces the rupture of the aggregate and requires a high energy demand to allow the pinned crack faces to open and the continued propagation of the crack.

6.1.4.4 Fiber pull-out and rupture

Incorporation of discrete, uniformly-distributed, randomly-oriented fibers into concrete has been one of the most effective toughness-building mechanisms of all time. Discrete fibers

have been used in building materials since biblical times when straw was added to mud bricks for reinforcement [104]. Fibers were first incorporated in concrete in the early 1900s when asbestos fibers were added for strength. In the 1950s and 1960s steel, glass, and synthetic fibers became common materials for fiber reinforcement. Until the early 1970s fibers were recognized for evenly distributing stresses in the concrete and adding compressive and flexural strength to unreinforced concrete. As fracture mechanics principles began to be applied to concrete, fiber reinforcement began to be recognized for its toughening role.

Fibers randomly distributed throughout the cement matrix only serve to distribute structural and material related stresses more evenly throughout the structure until cracking occurs. For example, the stresses in the concrete beneath a point load, such as a vehicle wheel load, on a fiber-reinforced slab will be better distributed throughout the cross section than it would be if the slab were unreinforced. This is because the many fibers in the paste help distribute the concentrated load from fiber to fiber spreading it over a larger area than would be realized in unreinforced concrete. In a similar manner, shrinkage or thermal stresses in a fiber-reinforced structure will be better distributed throughout the structure because of the action of the fibers. Once the concrete cracks, the fibers take on their more prominent role of a toughening mechanism. Referring to the crack-wake zone or the fiber-bridging zone in Figure 6.1, when a crack forms this zone of the cement paste, the cement matrix can no longer transfer load-carrying capacity across the two crack faces. But as was discussed in the aggregate pinning and aggregate bridging mechanisms, the two crack faces cannot open until they overcome the load-carrying capability of the fibers (and aggregate) that cross the closed faces of the crack. For the fibers, this load-carrying capacity manifests itself through a number of toughening mechanisms including: matrix fracture, fiber/matrix interface debonding, post-debonding friction, fiber fracture, stress

redistribution, and fiber pull out. Of these, fiber/matrix interface debonding, post-debonding friction, and fiber pull out account for the greatest energy consumption [34].

6.2 Fracture toughness experiments

6.2.1 Fracture toughness of unreinforced VHSC

The majority of reasons to make a concrete as strong as VHSC involve not only its compressive load-carrying capacity but also its very high tensile strength. For military purposes, tensile strength and toughness are critical properties for blast and penetration resistance. Unreinforced VHSC has very-high compressive strength (in the range of 235-267 MPa) and tensile strength that is often comparable to the compressive strength of low-strength concrete (in the range of 14 MPa). However, it is brittle and lacks the toughness necessary to resist tensile loads. The most commonly adopted solution is to add distributed fibers to restore some of the toughness and ductility. To explore these properties in the baseline VHSC, a set of experiments was conducted to determine the fracture toughness of the material without distributed reinforcement for later comparison with fiber-reinforced VHSC and other concrete materials.

6.2.1.1 Experimental procedure

A mixture of baseline VHSC as described in Table A3 of Appendix A was made to produce 50.8-mm compressive strength cubes and 3 fracture-toughness beams 355.6 mm in length and 76.2 by 38.1 mm in cross section. For this set of experiments, the powder Disal™ HRWRA was replaced with W.R. Grace ADVA 170™ at the dosage of 7.22 ml/kg of concrete. The mixing was done in the floor-mounted 28.92-l Hobart mixer. Standard mixing and curing procedures described in paragraphs 5.1.2 through 5.1.7 were used and all specimens received heat curing.

The flexural-toughness beams were water-jet cut to produce a notch 25.4 mm deep and 1 mm wide in the bottom third of the beam at its mid-point. For purposes of calculating fracture toughness, dimensions of each beam were taken with a micrometer and averaged for calculation. Knife-edge tabs were epoxied to the beams on both sides of the cut notch to accept a crack-mouth-opening-displacement (CMOD) gage to provide displacement feedback to the hydraulic loading system. Flexural-toughness testing was done on a 220 kN MTS closed-loop hydraulic testing machine and were loaded in displacement control at a rate of 0.08 mm/min. to failure. Time, load, and CMOD were collected for each test. Fracture toughness, K_{Ic} , was calculated from these data. A detailed account of the methods and calculations used for this experiment is given in Appendix C.

6.2.1.2 Results of unreinforced VHSC fracture toughness tests

Three beams were tested to failure. The fracture toughness, K_{Ic} , and the critical CMOD were calculated from the load-CMOD curve by the Two-Parameter Fracture Model (TPFM) of Jenq and Shah [105] using a numerical technique proposed by Navalurkar et al. [106] to calculate the unloading compliance, C_u (Refer to Appendix C). The results are presented in Table 6.1 and Figure 6.2. Average values for peak-load, K_{Ic} , critical crack-tip-opening dimension (CTOD_c), and G_f , are given in the figure.

Table 6.1 Fracture toughness properties of unreinforced baseline VHSC

Specimen	Fracture toughness, K_{Ic} , MPa- \sqrt{m}
Beam 1	1.02
Beam 2	1.04
Beam 3	1.12

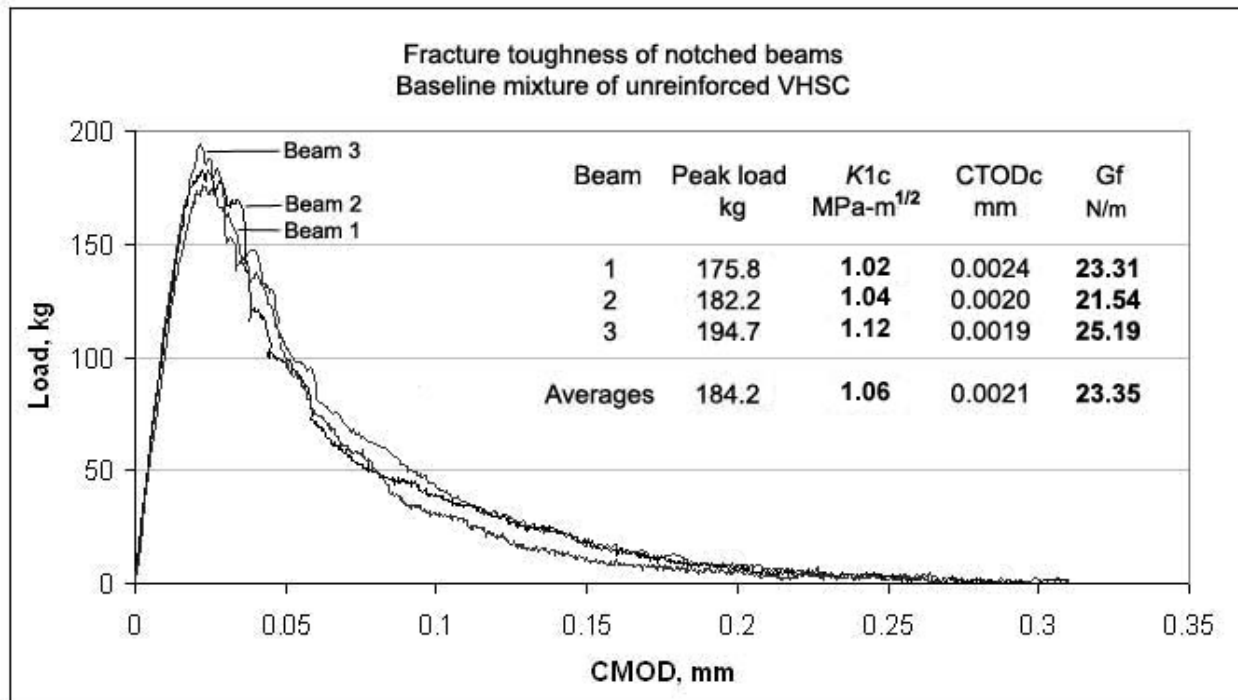


Figure 6.2 Fracture toughness of unreinforced baseline mixture of VHSC

6.2.1.3 Discussion of unreinforced VHSC fracture toughness properties

The average value for fracture toughness found in these experiments is not remarkably different from values reported in the literature for more conventional concrete materials. Karihaloo [107] reported fracture-toughness results based on extensive test data from many laboratory experiments for concrete having f'_c in the range of 21 to 110 MPa. In those data, mean values of K_{Ic} ranged from 0.064 to 1.759 MPa- \sqrt{m} . A scatter plot of compressive strength against fracture toughness from Karihaloo's data shows a shotgun distribution of data points, but a linear trend-line through the data shows a slight decrease in fracture toughness with increasing strength. This follows from the increase in brittleness that accompanies high-strength and the fracture toughness will be affected by this brittleness. It should be noted that the 110-MPa concrete produced the 0.064 MPa- \sqrt{m} fracture-toughness value.

Shah et al. [28] also reported a large body of test results from published work. In this body of work, the fracture toughness for concrete ranging from 25 to 110 MPa varied from 0.560 to 2.130 MPa- $\sqrt{\text{m}}$. Unlike the Karihaloo data, the 110-MPa concrete in this data set had the highest fracture toughness and critical-fracture energy. Shah's data also reported values of critical-fracture energy ranging from 8.57 to 80.23 N/m and CTOD_c from 0.0018 to 0.05 mm.

The CTOD is integral in defining the length of the plastic fracture zone in front of the crack-tip. From LEFM, the stress in a material at the tip of an infinitely sharp crack is infinitely large. But from mechanics of materials we know this is an impossibility, and the highest stress attainable is the material's yield stress. To account for this incongruity, a zone of plastic deformation must exist in front of the actual crack. The length of the plastic deformation zone is related to the effective elastic crack length calculated in the TPFM. It is also related to the CTOD which can be defined as the crack-opening of the effective elastic crack at the location of the tip of the actual crack. That opening is proportional to the length of the effective elastic crack. Figure 6.3 shows the relationship of the plastic zone to the yield strength of the material. The asymptotic curve in the $\sigma - r$ field defines the yield stress – plastic fracture zone relationship. For a material with low σ_{ys} the length of the plastic zone is r_{pl} . For a material with higher σ_{ys} , the yield stress intersects the asymptotic curve at a higher stress and defines a smaller plastic zone length, r_{ph} . Since the CTOD is proportional to the length of the plastic fracture zone, a smaller r_p would reflect a smaller CTOD. In the data from the unreinforced VHSC beams, the CTOD_c averaged to 0.0021 mm. Since the CTOD may be used as a measure of the magnitude of the crack-tip plastic fracture zone, a small value of 0.0021 mm suggests that the fracture process zone in front of the crack tip in VHSC may be small in comparison to the actual crack and that VHSC may respond favorably to LEFM criteria.

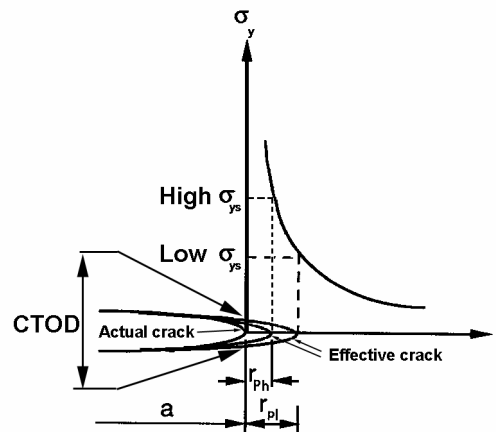


Figure 6.3. Plastic fracture zone, effective elastic crack, and CTOD relationship at the crack tip.

6.2.2 Fracture toughness of steel macrofiber reinforced VHSC

As has been pointed out earlier, because of its very-high strength, VHSC is brittle and needs to be reinforced with distributed macrofibers to restore some ductility and toughness. To explore the level of toughness imparted by macrofibers, a series of VHSC beams, containing distributed steel macrofibers, were fabricated and tested to determine their fracture toughness. The results revealed the contribution the fibers make in toughening the concrete, but also revealed information about the assumption of even distribution of fibers in laboratory-scale specimens and the impact that has on fracture-toughness results.

6.2.2.1 Experimental procedures

Two identical batches (mixtures) of baseline VHSC were made to cast four fracture beams and six compressive strength cubes from each batch. Each mixture contained the proportions of materials presented in Table A3 of Appendix A plus an addition of 3.1% by volume of concrete of Bekaert ZP305™ hooked-end, distributed, steel fibers. The fibers were 30 mm in length and 0.5 mm in diameter. Two identical mixtures were made to evaluate the mixture-to-mixture variation in the results. Each mixture was large enough that the floor-

mounted 28.92-l Hobart mixer was used. Mixing was done according to the procedures described in paragraphs 5.1.2 through 5.1.7 up through the point where the mixture became a paste. At this point, enough mortar was removed from the mixing bowl to make six 50.8-mm cubes for compression testing. The mixer was again started and the 3.1% steel fibers were added to the mixture and allowed to mix for 10 minutes before casting.

Forms to produce beams 355.6 mm in length and 76.2 by 38.1 mm in cross section were used to cast the four beams from each mixture. The forms were placed on a vibrating table and the fresh mixture scooped into the forms in half-depth layers. Each layer was rodded with a steel, slump-test rod to even the mixture before the next layer was added or before finishing the beam. Curing for the cubes and beams was as given in 5.1.5 for heat curing.

When the beams were fully cured, they were sent to be notched for the flexural testing. Because of the way the beams were cast, one of the two 355.6- by 38.1-mm faces was cast against the formwork and the other was trowel-finished. For notch cutting, all beams were oriented so that the notch would cut through the formed face. This was done so that the formed face would be the face that was resting on the support rollers in the test set-up. The notch was cut in the center of the beams with a high-pressure water-jet spray that cut a square notch 25.4-mm deep in the tension face of the beam. The width of the notch was approximately 1 mm wide. The beams were labeled B1-1 to B1-4 for the first mixture and B2-1 to B2-4 for the second mixture. The testing set-up and procedures were the same as described in paragraph 6.2.1.1 above.

6.2.2.2 Results

The compressive strength of each mixture was based on the average of the six cubes made and are presented in Table 6.2. The

f'_c, MPa	
Mixture 1	207.8
Mixture 2	228.5

fracture toughness, K_{Ic} , as calculated by the TPFM requires an unloading compliance parameter that establishes the elastic and plastic contributions to the CMOD at the point of unloading. This works well when there is nothing hampering the elastic recovery on the unloading cycle. But, in fiber-reinforced concrete when the Load-CMOD test reaches peak load (and goes just beyond that load to establish a point for collecting the unloading compliance), the concrete specimen has already cracked and the steel fibers in the crack wake are already pulling out of their sockets on one face of the crack. The test specimen will try to recover the elastic portion of the CMOD if unloaded at this point, but the fibers that have pulled from the concrete will exert a resisting force that will hamper accurate unloading measurement. In this case conducting the fracture toughness test without the unloading cycle and using the numerical equation proposed by Navalurkar to estimate the unloading compliance avoids this problem. The fracture toughness values for the eight beams were calculated this way and are presented in Table 6.3 and Figures 6.4 and 6.5. Additionally, because further toughening information can be realized by describing the results through toughness indices (TI), these data are analyzed by the method of ASTM C 1018 and presented in Table 6.4.

Table 6.3 Fracture toughness results for individual FRC VHSC beams

Beam	Peak Load, kg	Fracture Toughness, MPa\sqrt{m}
B1-1	645.2	3.78
B1-2	790.1	5.37
B1-3	458.5	2.54
B1-4	766.6	5.60
B2-1	845.9	5.96
B2-2	736.7	4.51
B2-3	602.9	3.81
B2-4	486.1	3.09

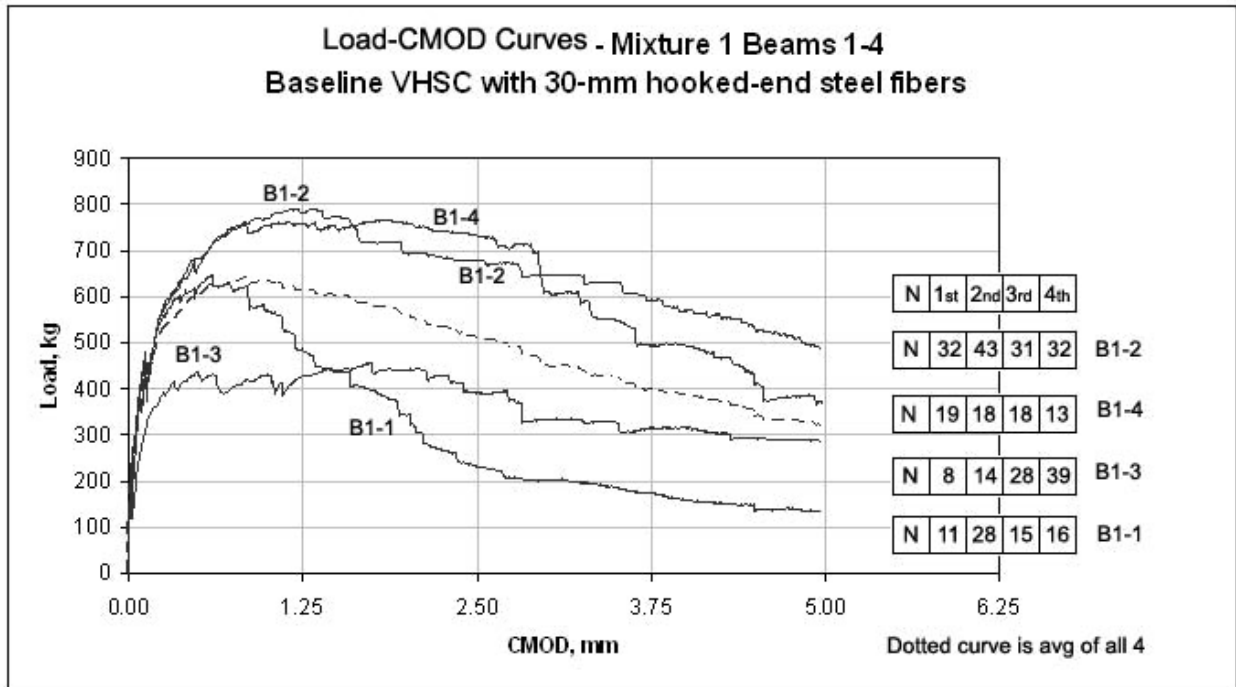


Figure 6.4 Load-CMOD curves for mixture 1

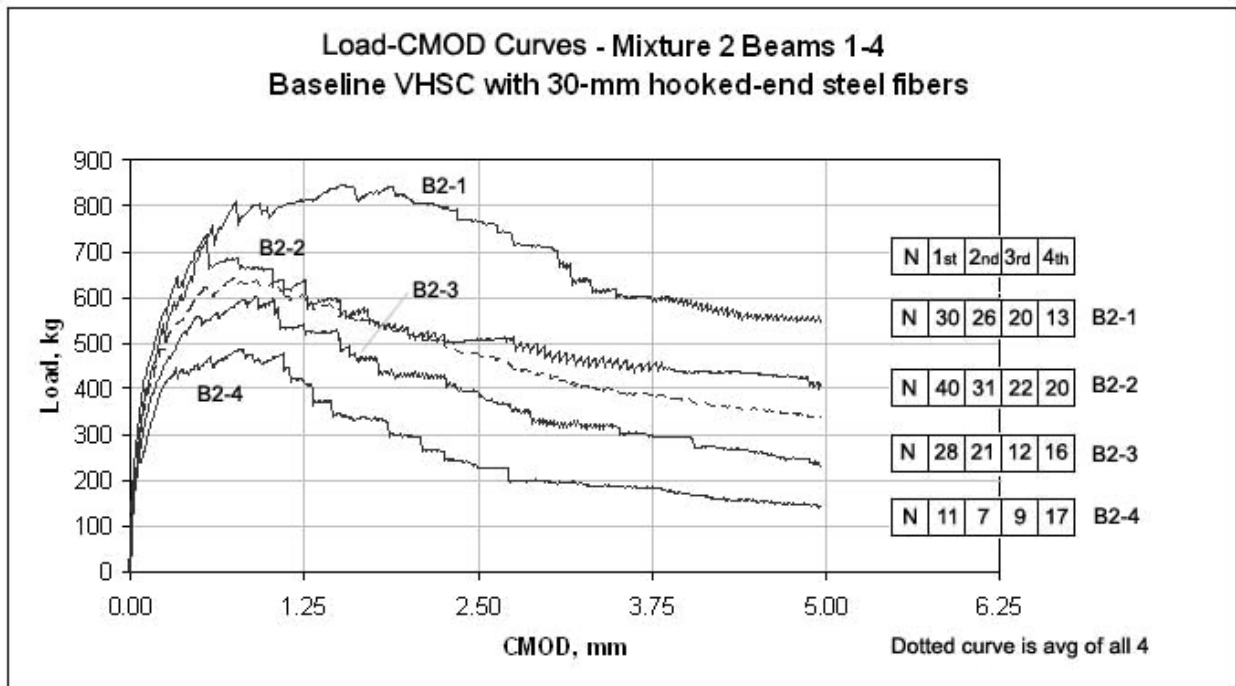


Figure 6.5 Load-CMOD curves for mixture 2

Table 6.4 Toughness Indices for the fiber-reinforced VHSC

FRC Beam	Area under Load-CMOD curve, kg-mm						Toughness Index				
	A_{f-c}	A_{15}	A_{110}	A_{120}	A_{140}	A_{180}	I_5	I_{10}	I_{20}	I_{40}	I_{80}
1-1	9.4	36.2	82.4	193.8	432.6	829.2	3.9	8.8	20.7	46.2	88.6
1-2	31.9	143.2	320.3	724.3	1517.3	2861.5	4.5	10.1	22.7	47.6	89.8
1-3	8.6	32.4	72.4	169.1	359.2	757.1	3.8	8.4	19.7	41.8	88.0
1-4	16.3	65.6	151.1	351.6	799.3	1697.6	4.0	9.3	21.6	49.0	104.1
2-1	60.8	275.6	625.1	1367.2	2657.5	--	4.5	10.3	22.5	43.7	--
2-2	18.3	78.9	181.8	416.9	853.7	1580.5	4.3	9.9	22.8	46.7	86.3
2-3	19.5	87.5	200.7	452.8	910.8	1560.3	4.5	10.3	23.3	46.8	80.1
2-4	28.9	121.4	257.1	533.1	906.3	1344.6	4.2	8.9	18.5	31.4	46.6

6.2.2.3 Discussion of the fracture toughness results

All fracture toughness tests were carried to complete failure of the beams. The CMOD at failure ranged between 5.0 and 5.52 mm, but for comparison between beams the load vs CMOD data were truncated at a 5-mm crack opening. The CMOD gage had a working range of 0 to 6.35 mm.

In each of Figures 6.4 and 6.5, there are four load-CMOD curves plus a dashed curve representing the average of the four curves on each figure. In both figures it can immediately be seen that there is a large within-mixture variation in the results of individual beams. Table 6.3 gives the individual peak loads and the fracture toughness results for the eight beams. On observing the fractured surfaces of each of the beams, it was seen that the distribution of the fibers across the fracture surface was not even. The total number of fibers crossing the fracture surface was different from beam to beam. In theory, the distribution of randomly oriented fibers should be uniform across the ligament, while in reality some beams had a high density of fibers close to the pre-cracked notch and others were very sparse in this area.

To study this phenomenon further, an accurate count of the fibers crossing the failure surface of each beam was made. The fractured face of the beam was divided into four regions

from bottom of the beam to top. The water-jet cut region contained no fractured or pulled out fibers so it was ignored in the analysis. This left the top 50.8-mm fractured ligament to be analyzed. This region was divided into four 12.7- by 38.1-mm quadrants that were labeled 1 (closest to the notch) through 4 (closest to the top of the beam) and the number of fiber ends in each quadrant counted. The results of this exercise are shown in the series of boxes to the right of each curve in Figures 6.4 and 6.5. The box containing an N represents the notch, followed by four boxes with the number of fibers found for each of the four quadrants.

The fiber pull-out and aggregate bridging in the crack wake zone are primarily responsible for the shape of the post-peak strain-softening portion of the Load-CMOD curve [29, 108] and it is often stated that the matrix is solely responsible for the properties of the load-CMOD curve prior to first-cracking load. Figures 6.4 and 6.5 show that the initial slopes of all the curves, up to a load of approximately 200 kg, are essentially the same. However, the magnitude of the peak load and the deformation associated with it are strongly affected by the number of fibers in the first quadrant of the ligament beyond the notch. In Figure 6.4, the peak load in each curve occurs, in order of descending magnitude, in beams B1-2, B1-4, B1-1, and B1-3 and the number of fibers found in the first quadrant for these beams were 32, 19, 11, and 8, respectively. In Figure 6.5 the peak loads, in order of descending magnitude, occur in beams B2-1, B2-2, B2-3, and B2-4 with fibers found in the first quadrant being 30, 40, 28, and 11. In both figures there is a correlation between the magnitude of the peak-load and the number of fibers found immediately behind the cut notch of the beam. A plot of peak-load vs number of fibers crossing the first quadrant is shown in Figure 6.6 and a linear trend-line applied to these data indicates increasing peak-load with increasing number of fibers in the first quadrant.

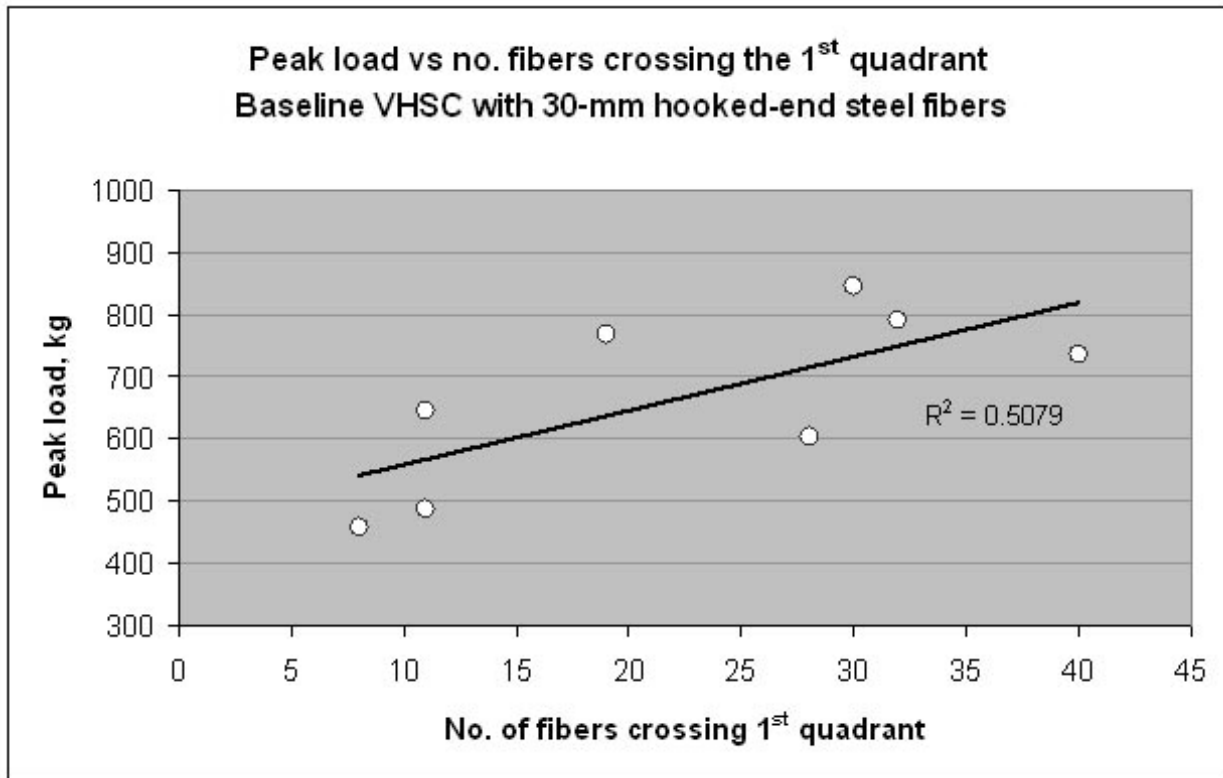


Figure 6.6 Peak load vs no. of fibers crossing the 1st quadrant in fiber-reinforced VHSC

Continuing with the issue of distribution of fibers in the fracture path, beams B1-2, B1-4, and B1-3 all maintain a high level of load carrying capacity in the post-peak region of the curve from 1.25 to 5.00 mm. The magnitude of the load for B1-3 is lower than the others and most likely controlled by the magnitude of its peak-load and the low number of fibers in its 1st quadrant. All three of these beams have higher numbers of fibers in quadrants 3 and 4. In contrast, beam B1-1 has high numbers of fibers in quadrant 2 but the number of fibers is significantly lower in quadrants 3 and 4 and the magnitude of its post-peak load-carrying capacity drops off in this region as well. In these instances, the amount of work being done at a particular point along the post-peak strain-softening curve is a function of the number fibers in the quadrant primarily representing that point and is in the area of the crack wake just behind the

crack front. Similar arguments supporting this observation can be presented for the curves B2-1 through B2-4 in Figure 6.5.

All of these observations reinforce a relatively intuitive property of fiber reinforcement in the post-peak strain-softening region of the curve. That is, the more fibers there are in the crack-wake-zone, the more energy is consumed in debonding and pull-out of the fibers, thus delaying the growth of the crack for a longer period of time and enhancing the material toughness.

Perhaps less intuitive, but none-the-less relative is the influence of the volume of fibers in the non-linear portion of the rising-load side of the load-CMOD curve and how they affect the magnitude of the peak-load. The volume of fibers here are distributing stress throughout the microcracking zone and reducing the stress intensity factor, K_I , at the site of ultimate fracture. This effect has also been mentioned by Barr et al. [108]. The more fibers available in this region to hinder the microcracking strain in advance of the developing crack-front, the stronger the matrix will be and the better equipped it will be to delay development of the peak load. The toughening effect of fibers on the rising-load side of the Load-CMOD curve will be further discussed in paragraph 6.2.2.4 on toughness indices of FRC VHSC.

One additional property that these experiments set out to explore was test variability. There was high variability in the within-mixture load-CMOD due to the differences in distribution of fibers throughout the cross section of each beam. However, the variability in the mixture-to-mixture results was almost nonexistent as can be seen in the comparison of the averages of the individual Load-CMOD curves from each mixture shown in Figure 6.7.

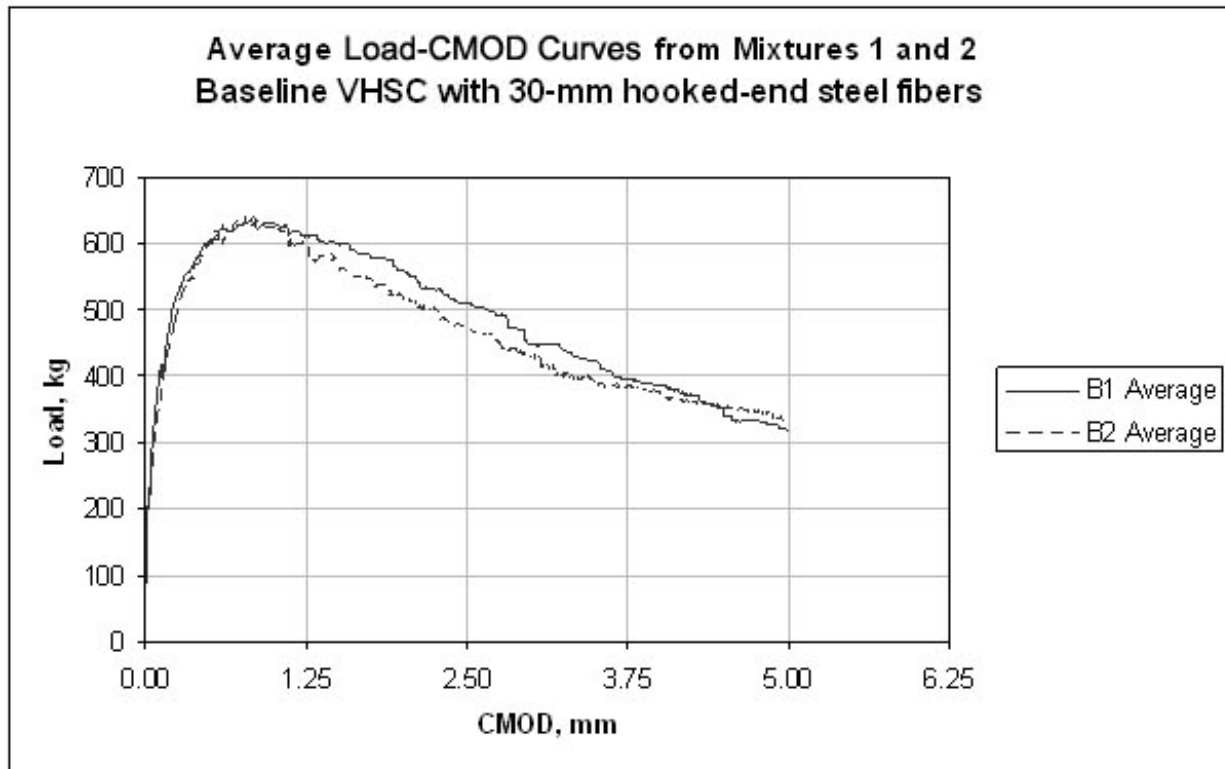


Figure 6.7 Comparison of the average Load-CMOD curves across mixtures.

6.2.2.4 Discussion of toughness indices results

The same set of eight load-CMOD tests used to calculate the fracture toughness of the fiber-reinforced VHSC was used to study the toughness indices (TI) of the material. The techniques established for calculating fracture toughness, K_{Ic} , have received greater focus in the research-literature than those used for calculating the TI and, as such, the fracture-toughness techniques are more reproducible and better suited for comparison among fracture-toughness studies. Techniques for determining the TI, on the other hand, are less standardized, often rely on guesswork to establish critical parameters, and use different criteria to define the different indices. However, if calculated correctly the TI can reveal information on the distribution of toughening energy throughout the Load-CMOD curve.

Several researchers have reviewed the various techniques used to determine fiber-reinforced concrete TI [8, 108, 109]. The better-known techniques from this group include: the ACI 544 Toughness index [110], the ASTM C 1018 Toughness Index [111] and the JSCE SF-4 method [109]. All these methods create toughness indices based on a ratio of the area under the load-deflection (or load-CMOD) curve to some multiple of the first-crack deflection, divided by the area under the curve to the first crack deflection. Those who have reviewed the methods find that it is difficult to accurately establish where first-crack occurs and as a result suggest that the deflection at the peak-load be used to indicate first-crack deflection.

Mindess et al. [112] published a mathematical technique to estimate when first-crack in fiber-reinforced concrete occurs. They based the first-crack location on the rising portion of the P- δ curve, between the values of 45 and 70% of maximum load, where the slope of the curve (measured over at least 20 data points and a deflection of at least 0.01 mm) is at least 5% less than the average slope between the 45 and 70% peak load values. This method, which satisfies the criteria of ASTM C 1018 [111], is straight forward to calculate and is within the non-linear portion of the rising P- δ curve. In situations where the location of the first-crack load and deflection is not obvious it is a more accurate technique for estimating the first-crack load than using the peak-load which introduces obvious errors. This technique was used for calculating the toughness indices of fiber-reinforced VHSC.

Five TIs, I_5 , I_{10} , I_{20} , I_{40} , and I_{80} were calculated for each of the eight beams. They were defined as

$$I_n = \frac{A_{In}}{A_{first-crack}} \quad (6.4)$$

where $A_{first-crack}$ is defined as the area under the load-CMOD curve from δ_0 to $\delta_{first-crack}$, and A_{In} is defined as the area under the load-CMOD curve from δ_0 to δ_{In} , $n = 5, 10, 20, 40,$ and 80 . The toughness index, I_n , is based on area ratios of a perfectly elasto-plastic material in which δ_{In} is $(n+1)/2$ times $\delta_{first-crack}$. For example, δ_{110} is 5.5 times $\delta_{first-crack}$. These indices were applied to the load-CMOD curves shown in Figure 6.8. The tabular results are shown in Table 6.4.

The dotted lines and the toughness index above each line in Figure 6.8 show the right-hand edge of the area under the load-CMOD curve covered by the particular fracture toughness index. The left-most dotted line in each curve demarks the load and CMOD at first-crack as calculated by Mindess. The technique provides plausible load-deflection points for the initiation of first-crack. For all eight curves, the load at first-crack falls between 45 and 60 % of peak-load. This is within the range in which the typical load-deflection curve begins to deviate from linearity indicating cracking in the matrix.

The subscript on each TI, 5, 10, 20 etc., are so named because a purely elasto-plastic material would produce a TI equal to the value of the subscript [108]. The averages of the eight TIs at each index level in Table 6.4 are $I_5 = 4.21$, $I_{10} = 9.50$, $I_{20} = 21.46$, $I_{40} = 44.14$, $I_{80} = 83.36$ and mimic this metric very closely. This is not to say that the FRC VHSC is an elasto-plastic material, it is merely mentioned to point out that the choice of first crack deflections and the TIs calculated using Mindess' formula for establishing first-crack is a better solution than choosing the peak-load to calculate the indices. Using the area under the curve to the peak-load as the denominator term in these eight experiments would only allow calculation of TIs I_5 and I_{10} before reaching the full deformation of the test.

The TIs give a measure of energy consumed along the Load-CMOD curve in relationship to the energy consumed to produce a first-crack. In each of the graphs in Figure 6.8, the first

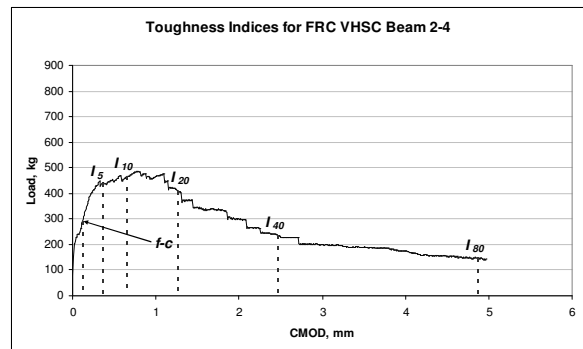
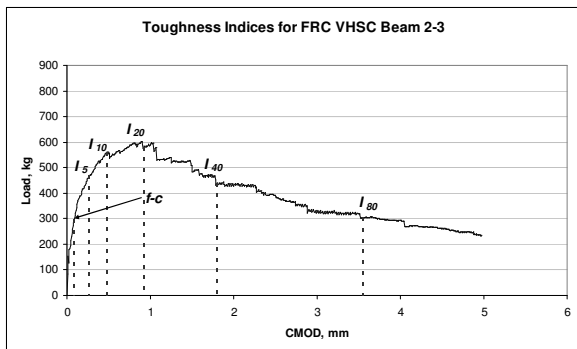
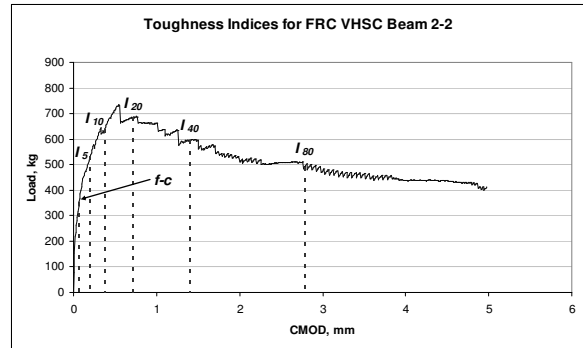
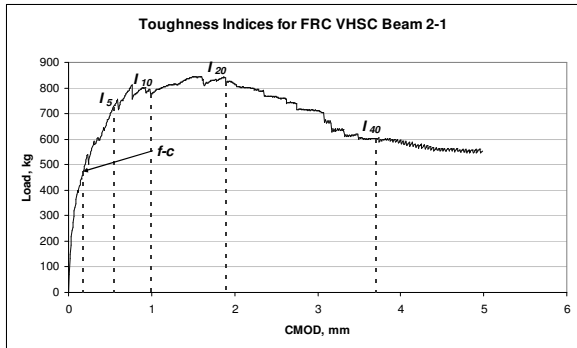
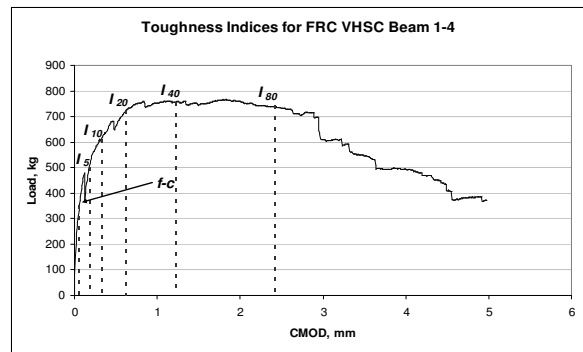
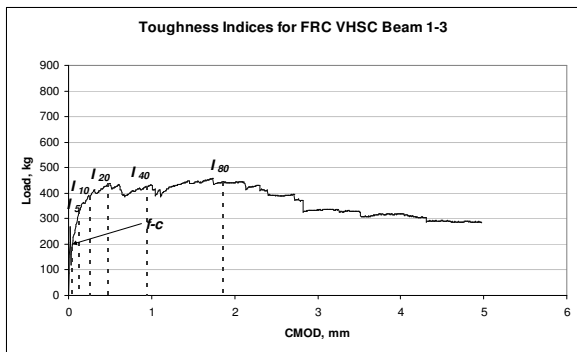
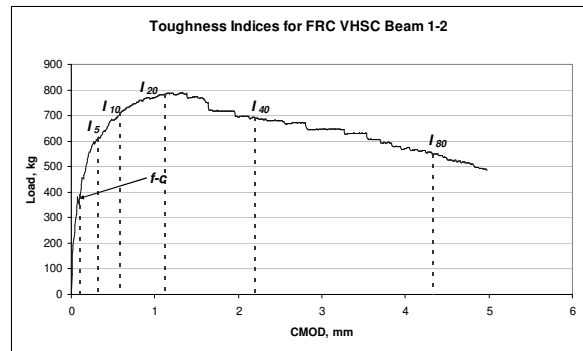
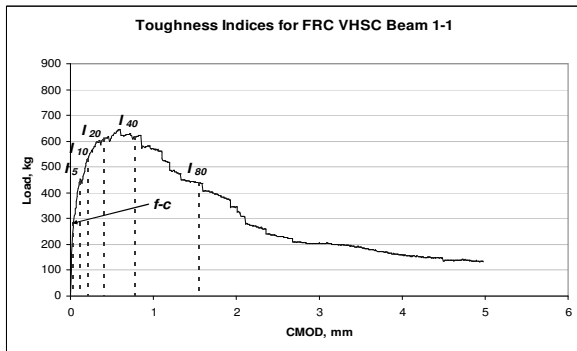


Figure 6.8 FRC VHSC load-CMOD curves

three TIs (I_5 , I_{10} , and I_{20}), all occur on the rising portion of the load-CMOD curve, the I_{20} index occurring close to peak load. This tells us that the steel fibers consume about 20 times the energy required to produce first-crack in the process of reaching peak load. Also, in the post-peak region of the curve, the steel fibers consume $I_{80} - I_{20} = I_{60}$ or about 60 times the energy required to produce first-crack. These data are information not provided by K_{Ic} .

Comparison of the average Load-CMOD curves for the FRC VHSC beams with the average of the Load-CMOD curves for the unreinforced VHSC beams in Figure 6.9 shows the energy consuming contribution of the steel fibers. The area beneath the average Load-CMOD curve for the steel-fiber VHSC (average of all eight beams) was 23.21 N/m, while the average area under the Load-CMOD curves for the unreinforced VHSC was 0.115 N/m. The energy consumed by the fiber-reinforced beams was $23.21/0.115 = 202.5$ times that of the same beams without the fibers.

The TIs for the average of the three unreinforced VHSC beams were: $I_5 = 2.95$, $I_{10} = 3.81$, and $I_{20} = 4.23$, much less energy consumptive than the FRC VHSC. For the unreinforced VHSC, Mindess' first-crack location technique did not find any significant deviation from linearity in the slope of the curve anywhere along the rising portion of the graph. This reinforces the finding that because of its high strength and brittle nature, the load-deflection curve of unreinforced VHSC tends to be nearly linear to peak load. As a result, the peak-load was used as the first-crack index in the TIs reported for these beams because a suitable pre-peak, first-crack location could not be found.

Accurate comparison of the FRC VHSC TIs with data from the literature was not easy. Many of the studies used a different method of calculating the TI or the volume of fibers was different from the 3% used in VHSC or the specimen size was different. In those studies that did

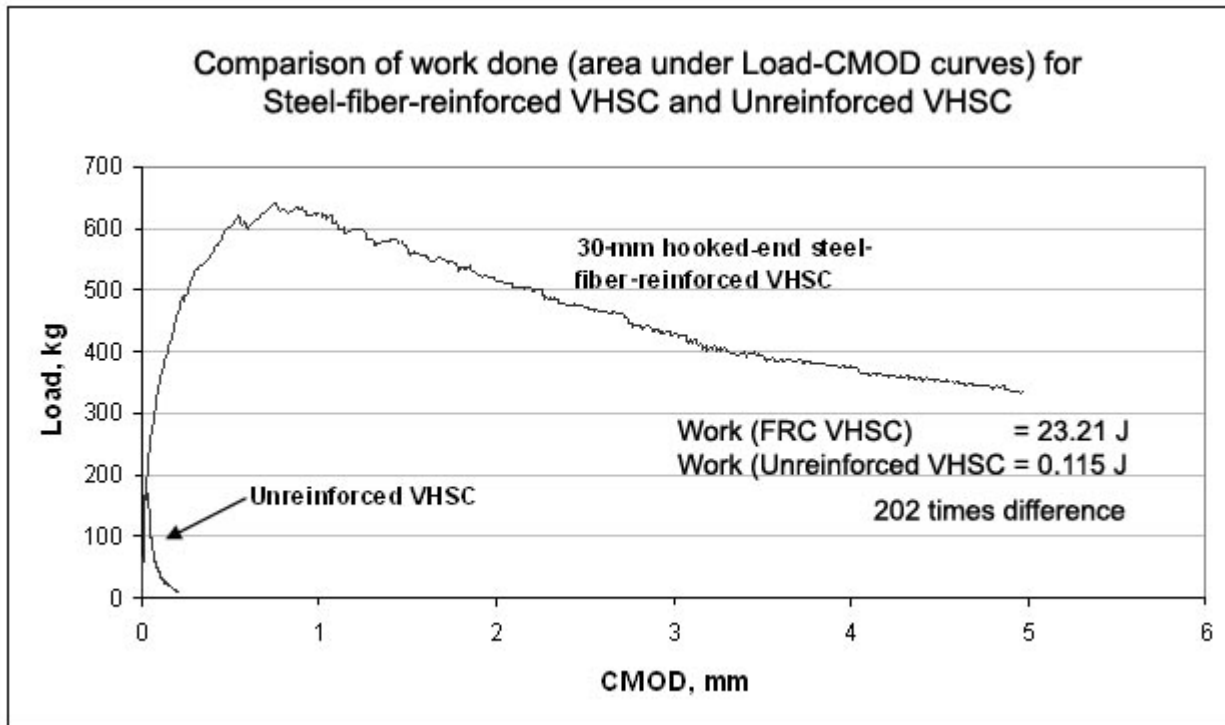


Figure 6.9 Comparison of work done for unreinforced and FRC VHSC.

use ASTM C 1018, the peak-load was used as the first-crack index [8, 108]. In others the strength of the concrete was significantly below that of the VHSC. Song and Huang [113] measured TIs of high-strength fiber-reinforced concrete beams, 150 by 150 by 530-mm made from FRC with compressive strengths between 85 and 98 MPa. They used ASTM C 1018 and estimated the first crack strength properly. Their highest volume of fibers used was 2% by volume for which they reported indices $I_5 = 6.5$, $I_{10} = 11.8$, and $I_{30} = 20.6$. The first two indices are much the same as the VHSC values, but at the I_{30} index the value was comparable to the VHSC I_{20} value. Jeng et al. [114] also used the ASTM C 1018 method and measured first-crack load and deformation when calculating the toughness indices of field-cut fiber-reinforced shotcrete beams. Their toughness beams were 150 by 150 by 600 mm, the various shotcrete specimens contained four different kinds of steel, three volumes of steel up to 2.5%, three

percentages of silica fume, and three different cement contents. They reported TIs ranging from 3.9 to 4.4 for I_5 , 6.5 to 8.4 for I_{10} , 9.4 to 13.6 for I_{20} , 12.0 to 18.9 for I_{30} , and 16.4 to 28.5 for I_{50} . As with the toughness results of Song and Huang, the I_5 and I_{10} indices were comparable with those of the VHSC but higher indices were considerably lower. Because there were so many variables involved in this work, it is hard to say what was responsible for the differences at higher toughness indices. Because the higher indices reflect energy consumption in the post-peak region of the load-deflection curve, any one of their material variables could have an effect on the bond and pullout resistance of the fibers.

6.2.3 Fracture toughness of VHSC with microspheres

In chapter 5 a study was described regarding the effects of the addition of ceramic microspheres on the compressive strength of the basic VHSC mixture. To complement that set of experiments, a series of fracture toughness experiments was conducted on the same materials to study the contribution of the microspheres to toughness.

6.2.3.1 Experimental Procedures

The set of experimental procedures outlined in paragraph 6.2.1.1 was used for the fracture toughness beams cast for these experiments. Two variations were made to the experimental procedures to accommodate these mixtures. First, the mixtures included the 3M Corporation G-800 microspheres and second, the w/c was adjusted to keep the w/s at a constant 0.0835. There were three levels of microspheres studied in the experiment, 0, 6, and 12% by volume of concrete and three beams were cast at each level of microspheres along with compressive strength cubes for heat-cured testing. The change in w/c to accommodate the constant w/s resulted in a 0.22 w/c for the 0% microspheres, a 0.23 w/c for the 6% microspheres, and a 0.25 w/c for the 12% microspheres.

6.2.3.2 Results for the microsphere toughness studies

The results of the compressive strength of the cubes accompanying this experiment are presented in Table 6.5. The fracture toughness results are given in two tables, Table 6.6 presenting pertinent beam property calculations, and Table 6.7 presenting the fracture toughness calculations. Sample calculations describing the method of computing these values can be found in Appendix C.

Table 6.5 Heat cured compressive strength for microsphere toughness experiments

Beam series	Compressive strength, MPa
B0	172.0
B6	202.8
B12	204.8

Table 6.6 Beam property calculations for VHSC microsphere toughness studies

Beam	Percent μ -spheres	P_{max} kg	a_o mm	a_c mm	E GPa	C_i mm/kg	C_u mm/kg
B0-1	0	175.82	26.35	27.36	44.62	9.2666E-05	9.9278E-05
B0-2	0	182.21	26.26	27.11	50.51	8.0910E-05	8.5775E-05
B0-3	0	<u>194.73</u>	<u>26.21</u>	<u>26.88</u>	<u>49.91</u>	<u>8.3060E-05</u>	<u>8.7002E-05</u>
Avg. B0		184.25	26.27	27.12	48.35	8.5545E-05	9.0685E-05
B6-1	6	181.30	26.00	26.61	40.52	9.9739E-05	1.0399E-04
B6-2	6	168.29	25.67	26.43	38.73	1.1152E-04	1.1763E-04
B6-3	6	<u>196.82</u>	<u>26.00</u>	<u>27.10</u>	<u>43.70</u>	<u>9.6182E-05</u>	<u>1.0383E-04</u>
Avg. B6		182.14	25.89	26.71	40.98	1.0248E-04	1.0848E-04
B12-1	12	173.00	25.84	26.72	48.01	8.8344E-05	9.3935E-05
B12-2	12	180.26	26.00	26.46	47.35	8.9824E-05	9.2759E-05
B12-3	12	<u>172.10</u>	<u>26.01</u>	<u>26.76</u>	<u>50.26</u>	<u>8.3631E-05</u>	<u>8.8078E-05</u>
Avg. B12		175.12	25.95	26.65	48.54	8.7266E-05	9.1591E-05

6.2.3.3 Discussion

The results of the heat cured compressive strength tests were similar to the G-800 microsphere strength tests of the first and second rounds discussed in chapter 5, paragraph 5.7.2.4 (there was also a third round in that study comparing G-800 to G-200 microspheres

Table 6.7 Fracture toughness calculations for VHSC with microspheres

Beam	Percent μ-spheres	$K_{Ic}, MPa \sqrt{m}$	CTOD_c, mm	G_f, N/m
B0-1	0	1.02	0.0024	23.31
B0-2	0	1.04	0.0020	21.54
B0-3	0	<u>1.12</u>	<u>0.0019</u>	<u>25.19</u>
Avg. B0		1.06	0.0021	23.34
B6-1	6	1.03	0.0020	26.03
B6-2	6	1.02	0.0023	26.89
B6-3	6	<u>1.17</u>	<u>0.0029</u>	<u>31.25</u>
Avg. B6		1.07	0.0024	28.06
B12-1	12	1.03	0.0021	22.17
B12-2	12	1.06	0.0016	23.76
B12-3	12	<u>1.01</u>	<u>0.0018</u>	<u>20.31</u>
Avg. B12		1.03	0.0018	22.08

not presented here). Figure 6.10 shows the current strength data (fourth round) along with the first and second round results. The first round data, which held w/c constant, show there was an increase in strength up to 6% microspheres. The second round data which held w/s constant and varied w/c showed negligible strength gain with increasing % microspheres. The current fourth round data, which also held w/s constant and varied w/c, shows strength increasing to 6% and then remaining the same at 12%. The current round of compressive strength data supports the conclusion that the G-800 microspheres add a modest increase in strength up to 6 volume % of microspheres.

The fracture toughness calculations resulting from these experiments indicate that the microspheres also have a small role in increasing the toughness of the VHSC. The majority of trends in the data in Tables 6.6 and 6.7 provide supporting evidence that the microspheres improve the matrix toughness up to a volume percentage of 6 %. Figure 6.11 a and b presents plots of the average values of fracture toughness, K_{Ic} , and fracture energy, G_f , respectively,

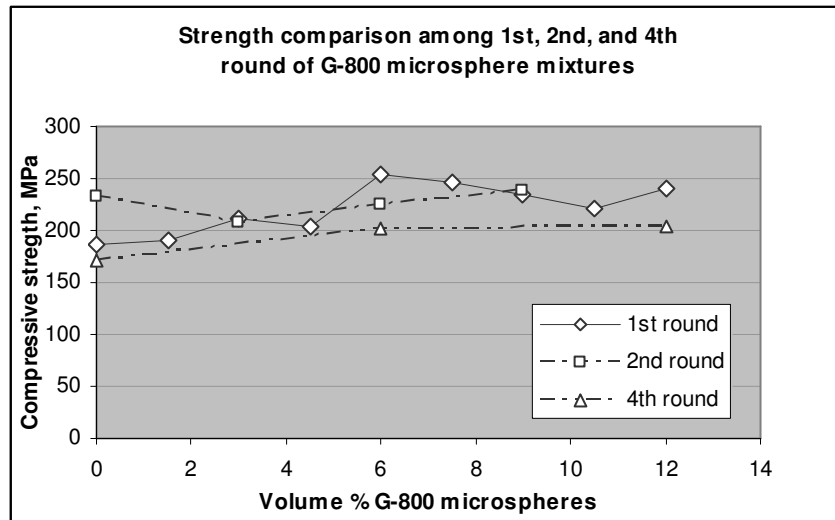


Figure 6.10 Compressive strength of current microsphere mixtures compared to previous results.

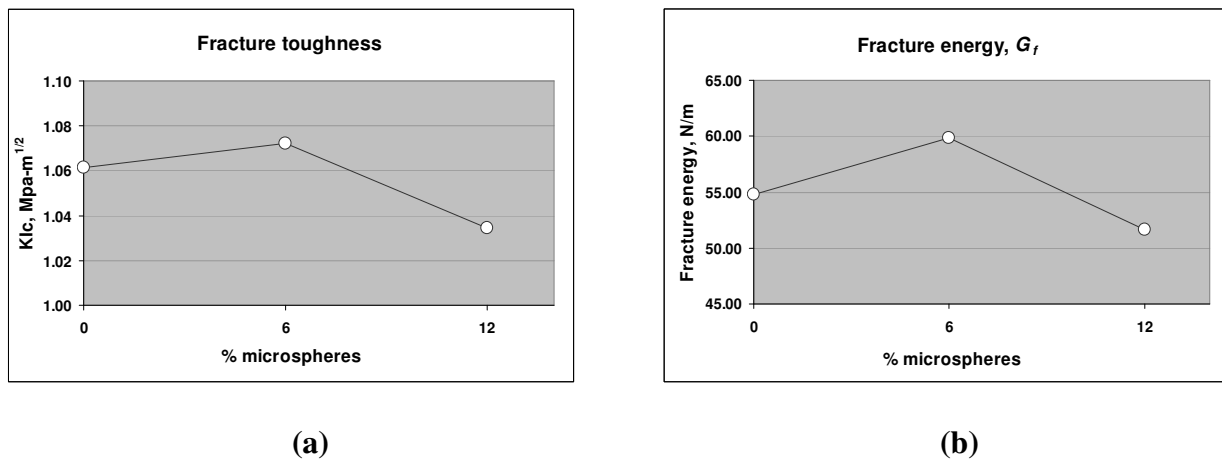


Figure 6.11 Fracture properties of VHSC with G 800 microspheres.
(a) Fracture toughness and (b) fracture energy

showing the trend of a small increase in toughness with increase of microspheres up to 6%. In comparison of fracture toughness of unreinforced VHSC, the fracture toughness of VHSC containing 6% G-800 microspheres increased 1%, providing a negligible increase in toughness.

The small toughening value of the microspheres comes from their strength, their slightly pozzolanic nature, and their ability to act as crack-trapping, crack-tip blunting, and aggregate

bridging mechanisms in the wake process zone. Because they are so small and are distributed everywhere throughout the paste, they are able to intercept microcracks and function as crack trapping and crack-tip blunting mechanisms. Their high compressive strength (greater than 400 MPa) and pozzolanic nature, allow them to act as strong aggregates with good interfacial transition zone properties allowing them to function as crack-face pinning toughening mechanisms.

It is not immediately clear why the strength and toughness of the beams decrease beyond the 6% volume capacity. The extremely small size and large surface area of the microspheres would imply a water demand that would lower the water available for hydration and potentially decreases the strength. This is reflected in the reduction in flow number with increase in percent microsphere shown in Figure 6.12.

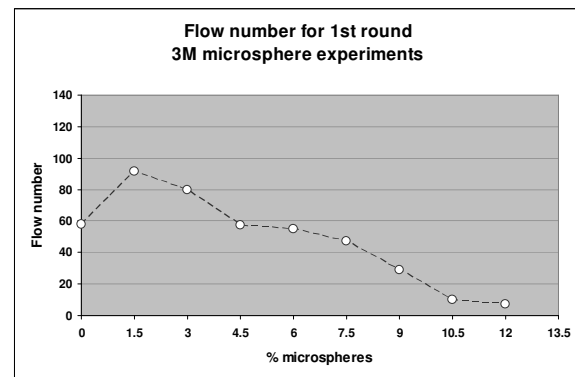


Figure 6.12 1st round G-800 flow numbers

6.3 Summary

Chapter 6 is the concluding chapter on the engineering choices that can improve the properties of VHSC. This chapter dealt with improving properties that deteriorate in the wake of primary properties that were improved. Specifically, when VHSC strength is significantly enhanced it becomes brittle and its ductility suffers. To restore some of the ductility, efforts to counteract the brittleness must be engineered into the material's fabric. This involves understanding and employing toughening mechanisms.

The first part of the chapter gave a comprehensive look at toughening mechanisms that may exist in concrete materials and where and how they act to consume fracture energy. Here

also much of literature review III on toughness was addressed. Following the review of toughening mechanisms, a study of the fracture toughness of unreinforced VHSC was documented to establish the baseline level of material toughness. The Two Parameter Fracture Model of Jenq and Shah [105] was used to establish fracture parameters. Toughness parameters of critical stress intensity factor, critical crack mouth opening displacement, and fracture energy were calculated.

In the next section, the primary method of providing toughness to VHSC was addressed. An experiment was conducted to establish the level of toughness provided by hooked-ended, 30-mm-long distributed, steel fiber reinforcement. Two identical mixtures were made to establish fracture toughness properties and to study within batch and batch-to-batch variations. The results of these experiments were compared to the unreinforced VHSC. For these experiments, fracture toughness K_{Ic} , and the ASTM C 1018 toughness indices were calculated. Finally, the toughness of VHSC containing ceramic microspheres was studied and compared to unreinforced VHSC to document their level of toughening the material.

6.4 Conclusions

6.4.1 Unreinforced VHSC toughness conclusions

An experiment consisting of three unreinforced, notched, fracture-toughness beams were cast and tested under crack-mouth-opening displacement control to produce load-CMOD curves for each specimen. Toughness parameters of K_{Ic} and $CMOD_c$ were calculated using the TPFM and evaluating the unloading compliance by a mathematical technique presented by Navalurkar et al. [106]. G_f was calculated from the fracture toughness and the material modulus of elasticity. The following conclusions can be made from these studies:

- 1) The mathematical technique used by Navalurkar uses the premise that the stiffness K for the concrete beam will decrease as the notched crack propagates, and the assumption is made that the unloading stiffness (inverse of the unloading compliance) decreases in a linear manner with the increase in displacement along the descending portion of the load-CMOD curve. Values of C_u calculated in this manner were reasonable and produced values of critical effective elastic crack length that were believable. It is concluded that this technique is useful and reasonable as a substitute when collecting unloading compliance data are not possible.
- 2) Values of K_{Ic} and G_f calculated for the unreinforced VHSC fell in the mid-portion of the range of published values for concretes with wide variations in strength. For these same data sets, the calculated $CMOD_c$ for VHSC fell at the extreme low end of the data range. From these values it is concluded that the fracture toughness of VHSC is not dissimilar to concrete materials much weaker than itself; and because the CMOD (which is linearly related to the CTOD, a measure of the plastic fracture zone in front of the crack tip) is very small, this signifies that the FPZ of the VHSC is also small and that VHSC would likely respond reasonably to analysis by LEFM.

6.4.2 Steel-fiber-reinforced VHSC toughness conclusions

From the results presented in paragraph 6.2.2.2 and the discussion in paragraph 6.2.2.3, the following conclusions about fracture toughness of steel fiber-reinforced VHSC can be made:

- 1) The Load-CMOD curves for each beam within its batch presented large variations in peak-load and shape of the pre-peak rising portion and post-peak

descending portion of the curves. It can be concluded there can be wide within-batch variations of individual beam fracture toughness values.

However, when the within batch results were combined and averaged to produce an average fracture-toughness value for each batch, the load-CMOD curves from each batch plotted on top of each other prompting the conclusion that the batch-to-batch variation was very small.

- 2) The within batch variation of the load-CMOD curves were studied by counting the number of fibers crossing the fracture plane in each of four quadrants that made up the fractured ligament of the beam and relating these numbers of fibers to the magnitude and slope of the load-CMOD curve. It can be concluded from these observations that a direct relationship exists between the number of fibers in the quadrant representing the front half of the crack wake zone (that portion of the crack wake zone where fibers are still actively pulling out of the matrix) and the magnitude and slope of the portion of the load-CMOD curve represented by this quadrant.
- 3) Conclusion 2 leads to a further conclusion that in small, laboratory fracture-testing beams where the smallest cross-section dimension of the beam is equal to or less than the length of the fiber being used, that directional fiber orientation can result that will have an effect on the fracture toughness. Because of directional fiber orientation and distribution, it should not be assumed that the distribution of the fibers across the fracture ligament of the beam will be uniform and randomly oriented.

- 4) The parameters most often used to measure the toughness of fiber-reinforced concrete are the ASTM C 1018 toughness indices. These indices call for estimating the displacement at first-cracking strength to establish a denominator value that defines the magnitude of each of the indices. Most research efforts consider finding this first-crack displacement troublesome and recommend the use of the peak-load to represent first-crack displacement. Mindess et al. [112] have proposed a mathematical relationship that estimates the first-crack displacement a characteristic distance along the upper half of the pre-peak load-CMOD curve. Both methods were calculated under these experiments and it is concluded that using the peak-load as indicator of first-crack is inaccurate and produces toughness indices that are lower than true values. Further, while the Mindess calculation is also an estimate, it produces toughness indices that are close to the ratios of the elasto-plastic model these indices were designed around and is a more accurate estimate of the toughness of fiber-reinforced VHSC.
- 5) From the data collected and toughness indices calculated in these experiments, it can be said that for VHSC reinforced with 3.1% steel fibers the toughness indices up to I_{20} occurred before the peak load. This indicated that the fibers consumed 20 times the first-crack energy in reaching peak load and that toughness indices up to I_{80} could be calculated before the test completed. This also indicates that at least 60 times the energy expended to reach first-crack was consumed in the post-peak, strain softening portion of the load-CMOD curve.

- 6) When the Load-CMOD curves for the eight fiber-reinforced fracture toughness beams were averaged, and the energy consumed as work calculated from these curves it was found that in comparison to unreinforced VHSC, 202 times the energy was consumed demonstrating the toughness energy provided by the steel fibers.

6.4.3 VHSC with microspheres toughness conclusions

From the results presented in paragraph 6.2.3.2 and the discussion in paragraph 6.2.3.3, the following conclusions about toughness from ceramic microspheres in VHSC can be made:

- 1) The techniques used to apply the TPFM to the unreinforced VHSC were used to calculate the beam properties in Table 6.6 and the fracture toughness values in Table 6.7 for three sets of beams containing 0, 6, and 12% of G-800 ceramic microspheres. From these data it can be stated that the fracture parameters of K_{Ic} , $CMOD_c$, and G_f increased as the loading of microfibers increased from 0 to 6% and with this increase it can be concluded that the microspheres provided a very modest 1% level of increased toughness.
- 2) It can be further concluded that the toughening value of the microspheres comes from their strength, their slightly pozzolanic nature, and their ability to act as crack-trapping, crack-tip blunting, and aggregate bridging mechanisms in the wake process zone, crack deflection mechanisms in the crack tip zone, and microcrack shielding mechanisms in the crack frontal zone.

Chapter 7 FRANGIBLE CONCRETE

7.1 Introduction

It was stated in the problem statement to this dissertation that the purpose of the work was to advance logical thought processes to reliably obtain specific material properties in the concrete produced. Up to this point, those thought processes have been geared to producing high-density, very-high-strength concrete. Those same thought processes can be directed to address properties at the opposite end of the concrete material spectrum. The military often has unique needs and applications for concrete materials. Where applications in the civil works environment are generally geared towards structural uses such as buildings, roadways, and hydraulic structures, military interests are more often focused on the use of concrete for defensive applications such as blast and penetration resistant structures. Very-high-strength concrete used in this capacity can be an effective and economical means of providing troops in the field with protection from shell fragments and small caliber weapons. However, when concrete itself is subjected to blast loading the pieces it breaks into can become projectiles that are lethal. This is a problem that resides at the other end of the spectrum. How can we make a structural concrete that will not become a shrapnel problem in dynamic blast-loading situations? The remainder of this chapter is devoted to describing efforts to solve this unique problem of developing concrete with high-performance properties of strength and frangibility.

7.2 Statement of problem and challenge

The problem arises when one considers the placement and detonation of a terrorist truck bomb. Security personnel establish perimeter security barriers around facilities that could be targets of terrorists. The security barriers, meant to prevent unauthorized vehicular access inside the perimeter, are often concrete block walls that are built far enough away from the facility to

render the force of blast from outside the perimeter ineffective in destroying the facility. These walls are also built tall enough to prevent terrorists from scaling them. The problem with this solution is that if the truck bomb is left on the outside of the standoff wall and detonated, the force of the blast will fail the block wall and send lethal sized pieces of concrete block into the facility. This makes the solution part of the problem.

Engineers from the ERDC were challenged to address this problem and develop a concrete material that would have sufficient load-carrying capacity under static loading conditions to perform as a typical standoff wall but that would break into non-lethal sized pieces when impacted by a blast force. The objective was to design a specialty concrete that would break up into pieces that may cut and wound, but would not be large enough to kill.

7.3 Background, and first series of experiments^{III}

The concept of a material that, on the one hand, has acceptable strength and, on the other, is expected to break into small particles is foreign to most engineering thought. It is the equivalent of asking the material to be weak and strong at the same time. Original thinking was clearly needed to arrive at a solution, and a materials science approach to the problem was adopted. Thinking on the microstructure level was critical to linking the properties and the processes necessary to achieve such a material. Understanding how the processes that can be applied (controlling the relative humidity, the temperature, the types of additives, and the component materials) affect the microstructure and how changes to the microstructure (modifying pore structure, affecting phase composition, creating microcracks) affect the properties (strength and fragility) provides a better knowledge of the desired material and a solid approach to achieving the desired properties.

^{III} The work of developing a slag/cement mixture summarized in this section is the work of Northwestern University done under contract to the ERDC. It is included for clarity of related work in this dissertation.

Following the above thinking, Jennings and Thomas found that for a material to be weak and strong at the same time, a network of purposefully developed microcracks had to be built into the matrix. The microcracks should be uniformly distributed throughout the matrix and remain small. While these microcracks would marginally reduce the physical properties of the concrete, they would not be structurally connected and a sufficient amount of the material's strength would remain. At the same time, the network of microcracks would be poised to complete the fracture process under application of a dynamic load, breaking the matrix into small pieces.

To achieve this network of microcracks, Jennings and Thomas realized drying shrinkage cracks must be engineered into the structure of the C-S-H. This can be accomplished by taking advantage of the network of water-filled channels in the C-S-H. If the water is driven out of these channels through heating the freshly set paste, large shrinkage stresses will occur that will produce the network of microcracks needed to create the weak and strong material desired.

7.3.1 Laboratory experimental development – phase 1

The research team organized the work into phases choosing variables they thought would influence the development of microcracks in the paste. For the first phase they chose eight variables at up to three levels per variable as shown in Table 7.1. They entered these variables into an experimental design optimization program that recommended 18 experiments be conducted. Specimens cast from the 18 mixtures were tested by collecting compressive strength from 50.8- by 101.6-mm cylinders and simulating a blast impact by dropping a 6.4 kg-cylinder from a height of 4.3 m through a tube to impact a 50.8- by 50.8-mm cylinder. Frangibility was determined by collecting and analyzing resulting fragments.

Table 7.1 Type and levels of the variables in the phase 1 experiments

Variable	Levels	Comments
% portland cement	0, 10, and 25	Remainder of binder is slag
Type of slag	1 or 2	Slags were grade 120
Sand/binder ratio	0 and 0.5	Sand may have an important effect on failure mode
Water/binder ratio	0.35 and 0.5	A low and high w/b would make a stiff or liquid paste
Chemical activator	Either none or 2% CaCl ₂	CaCl ₂ is known to increase OPC drying shrinkage
Curing time	7 and 28 days	Longer curing promotes more hydration and greater strength
Curing temperature	20 and 60 °C	Does higher temperature affect drying shrinkage?
Drying treatment	24h@110 °C or 50%RH@20 °C	Does speed of drying affect shrinkage?

7.3.2 Results from laboratory development – phase 1

The findings from the phase 1 matrix revealed that overall, the frangibility of specimens was good and their compressive strength experiments compared adequately to the compressive strength of conventional concrete block. Adding OPC to the slag reduced fragmentation and increased strength as did increasing the sand/binder ratio. Further, the elevated curing temperature reduced strength and oven drying increased it.

7.3.3 Laboratory experimental development - phase 2

Jennings and Thomas used the results of phase 1 to modify the input variables for phase 2. Three variables were dropped from the design and one was added and the levels in several variables were increased. The type of slag was removed because both slags behaved similarly. In phase 1, the higher w/b gave better frangibility so it was set as a property and removed from the experimentation. Additionally, the drying treatment was removed from the matrix and the 110 °C for 24 hours drying procedure was adopted as the default. Additional changes to the phase 2 matrix included: adding a 3-day curing time level, adding an 80 °C curing temperature level,

replacing 2% CaCl_2 with 2% NaOH , adjusting the % OPC downward, creating a new variable of sand type (coarse or fine), and measuring the amount of bound water in conjunction with the drying treatment.

Phase 2 experimental procedure was similar to phase 1 with the exception of measurement of the bound water which was found to be an important variable because of its relationship to the degree of hydration of the matrix. Phase 2 experimental results reflected lower strength than phase 1 and the fragmentation was higher largely due to the use of less portland cement and sand. Also, results showed that specimens tested wet had higher strength and lower fragmentation than specimens tested dry, due in large part to the opportunity for those tested wet to rehydrate.

7.4 ERDC preliminary blast-load studies on the 18 mixtures of phase 2

7.4.1 Background

Because the contractor did not have the capability to conduct any blast loading on the 18 mixtures he made, the ERDC conducted a supplemental set of experiments on the phase 2 mixtures, making use of a confined blast chamber in its inventory, Figure 7.1. The blast chamber is capable of directing a confined blast force of 689 kPa against a plane approximately 1.22 m in diameter. This set of experiments would serve to compare the damage to the slag mixtures from a simulated blast and failure by impact. It would also help rank the 18 mixtures from most to least frangible.



Figure 7.1 1.22-m blast chamber

7.4.2 Experimental procedures

Eighteen mixtures of phase 2 with varying amounts of slag, cement, sand, and activator were cast from February 28 to March 16, 2003. Enough mortar was made in each mixture to cast one panel 152.4 mm on a side by 19 mm thick and three cubes, 50.8 mm on a side. The mixture details are given in Table 7.2. In this suite of experiments, the term binder refers to a mixture of slag and OPC. Where a mixture contained a given wt % of OPC, the remaining wt % (100% - wt % of OPC) was slag. Table 7.2 also shows the curing environment of each mixture. Subsequent to curing, each of the panels and cubes was subjected to 72 hours of hot air drying at 101 °C. The curing environments and hot air drying were designed to enhance the fracturing of the mixtures.

Table 7.2 Experimental design for matrix 2

Experiment number	% OPC	Sand/binder ratio	Sand type	NaOH activator	Cure temp.(°C)	Cure time (days)
1	10	0.25	coarse	2%	80	21
2	5	0.25	fine	2%	80	21
3	0	0.12	coarse	2%	60	21
4	5	0.12	coarse	no	60	21
5	10	0	n/a	2%	20	21
6	0	0	n/a	no	20	21
7	5	0.25	fine	no	80	7
8	10	0.25	coarse	no	80	7
9	5	0.12	coarse	2%	60	7
10	0	0.12	fine	no	60	7
11	10	0	n/a	2%	20	7
12	0	0	n/a	2%	20	7
13	0	0.25	coarse	2%	80	3
14	0	0.25	fine	no	80	3
15	10	0.12	coarse	no	60	3
16	10	0.12	fine	2%	60	3
17	5	0	n/a	2%	20	3
18	5	0	n/a	no	20	3

After drying, the specimens were stored in controlled laboratory air conditions until they were tested in the 1.22-m diameter blast chamber on September 9, 2003. At the date of blast testing, the specimens were approximately 6 months old.

7.4.3 Blast environment

A frame designed to hold the specimens inside the blast chamber, Figure 7.2, was made from welded 25.4 mm. angle iron and had 24 compartments to house specimens. Separate canisters beneath each compartment were installed to capture the fragments from each specimen. In this test there were 18 specimens, 2 conventional concrete specimens, 2 compartments housing steel plates with a pressure sensor mounted in their centers, and 2 compartments filled with wood to prevent blast pressures from going around the specimens. Sixteen

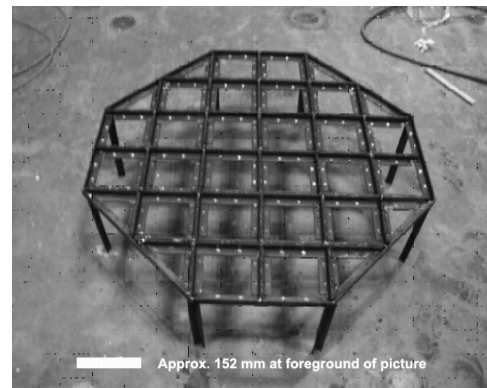


Figure 7.2 Specimen housing frame

hundred grains of pentaerythritol tetranitrate (PETN) (4 ropes of 50 grain detonation cord, each 1.2 m long in each of 2 baffle tubes (see Figure 7.1)) were used to affect a peak pressure of 517 kPa at the surface of the specimens. The peak pressure, measured by pressure sensors during the test, was between 420 and 655 kPa. The gage reading 655 kPa failed during the test and showed erratic reading before failure, calling into question the validity of the 655-kPa readings. The remaining gage peaked at 9 milliseconds and maintained greater than 207 kPa for 500 milliseconds.

7.4.4 Blast chamber results

The visual results of the test after opening the blast chamber and cleaning the surface of the specimens are shown in Figure 7.3. Of the 18 specimens, 14 failed under the blast shock and

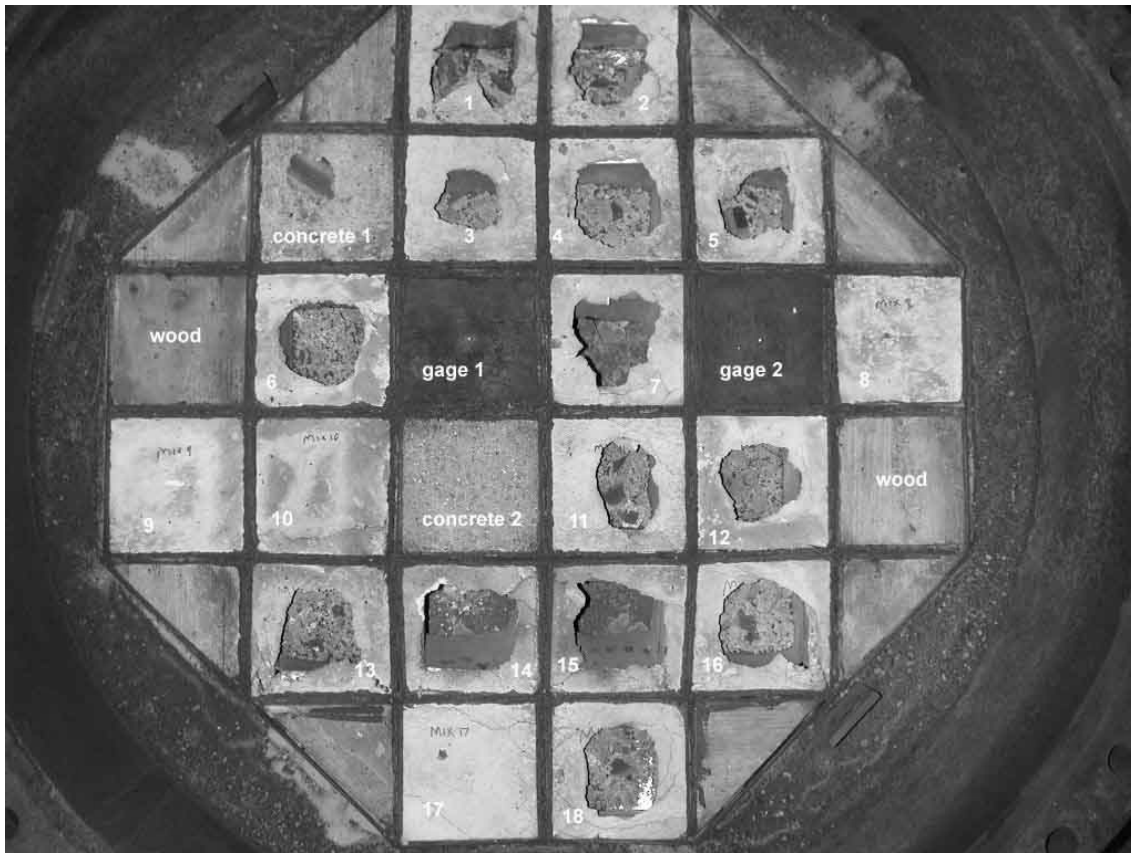


Figure 7.3 Condition of the specimens after the blast. Each cell is 152.4 mm on a side.

the remaining 4 cracked but did not fail (numbers 8, 9, 10, and 17). Neither of the two conventional concrete specimens failed. Of the 14 specimens that failed, data from 3 experiments (numbers 7, 14, and 15) were lost because the blast failed the bottom of the metal canister designed to catch the fragments and the fragments were scattered to the bottom of the blast chamber. The fragments from the remaining mixtures were isolated in individual canisters mounted below the specimens.

7.4.5 Blast load analysis

As shown in figure 7.3, the blast fractured only the center portion of each panel because the edges were supported by the flange of the angle iron. Only the particles that were collected in the canisters were included in the analysis. These particles were collected, and sieved through a

set of sieves for separating sand-size material (#4 sieve (4.75mm), #8 (2.38mm), #16 (1.76mm), #30 (0.60mm), #60 (0.3mm), #100 (0.1mm), #200 (0.075mm) and pan). Particle size gradations for the 11 mixtures that were successfully captured in the canisters are shown in Figure 7.4.

Gradation Analysis of Matrix 2 Experiments under Blast loading

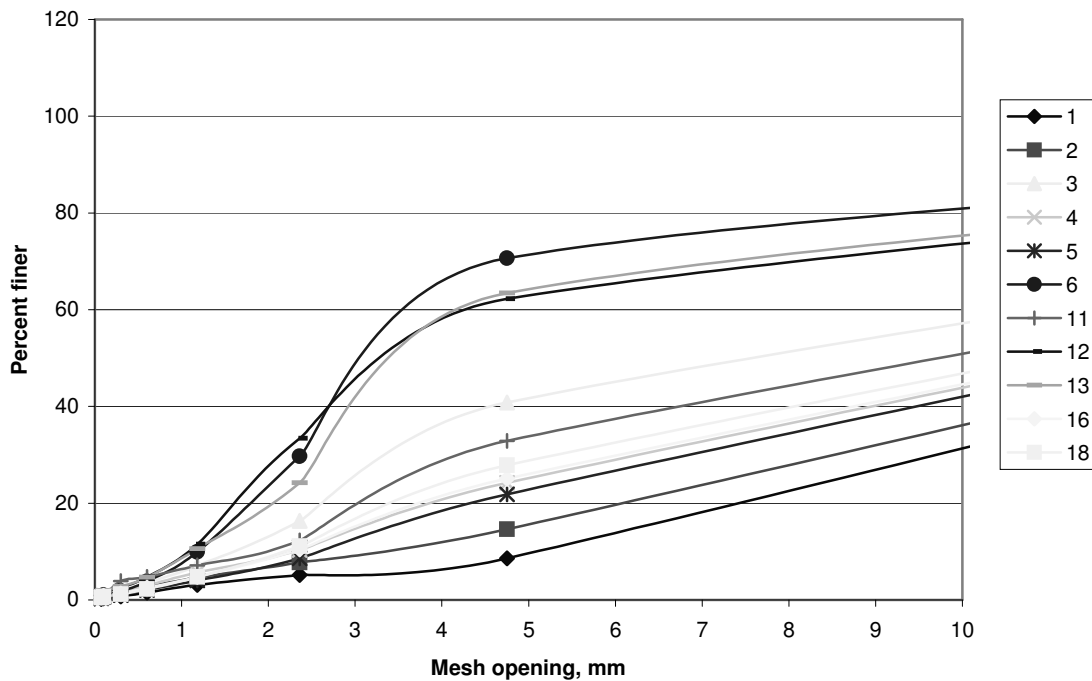


Figure 7.4 Gradation curves of the 11 mixtures that fractured and could be analyzed

7.4.6 Discussion

The largest spread of particle mass is shown for the mass passing the #4 sieve (4.75mm opening). One of the metrics for successful development of the Frangible Concrete was particle sizes less than 4.75 mm. Three mixtures (mixtures 6, 12, and 13) had the greatest mass percentage of particles passing the #4 sieve and all smaller sieves. These mixtures are highlighted in table 7.2. All three mixtures are composed of 100% slag as binder, potentially indicating that the higher the percentage of slag, the greater the tendency to break apart in small pieces. This is possibly the result of greater shrinkage in slag than in OPC and the weaker

strength of slag compared to a slag/cement binder. Of the four mixtures that did not break under the blast pressure, three contained some percentage of OPC. In general, those mixtures with the smallest mass passing the #4 sieve (mixtures 1, 2, 4, 5, 16, and 18) all contained either 5 or 10% OPC in the mixture.

The other variables in Table 7.1 do not seem to correlate well to the results of this blast experiment. The sand to binder ratio is an instance. Two of the three mixtures that fractured best (mixes 6 and 12) had no sand while the third (mix 13) had the maximum amount. In the results of matrix 2 impact tests conducted at Northwestern University, the researchers could not make a distinct correlation between presence of sand and compressive strength partly because three of their independent variables; sand size, sand type, and curing temperature were, themselves, correlated. They stated that the sand could influence the size of fragments because it would create sites for microcracks. Under the blast work done at ERDC there is no direct correlation between sand content and fragility. Likewise amount of activator, curing temperature, and time also cannot be correlated with the size of fragments.

The three companion cubes from each mixture blast-tested at ERDC were sent to Northwestern University to be tested under the impact loading used in the first phase of the Frangible Concrete contract to determine if the size of particles produced by a simple drop-hammer impact test could be a good indicator of what would result from a blast test. Two of the cubes were failed in static compression to determine the mixture strength at 180 days while the third cube was subjected to impact loading. The results are shown in Table 7.3. The mixtures in column 1 are sorted by the ranking of the blast experiments in column 3 (mix 1 = best results, mix 11 = worst). The impact experiments are also ranked from 1 to 11 (column 4), but they are

Table 7.3 Comparative results of blast experiment and impact experiment

Mixture number	Blast experiment		Impact experiment		
	Percentage of particles smaller than 4.75 mm	Ranking of blast experiments	Ranking of impact experiments	Percentage of particles smaller than 4.75 mm	Compressive strength, MPa
6	70.7	1	1	96.9	9.6
13	63.4	2	2	80.7	4.9
12	62.2	3	5	67.5	8.4
3	40.8	4	4	73.9	7.1
11	32.9	5	8	41.2	11.1
18	27.9	6	11	26.0	12.7
16	25.1	7	7	49.6	7.8
4	24.2	8	6	57.9	7.1
5	21.9	9	3	75.9	12.5
2	14.6	10	10	31.6	9.6
1	8.6	11	9	34.7	10.8

ordered to match the mixture numbers in column 1. Columns 2 and 5 represent the percentage of particles passing the #4 sieve for the blast and impact experiments, respectively.

Compressive strength (column 6) of the 11 mixtures ranged from 4.9 MPa to 12.7 MPa with the three best fracturing mixtures in the low to lower-middle of this range. This is expected since the best fracturing mixtures contained no cement and would have lower strength associated with slag. The most interesting correlation between the blast and impact experiments is the ranking of the mixtures. In both sets of experiments, 3 of the 4 top mixtures were ranked the same (1st, 2nd, and 4th) and overall, 5 of the 11 experiments were ranked identically with the remaining experiments being, for the most part, no more than two rankings different from each other. This result implies that the use of a drop-hammer impact loading is useful in predicting the results of a blast experiment similar to the one conducted at ERDC. The percentage of particles passing the #4 sieve is higher in the impact experiments because the impact weight continues to fall on the specimen after initial impact causing further damage, whereas with the blast

experiments the initial impact and blast pressure fall off after a few milliseconds and the remaining pressure causes little additional damage.

7.5 Laboratory experimental development - Phase 3

The last phase in this section of the frangibility work used a matrix of materials designed to further test the effects of NaOH and to separate the effects of curing temperature and sand addition. The variable list for this matrix was the smallest of the three. Input parameters that were no longer varied included: the binder (which was set as 100% slag number 2), the w/b set as 0.5, and the drying treatment set at 110 °C for 24 hours. Variables still included were: cure time (now limited to 3 and 7 days), cure temperature, wt % NaOH (now including 0, 2, and 4%), and sand/binder ratio.

When the data of the phase 3 matrix had been analyzed, Jennings and Thomas [115] found that the strengths were lower and the degree of fragmentation remained about the same as in the phase 2 matrix. This was partially due to data averaging and elimination of the 21-day hydration time. Using the averaged results at each level, the effect that stood out the most was the significant decrease in strength with curing temperature. Higher curing temperatures reduce the amount of bound water implying that the reduction in strength may be due to reduced hydration. Results from the phase 3 matrix showed: longer curing time increased the degree of hydration, the strength, and the fragmentation; the effects of NaOH are different at different concentrations; and adding sand to the binder caused a small decrease in the fragmentation allowing a conclusion that the curing temperature in the phase 2 matrix was responsible for the reduced strength.

Jennings and Thomas [115] concluded from the laboratory studies that it is feasible to produce a slag material that has static compressive strength in the range of 10.3 to 13.8 MPa that

under impact loading can break into pieces smaller than 4.75 mm in its largest dimension.

Among the important findings from the study is the relationship between degree of hydration of the matrix and the percentage of the mixing water considered bound water. As would be expected, an increase in the degree of hydration would be accompanied by an increase in the matrix strength and an increase in the percent of bound water. However, one would expect that as the strength increases, the degree of fragmentation would decrease. Jennings and Thomas [115] found that at low percentages of bound water, the degree of fragmentation increases up to a broad defining range of between 7 and 12% bound water and thereafter decreases. They found that to have a mixture with good strength and frangibility, a high percentage of slag was required along with the drying treatment of oven drying at 110 °C for 24 hours.

7.6 2004 field blast test of Frangible Concrete

7.6.1 Description of the Frangible Concrete block mixture

The last task at the conclusion of phase 3 development of Frangible Concrete was to fabricate enough blocks to build a wall that would be part of a full-scale, field blast test. The blocks were fabricated using a partially automated block-making machine (Atlantica Maq; São Paulo, Brazil) that forms a 2-cell block with wall thickness of 25.4 mm. Dimensions of the block are different from standard American block and are given in the sketch

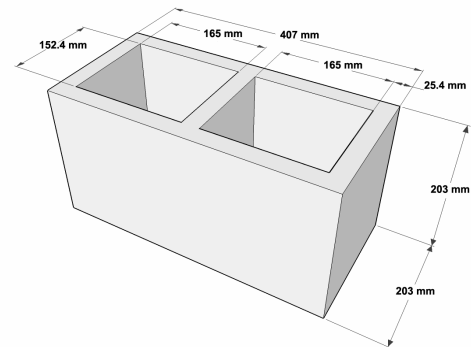


Figure 7.5 Frangible Concrete block dimensions

in Figure 7.5. Under normal conditions, the blocks would be made from the mixture chosen as having the best properties of strength and frangibility from the 48 individual mixtures tested over

the three phases of the first effort. However, a property that was not studied, slump, played a pivotal role in forming the mixture design for the machine cast blocks.

Because mass produced blocks must be demolded immediately, they have to be able to hold their shape and support their own weight immediately and therefore must have zero slump. Since slump was not a variable in any of the experimental design matrices, an adjustment to the best results had to be made. Production of a block that is free of defects, has zero slump, and will stay together in an acceptable manner, requires the sand-to-binder ratio to be raised significantly from the range of 0 to 0.5 (which was acceptable when some slump was allowable) to a level of 5. (see table 7.4) The zero-slump requirement further affected the mixture design and those variables and levels established in matrix 2 and 3. This mixture uses 100% slag which was a different slag from those used in the three matrices experiments. The previous activator, NaOH, was not as effective with the new slag so a stronger formulation of sodium silicate was needed.

Table 7.4 Frangible Concrete mixture design used to make block for the 2004 blast test

% Slag	Sand/binder	Water/binder	Activator	Cure temp	Dry temp
100 (Lafarge NewCem)	5	0.5	2.13% Na ₂ O and 3.75% SiO ₂	5 days at 20 °C	110 °C for 24 hours.

7.6.2 Fabrication of the walls

The blocks that were fabricated for the blast test were shipped to the field site, and the test wall and a conventional block wall were built on site. The two walls were built side by side on a reinforced concrete footing. The two walls are shown from

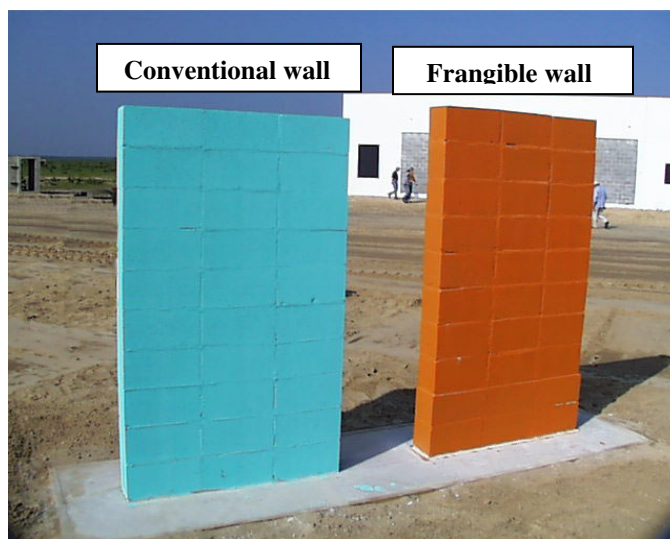


Figure 7.6 Test walls ready for blast

their down-range side in Figure 7.6. They were each three units wide by ten units high, built in stack bond and were built with their blast-side faces on a line perpendicular to a radial line from ground zero (GZ) at a distance of approximately 4.75 m. The first two courses in both walls were filled with grout to anchor them to reinforcing bars in the foundation. The remaining courses had no grout or reinforcement. The walls were painted different colors for post-test fragment identification. On the down-range faces, the conventional wall was painted turquoise and the Frangible Concrete wall orange. The blast face of the conventional wall was yellow and the Frangible Concrete wall purple.

7.6.3 Post-blast data collection and analysis

The major chore of post-blast data collection was to walk the down-range debris field and locate pieces of block from the blast^{IV}. Distances and angles from GZ to pieces of block were recorded using a theodolite with distance measuring equipment. The field team locating debris carried a reflecting stadia rod and a scale to weigh pieces of block. Angle and distance from GZ were calculated, and color and weight were recorded for each piece recovered. A summary of the data collected is given in Table 7.5.

Table 7.5 A summary of fragment data collected from block wall blast analysis

Wall	Face	Number of fragments	Mass range, kg	Median mass, kg	Mass found by color, kg	Percent of total wall	Total mass found	Percent of total wall
Conv. block	Yellow (facing GZ)	43	0.45 - 2.7	0.9	46.0	18.63	98.9	40.01
	Turquoise	31	0.45 - 5.9	1.4	52.8	21.38		
Frangible block	Purple (facing GZ)	13	0.45 - 1.8	0.9	13.6	4.50	43.8	14.31
	Orange	33	0.45 - 1.8	0.9	29.7	9.82		

^{IV} Details of the type and magnitude of the field blast event are sensitive military data and are not critical to the content of this dissertation. It can be said that the magnitude was sufficient to destroy both walls.

The fragments documented in Table 7.5 are the large pieces from each wall, those that weighed greater than 0.45 kg. There were smaller pieces as documented in Figure 7.7, showing the small fragments from the Frangible Concrete wall (left) and the conventional wall (right). The data in Table 7.5 show that there were large pieces remaining intact from both walls. The fact that the number of fragments, the range and median of fragment mass, the total mass found and weighed, and the collected piles of small pieces shown in Figure 7.7 are all smaller for the Frangible Concrete wall indicates that the Frangible Concrete blocks were more frangible than conventional block. However, the mass of the pieces from the Frangible Concrete wall that were recorded document the fact that the Frangible Concrete blocks did not meet total expectations for frangibility of 90 weight percent of pieces to a size less than 4.75 mm.



Figure 7.7 Small fragments not recorded, Frangible wall left, Conventional wall right.

7.6.4 Discussion of 2004 wall blast results

This field test, while not meeting the goals set for successful demonstration of the concept of Frangible Concrete, showed that even with a number of the input criteria being modified significantly that the Frangible Concrete was more frangible than conventional block and a concept worth further development. Based on the recovery criterion being set at a

minimum mass of 0.45 kg, 40 % of the conventional wall was recovered as compared to 14.3 % of the Frangible Concrete wall. This metric makes a further statement that the 85.7% of the Frangible Concrete wall that was not recovered weighed less than 0.45 kg. Refer again to Figure 7.7 and the representative sample of small pieces that were recovered but not recorded. These fragments appear to be from 12 to 25 mm long, based on the boot markings in the dirt, and perhaps are no heavier than 6 to 10 g based on material density. Even though this was not the optimal mixture design, the concept of a Frangible Concrete is viable.

Several factors are key to this mixture design failing to meet minimum criteria. Opportunities to participate in major field explosive events, such as the July 2004 event, are very rare. Usually the full 360-degree foot print surrounding GZ has been taken for months before the event. To be offered 35 degrees of arc at 5-m distance at the last minute required making blocks at a hurried pace with available materials. Trial mixtures that worked well under laboratory impact conditions had to be modified to meet installation deadlines for this major field test. The type of slag was changed from SuperCem grade 120 to NewCem Grade 120 as the result of availability. It was the same grade, but different formulation. It is often stated in the literature that different slags are affected differently [116] by amounts of activator, and different types of activator. Both changed factors were present in this case. In the experimental design, sodium hydroxide was identified as the best activator for the SuperCem slag. With the NewCem slag, it was not sufficiently active and a sodium silicate activator was substituted. The mixture design used to make the blocks was sufficiently different from the one recommended by the design of experiments work that it would be difficult to predict the behavior of the blast test blocks from the laboratory fracture data.

Another approach to explaining the presence of large pieces of Frangible Concrete in the post-blast environment is stress distribution. As a structural member populated throughout with a system of microcracks is hit by a blast force, initially the stress is uniform and all the microcracks will grow. As the stress on the member grows, microcracks will grow, propagating the most in areas where the structure is the weakest. This process relieves stress on some microcracks and concentrates it on others preferentially fracturing the concrete in the weakest areas and relieving stress in the stronger ones. In a material such as Frangible Concrete that is designed to develop microcracks, it is unrealistic to believe that all areas will have the same fracture potential and all microcracks will propagate and fracture equally.

7.7 A new approach - description of no-fines concrete

No-fines concrete is a special type of concrete that, as the name implies, contains no fine aggregates but coarse aggregate particles in a cementitious matrix. This form of concrete was used as a structural material in walls and houses in the early part of the 20th century [117] and its popularity as a building concrete has been much greater in Europe than in North America.

In its conventional form, no-fines concrete consists of pieces of coarse aggregate of a single particle size (usually the size of coarse aggregate in conventional concrete, between 9.5 and 19 mm), coated with a shell of cement paste and consolidated into a packed configuration where each aggregate particle touches each of its neighboring aggregate particles in at least one location. During the hardening process, at the sites of aggregate-to-aggregate contact, the paste from one aggregate particle mixes with the paste from the neighboring particle providing a paste bridge that structurally connects the two aggregate particles together. This creates an environment where the touching aggregate particles form a structural framework for carrying

load from one point to another and the cement paste shell functions to hold the aggregate particles in place and assist in transferring load from particle to particle.

In properly proportioned no-fines concrete, the volume fraction of the cement paste should be just enough to coat the aggregate particles with an even coating of paste that is stiff enough (low enough w/c) that it will not slump away from the aggregate before setting. The volume of void space between the coated pieces of aggregate should be fully percolated so that water can freely pass through the concrete.

7.8 Laboratory experimental development of no-fines Frangible Concrete

When it was realized that the change in type of slag and the necessary zero-slump alterations to the mixture design had adversely affected the frangibility performance of the block, it became apparent that further modifications of the mixture design were necessary. It was at this time that the no-fines concept was suggested as a new direction to improve the material frangibility. The suggested concept was similar to conventional no-fines concrete described above in that the mixture would not have fine aggregates, but with a no-fines version of Frangible Concrete the aggregate is uni-modal and sized to be smaller than 4.75 mm. The no-fines concept is conducive to frangibility for a number of other reasons. The slag binder is a neat paste rather than a sanded mortar. The neat paste is more prone to develop microcracks on drying than a mortar. Fracture of the Frangible Concrete block down to the individual aggregate particles only depends on failure of the paste at the interparticle contact points. Since the void space in the no-fines Frangible Concrete is continuous, this allows pressures from the blast to get between the uni-modal particles to put pressure on the block from the inside.

The suggestion to explore the no-fines concept was met with general approval and the contractor began a set of designed experiments to optimize the cementitious material, the w/b, the maximum size aggregate, and a range of aggregate sizes if necessary.

The contractor started a new series of designed experiments. Considered as variables in this design were: an angular coarse aggregate in the range between 4.75 mm and about 10 mm or a rounded, smooth aggregate in the range of 2.36 mm to 4.75mm that when mixed with different paste configurations yielded a compressive strength greater than 6.9 MPa; both OPC and Alkal-Activated Slag (AAS) pastes that had to be stiff enough to cling to the aggregate without sloughing off and filling in interparticle voids; slag activation chemical; w/b of 0.4 to 0.45 to meet the stiffness requirement; oven drying versus air drying; and an important aggregate-to-paste (a/p) ratio that would be key to success or failure. If there was too much paste the Frangible Concrete would be too strong and not fracture into aggregate size pieces and if there was too little paste the Frangible Concrete would be weak.

The above components were considered and a choice of variables was made based on the understanding of the material gained from the first three laboratory phases. Table 7.6 gives the variables and levels that went into the experimental design along with the components that were held as constants.

Table 7.6 Variables and levels in the experimental design

Variable	Levels	Comments
w/b	0.4, 0.45	w/b must make stiff enough paste to cling to aggregate
a/p	2.6, 3.1, 3.6	Aggregate to paste ratio must be just right. Too much or too little paste yields poor quality
Cure time, days	3, 7	days at 20 °C
Components in the mixture that were kept constant		
The binder was 100% NewCem slag activated with 2.13% Na ₂ O and 3.75% SiO ₂ by weight of slag, gravel aggregate 2.36 mm – 4.75 mm in size, room temperature curing conditions, and drying in an oven at 110 °C for 24 hours.		

7.8.1 Laboratory impact test modifications

Through discussions with the ERDC, it was established that the impact machine the contractor was using was too severe in the way it impacted the specimen and needed to be modified. The cartoon in Figure 7.8 shows the old impact machine to the left and the modification to the right. The old impact mass would hit the specimen and impart a shock load but then would continue to crush the specimen. In the new design the drop height has been reduced considerably and a set of stop studs have been added in the base of the tray to arrest the inertia of the drop mass. This better simulates just the blast impact.

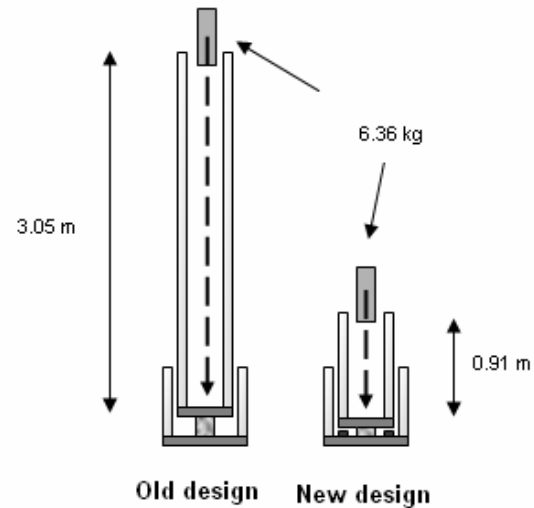


Figure 7.8 Modified impact tower

An experimental design was created and the mixtures tested both under laboratory impact and in compression. All mixtures in the design had the components mentioned in the lower half of Table 7.6. The most favorable mixture in terms of strength and fragility had a w/b of 0.45, an a/p of 3.6, and 7 days hydration time. The mixture had dry compressive strengths of about 13.8 MPa and about 88% of fragmented particles were less than 4.75 mm.

The final metric under the contract with the ERDC was to produce enough frangible blocks to build a test wall for a second field blast event. In response to this metric the contractor built 60 blocks which were palletized and shipped to the ERDC for storage. A field event in which a physical footprint was available for a frangible block wall test occurred in July 2007.

7.9 Analysis of 2007 Frangible Concrete wall field blast test

7.9.1 Description of the Frangible Concrete wall test set-up

The 2007 Frangible Concrete wall blast test took place at Eglin Air Force Base, Florida. This range has been used by the Department of State and the Army for large-scale blast and impact testing for more than a decade. The current series of events includes both Department of State and Army experiments, including the Frangible Concrete peripheral wall. Figure 7.9 shows the layout of the blast field and the stand off distances from each experiment to GZ (perimeter wall O'Neil is the Frangible wall experiment). The distance from GZ to the face of the perimeter walls is 3.05 m. This proximity simulates the damage a large truck bomb would have if parked just outside the wall.

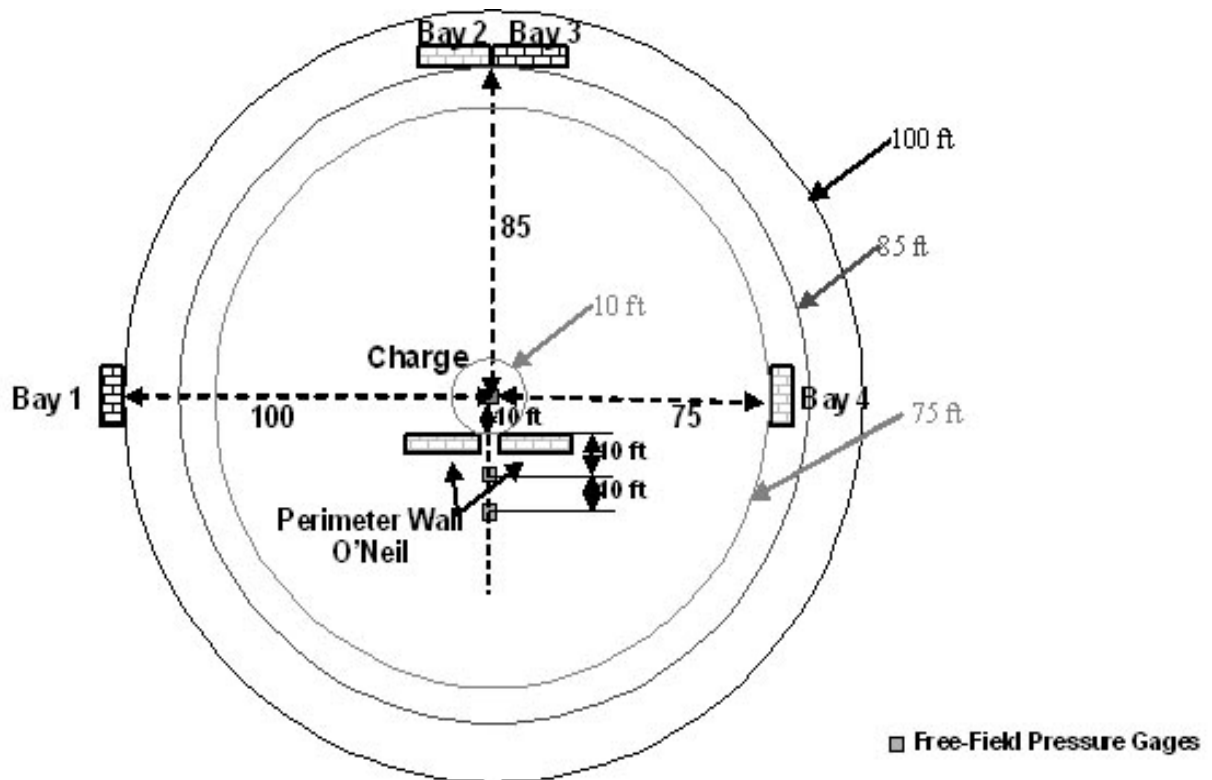


Figure 7.9 Layout of the blast field and stand-off distances to each experiment

Figure 7.10 shows the two walls from the down-range side. The walls are seated on a reinforced footing with #4 bars spaced to fit in the block cavity. Each wall is 5 blocks wide and 11 courses high. The walls are different heights because the Frangible Concrete blocks do not match U. S. standard dimensions. The walls are unreinforced except for the bars

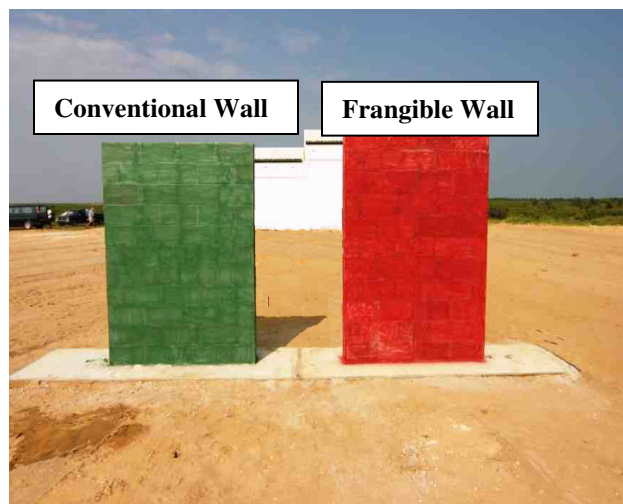


Figure 7.10 Block walls ready for testing

extending from the foundation. These bars extend into the second course and the first and second course cavities have been filled with grout to anchor the walls to the foundation.

7.9.2 Post-blast collection of data and analysis

The technique for collecting debris from the blast was identical to the routine used in 2004 (refer to paragraphs beginning at 7.6.3). The force of the blast was recorded on two free-field pressure gages that were buried in the sand 3.05 and 6.1 m down range from the front face of the walls and on a line between the two walls perpendicular to the plane containing the front face of the walls. The data these gages recorded are given in Table 7.7. The free field gages were down-range relative to the front face of the wall so the

incident pressure on the face of the wall would be higher than these figures attest. Using the Pressure-Range feature

of the Army's blast calculation program, ConWep [117], the theoretical impact and reflective pressure-distance relationships for a blast of this nature can be calculated. This is shown below in Figure 7.11 along with the actual data collected from the field work plus an extrapolated data

Gage	Distance from GZ, m	Incident pressure, MPa
FFA	6.1	2.77
FFB	9.15	1.00

8/28/2007

Pressure vs. Range

Hemispherical Surface Burst

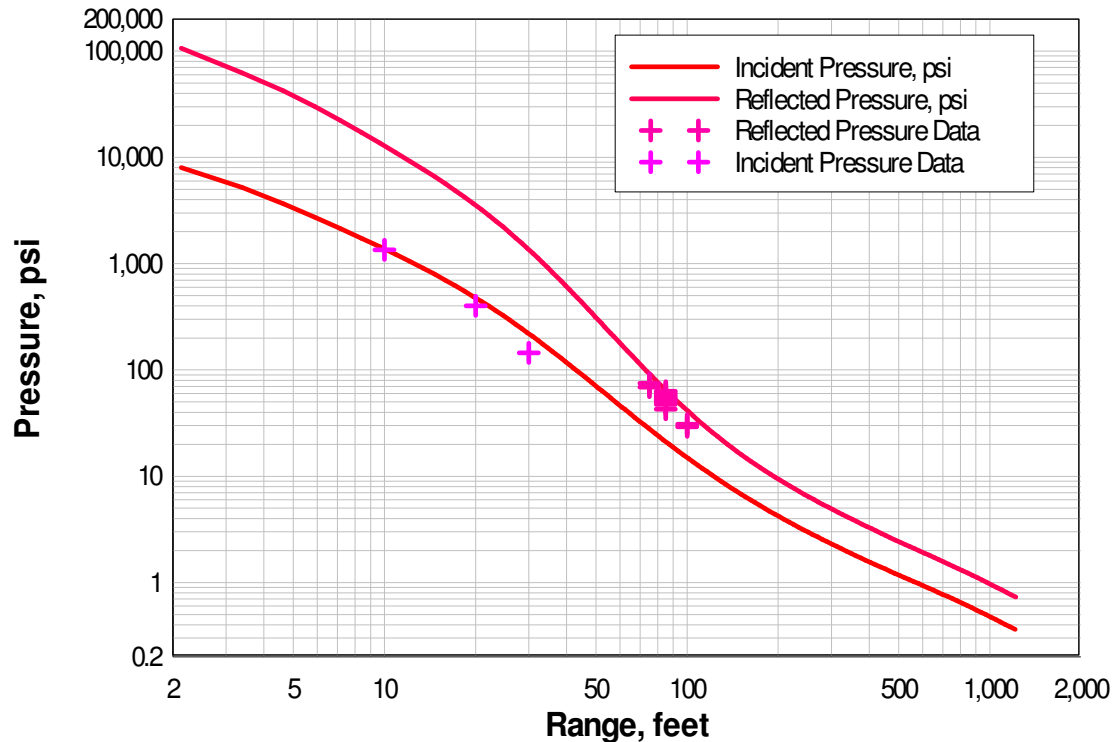


Figure 7.11 Actual pressure vs range data plotted on theoretical incident and reflected pressure curves calculated using USACE ConWep

point at 3.05 m from GZ. The extrapolated data point is at the face of the wall and is 9.31 MPa. The actual incident data are different from the theoretical curve because the ConWep calculates its values for a perfect hemispherical blast and the actual blast was not hemispherical.

Table 7.8 gives the results of the fragments recovered from the blast and Figures 7.12 and 7.13 show the fragments collected. A comparison to the results from the July 2004 blast, Table 7.5, is made. Fewer and smaller fragments were collected in the most recent blast when compared to the 2004 data. This is due in part to the proximity of the walls to GZ. While the size of the two blasts were approximately the same, the walls from the 2004 blast were approximately 4.75 m from GZ while in the current event they were 3 m away. The current pressure at the

surface of the wall is 1 3/4 times as large as the pressure from the former blast. This difference in pressure can explain the difference in size and number for the two conventional block walls because the blocks are supposedly the same from one test to another.

Table 7.8 A summary of fragment data collected from July 2007 block-wall blast

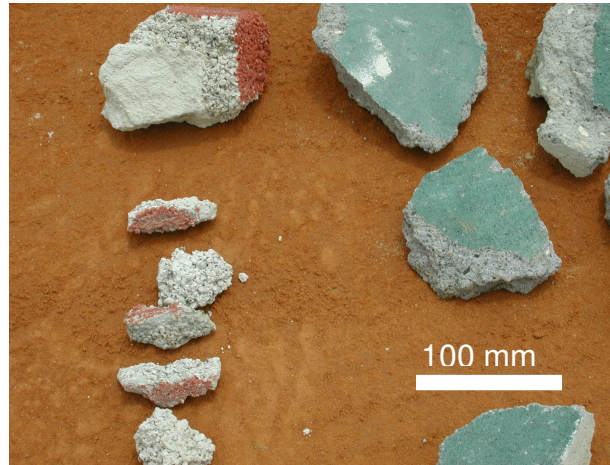
Wall	Number of fragments	Range of fragments in grams	Median value, g	Total mass recovered, kg	% total wall
Conventional	59	28.35 - 1048.95	170.1	16.30	3.52
Frangible	6	28.35 - 113.4	70.87	0.43	0.07



Figure 7.12 Photograph of the 70 pieces collected from the blast

But the large number of Frangible Concrete fragments found in the 2004 blast as compared to the six fragments found in the 2007 blast, Figure 7.12, requires a different explanation.

The difference between the 2007 Frangible Concrete and the 2004 Frangible Concrete is the



7.13 Detail of Figure 12

concept of particle packing. The difference lies in the composition of the aggregates in the two

mixtures. In the 2004 Frangible Concrete mixture, many factors were in place that encouraged particle packing to occur. The sand is an angular, multi-sized material that because of its many sizes of particles can pack together more efficiently reducing void space between particles. The mixture was vibrated which further compacted the aggregate particles. Also, the paste was proportioned to be similar to a concrete block, providing ample paste to fill in the voids between the particles. In the 2007 no-fines Frangible Concrete mixture there were many factors that discouraged a strong matrix and particle packing. The use of uni-sized aggregate that is rounded in shape puts the packing density somewhere between 52.4 % for simple cubic packing, and 74.05 % for face-centered cubic packing. While face-centered cubic packing is high for uni-sized particles, both densities are very low in terms of multi-sized particle packing and leave a large percentage of space as void space. These arrangements of spheres minimize the point-to-point contacts between particles thereby minimizing the number of points where an aggregate particle can bond to its neighbor. The paste formulation and processing have been shown to be effective in developing microcracks in the matrix that will propagate under dynamic load.

7.10 Summary

This chapter presented the concept of engineering a cementitious material from the opposite extreme of engineering for ultra-high strength. In this chapter engineering thought and knowledge of the microstructure of cement were brought to bear to develop a completely new form of concrete. The chapter began with a challenge to develop a concrete strong enough to carry structural loads yet frangible enough to fracture into small non-lethal pieces when impacted by a blast load. The first phase of development involved bringing together knowledge of how cements function at the microstructural level and applying that knowledge to obtain a condition that is normally avoided, to develop a matrix of microcracks. An experimental design was developed and the concept tested. The laboratory success of the first phase led to two follow-on phases that were meant to refine the design.

A first field blast test was conducted to compare the frangibility characteristics of the new material to conventional block materials. While the concept of pre-microcracked slag cement was verified and the new material was more frangible than conventional materials the first test failed to meet developmental criteria for success. Understanding the causes of the setbacks led to a redesign of the aggregate portion of the composite to approach the system from a no-fines concrete approach. Laboratory study was again conducted in preparation for a second field blast test. The results of that test confirmed the success of the changes and the successful development of a Frangible Concrete block.

7.11 Conclusions

7.11.1 Phase 1 conclusions

The results from execution of the Phase 1 experimental matrix yielded the following conclusions:

- 1) The overall strength of the mixtures was acceptable and the frangibility of the specimens was good, yielding fragments in the range acceptable to the Army
- 2) Higher levels of OPC in the mixture increased the strength and reduced the frangibility.
- 3) Initial results confirmed that developing a microcrack structure in slag cement through early-age heat drying of a slag/cement matrix was a viable concept.

7.11.2 Phase 2 conclusions

Phase 2 consisted of a refinement of the experimental design developed in Phase 1. A similar set of specimens were fabricated and impact tested with the following conclusions being drawn:

- 1) The w/b of Phase 1 was appropriate and adopted as a material constant.
- 2) Specimen drying at 110 °C for 24 hours was also adopted as a default
- 3) The measurement of the bound water was important because it reflected on the degree of hydration and the level of strength and frangibility.

7.11.3 Conclusions from the ERDC preliminary blast-load studies

The experiment of subjecting panels of the slag/cement mixtures provided a means of comparing the results of fragmentation by drop-hammer impact with that of a small blast force.

This allowed the following conclusions to be drawn:

- 1) The blast loading delivered in the small-scale blast loader was sufficient to fail the majority but not all of the specimens. This confirmed the magnitude of the blast force was in the right range for testing the specimens because some of the specimens were stronger than others and the strong ones would survive a loading in the correct range.

- 2) Of the 20 specimens tested, the three that had the highest weight of pieces that met the fragment size requirement were made from 100% slag while three out of the four specimens that did not fail contained some level of OPC, leading to the conclusion that 100% slag mixtures were the most frangible.
- 3) The three specimens that were the most frangible in conclusion 2 above were also among the weakest in compressive strength ranging from 5 to 10 MPa. This led to the conclusion that in order to be a superior frangible material the best mixture had to balance the high frangibility with acceptable strength.
- 4) The results from the comparison between the blast and impact tests presented in Table 7.3 show that the fragmentation produced by the drop hammer was similar to that produced in the blast chamber, based on the top ranking mixtures producing the highest frangibility. From this it can be concluded that an impact drop hammer apparatus similar to the one designed by Northwestern engineers is a reasonable substitute for a small confined blast chamber.

7.11.4 Phase 3 conclusions

Like Phase 2, Phase 3 continued to refine the input parameters to the Frangible Concrete design. The experiments showed that longer curing time increased the degree of hydration and the strength; the effects of NaOH are different at different concentrations; and adding sand to the binder caused a small decrease in the fragmentation. The major conclusion from this Phase was:

- 1) From the laboratory studies that it is feasible to produce a slag material that has static compressive strength in the range of 10.3 to 13.8 MPa that under impact loading can break into pieces smaller than 4.75 mm in its largest dimension.

7.11.5 2004 field blast test conclusions

From the results presented in paragraphs 7.6.3 and 7.6.4 the following conclusions can be made about the first blast field test:

- 1) The failure of the Frangible Concrete to meet minimum criteria is attributable to two factors. First, the block material that was brought to the field blast test was only a best approximation to the material developed in the two years of experimental testing; and second, Frangible Concrete was evolving into was a high-sand content, zero-slump material that was not too different from conventional block. From this it is understandable that their strength and frangibility would be similar.
- 2) Examination of the cross section of a large fragment of Frangible Concrete revealed a heavily sanded mortar in which the slag paste completely filled the space between the aggregate particles, providing a matrix that was stronger than anticipated. The forced microcrack, high-slag-content paste was a good concept but its execution was a failure. What was needed was an approach that minimized the efficiency of particle packing to achieve a material that was strong yet frangible. That approach was to be found in “no-fines” concrete technology.

7.11.6 2007 field blast test conclusions

The results of the field blast test in 2007 were much more successful. Only six fragments that were large enough to be considered lethal fragments were recovered, and one of them was a grouted piece from the bottom two courses. In contrast, 59 lethal-sized fragments from the

conventional wall were recovered. The following conclusions can be drawn from the second field blast test:

- 1) The success of the no-fines Frangible Concrete field blast test can be attributed to the low-particle-packing arrangement of the uni-modal particles and the pre-fractured slag-cement paste that acts as binder.
- 2) Because the aggregate particles are smaller than the 4.75 mm maximum acceptable fragment size and a blast force is expected to complete the fracture process at the contact locations where neighboring aggregate particles touch each other, the Frangible Concrete is designed to disintegrate into non-lethal fragments meeting Army criteria for a Frangible Concrete.

7.11.7 Chapter conclusions

The work from the first three phases of the Frangible Concrete block effort as well as the results of the 2007 wall blast test at Eglin AFB have resulted in the development of a new concrete material that has acceptable load-carrying capacity under static loading conditions and which has shown, to date, better frangibility characteristics than conventional concrete blocks. It can be concluded from this work that the use of blast furnace slag as a binder, alone or in combination with small quantities of portland cement, can be processed to provide a cement matrix that is highly populated with microcracks, and that when the paste is coated on a uni-modal sized aggregate in a no-fines arrangement of particles, and impacted by a dynamic blast force, it will fracture into small pieces.

One of the major truths about creating very-high-strength concrete is to minimize formation of microcracks. Because Frangible Concrete is a completely new concept, much of what is considered conventional thought does not apply. From data collected here in three

matrices of experiments and 48 different mixtures of OPC, slag, chemical activators, and sands; with varying properties of w/b, s/b, curing time and temperature, and drying criteria; much was learned about creating microcracks rather than preventing them. It can be said that the research and development that went into Frangible Concrete is truly a case of engineering a high-performance material to meet highly specific needs.

From fragments collected from both test walls after the July 2004 field blast event, it was found that the Frangible Concrete wall fragments were less numerous and smaller than the fragments from the conventional block wall. However, even though it could be concluded that the concept of designed microcracking in slag cement pastes was valid and that Frangible Concrete performed better than the conventional concrete block, the size of the fragments did not meet Army criteria for successful frangibility. This was because the aggregate particles in the matrix were packing too well and there was too much paste cementing them together. It was concluded that the current approach to producing a Frangible Concrete was ineffective and that a new approach that limited the efficiency of the particle packing was needed.

The concept of no-fines concrete dates back over one hundred years. It was used in Western Europe for inexpensive building construction during the nineteen thirties when cement was in short supply. No-fines concrete is a highly desirable formulation of Frangible Concrete material in which the uni-modal aggregate limits the particle packing capabilities of the matrix, thus fostering its frangibility.

A series of designed experiments was conducted in which slag cement and the concepts developed to encourage the growth of microcracks in the cement were employed. Studied in the experiments were two aggregate types of two different size ranges: two types of cement OPC and AAS and two w/c's and two aggregate-to-paste ratios. Specimens were cast and tested in a

modified impact tower redesigned to better simulate the impact forces on the Frangible Concrete and full scale blocks were cast to be destroyed by a high-charge bomb blast.

Results showed the most desirable properties of Frangible Concrete with the proper matrix of fine microcracks were produced under these circumstances: the coarse aggregate component is a uni-modal gravel no larger than 4.75 mm in diameter, the cementitious binder is high in AAS, the w/b is sufficiently low to insure that the paste is thick enough to cling to the aggregate and will not sluff off, the a/p is maintained with just enough paste to thinly coat the aggregate and not so thick that the paste could fill void spaces between aggregate particles (in the case of current materials that ratio is 3.6), and that proper drying of the slag binder is employed. From the results of these experiments, it can be concluded that the formulation developed and explained here is fully viable in producing a Frangible Concrete that meets the Army's criterion for non-lethal debris.

Chapter 8 GENERAL CONCLUSIONS AND FUTURE WORK

8.1 Engineering high-performance materials

The two concrete materials at the center of discussion in this work, Very-High-Strength Concrete and Frangible Concrete, are high-performance materials because they each fulfill a special need that can not be addressed by conventional concrete materials. Their component materials and mixture proportions were both derived based on how well those materials and proportions blended together to produce a concrete that could do something no other concrete could do. It should come as no surprise that the path way to achieving their separate, special capabilities is the same even though the results they produce turn out so differently. They both use extensive knowledge of the functioning of cementitious materials at all levels of the microstructure and judicious thought about the choices of component materials to use that perform the best at achieving their individual goals.

It is a conclusion of this work that the embodiment of the process of engineering a high-performance material involves a firm grasp of the goals to be achieved, use of all the knowledge that can be brought bear to understand what processes will be beneficial to the solution and what ones will hinder it, and judicious choice of component materials and how they are combined to maximize the benefits and minimize the detriments along the path to the solution.

It is further concluded that the development of both VHSC and Frangible Concrete follow this path way and have met their separate goals, not because they are composed of highly exotic materials generally missing from conventional concretes, but because conventional materials have been used through studied knowledge and application of the properties they can bring to the solution.

8.2 Overall conclusions on VHSC

8.2.1 Strength considerations

The research conducted here has brought a measured level of strength increase to VHSC, in some cases only small improvements while in others the contribution has been noteworthy. Compared to the Neeley and Walley work [47], the current research produced a reproducible increase in compressive strength to 266 MPa when cured at 90 °C for 13 days with occasional individual breaks reaching 276 MPa. This represents an increase of from 11 to 23% over early VHSC work depending on how one views their results. Strength increases have been achieved through changes made to the baseline mixture proportions, the use of more efficient HRWRAs, and the addition of microfibers and microspheres.

What can be concluded from the research conducted here is that all the strength gains came from ordinary concrete materials, among them, aggregates, silica fume, and HRWRAs. It can be stated that aggregates play an important role in strength giving properties when they are combined with materials that allow their physical properties to be a part of the composite strength. Silica fume provides several benefits including: its ability to produce pozzolanic C-S-H, its excellent ITZ developing properties, and its micro-fine particle size to act as a superior filler material dramatically reducing porosity. And micro-inclusions, while providing only small contributions, nonetheless provide energy consuming toughening mechanisms that allow the matrix to perform at a greater level.

8.2.2 Rheology considerations

As discussed in Appendix B, VHSC can have a fluidity ranging from no-slump to self-leveling. Because it is very dense and highly populated with small particles, it would be impossible to perform as a construction material without the benefit of HRWRAs. It only takes a

small knowledge of the chemistry of the third generation water-reducers to reap great rheological benefits from these materials. It can be concluded that these chemicals provide the ability to minimize one of the detrimental side effects of the beneficial properties of high density and allow almost designer choices of rheological properties.

8.2.3 Toughness considerations

As the strength levels of concrete materials continue to increase, they behave more like ceramic materials and less like concrete materials. The fact that the stronger VHSC becomes the more brittle it gets is one of the major detrimental side effects of its superior strength. True to the philosophy of engineering the properties of VHSC, restoring ductility and adding toughness is paramount among design goals.

From the research conducted here several conclusions can be made that are important to improving VHSC toughness. From the comparisons between unreinforced and fiber reinforced VHSC, it can be concluded that the path of fracture through unreinforced VHSC encounters very few crack arresting mechanisms because of its dense, homogeneous matrix and the path is straight, the fracture surfaces are smooth, and little fracture energy is consumed. It can be further concluded that the fibers add a tremendous toughening advantage to the material, consuming large amounts of energy in the process of crack growth primarily by fiber debonding and pullout mechanisms. It is also a conclusion from this research that micro-inclusions such as microspheres do provide a toughening effect but their consequence is much less pronounced than distributed steel fibers

It is interesting to note that while the fracture toughness of VHSC is not remarkably different from lower strength concretes, its critical $CMOD_c$ is among the smallest recorded for concrete materials. That coupled with the linear relationship between $CMOD$ and $CTOD$ in an

effective elastic crack model encourages the conclusion that the FPZ in VHSC is also small and that VHSC may respond well to LEFM principles.

8.2.4 Areas for future VHSC work

The definition of high strength concrete today will be the definition of normal strength concrete tomorrow. There will always be room for improvement in the areas of strength, rheology, and toughness. One area to explore is the realm of nanomaterials. As carbon nanotubes become stronger, less expensive, and easier to work with they will perhaps provide major breakthroughs in research into micro-toughness. Research into cross-linking polymers with cements also provide new directions for advancement. Efforts in this field began a quarter of a century ago and little progress has been made in the interim. With the greater knowledge of chemistry available today, advancements in this area are highly possible.

8.3 Overall conclusions on Frangible Concrete

8.3.1 A new high-performance material

One of the most important conclusions that can be drawn from this portion of the dissertation is that Frangible Concrete represents a new category of high-performance concrete, one that possesses both strength and weakness at the same time. This, in itself, is a significant accomplishment and a testament to the power of engineering a material to achieve a specific goal. Although Frangible Concrete's primary purpose is to minimize casualties from military threats, it is concluded that its usefulness can be expanded into a number of other areas quite easily. For example, it can be directly translated into automotive crash barriers to absorb impact energies during collision. Because its structure is completely percolated, it can become a thermal insulating barrier trapping dead air in the percolated cavity and controlling heat transfer across its mass, with the application of a skin material on both its faces. Also, without the application of a

skin, the mono-sized aggregate and the tortuous percolated pathways through the material provide a good environment for trapping sound allowing it to serve as a sound barrier material.

Even though the Frangible Concrete design started out as a sanded-mortar matrix similar to a concrete block design, and although it performed below expectations in the 2004 field test, it can be concluded that it did perform better than the conventional block material and that the slag cement matrix, heat-treated to induce pre-formed microcracks, is a valid approach to achieving strength and frangibility at the same time. It is a further conclusion that when the slag paste was used to coat a mono-sized aggregate, two important conditions emerged: 1) the coated aggregate settled into an aggregate-to-aggregate contact orientation providing a solid particle bridging effect that results in good compressive-load bearing strength; and 2) the consistency of the paste was such that it clung to the aggregate particles and only contacted other areas of paste where there was aggregate-to-aggregate contact. When the paste hardened it created a very exclusive bond, only at these contact points, that was strong enough to maintain the interlocked and bridged aggregate orientation but frangible enough to fracture under dynamic blast load.

It can be finally concluded that from the results of the 2007 field blast test that the no-fines version of Frangible Concrete was successful in meeting its design goals.

8.3.2 Areas for future Frangible Concrete work

Frangible Concrete has been proven to work under controlled field blast conditions, but there are many areas that need further attention before it is a completed material. The issue of paste durability in outdoor and aggressive environments has not been addressed. More details need to be worked out regarding the consistency and volume of the paste used to coat the aggregate. The consistency used for the field blast experiments was similar to that of fresh pudding. It was thick enough to insure the paste clung to the aggregate and did not fill the spaces

between particles but was by no means optimized. Likewise, the volume of paste is a critical property. Too much paste will leave excess to fill in the spaces between aggregate particles and too little will compromise the strength. A mathematical relationship to determine the necessary volume of paste based on the diameter of the mono-sized aggregate, its volume, and the thickness of the paste coating each aggregate needs to be worked out. Lastly, work is needed to refine the relationship between strength and frangibility. It is an important conclusion from the work that as the strength of Frangible Concrete increases its frangible nature decreases and vice versa. There is a “sweet spot” somewhere in the strength/frangibility range that optimizes both properties by sacrificing some of each. Finding this spot would add a further level of material engineering to this new high-performance concrete.

REFERENCES

1. The concrete centre, "The benefits of concrete," 2007, <http://www.concretecentre.com/main.asp?page=13>
2. Minson, A., "Concrete has many benefits," 2007, <http://www.building.co.uk/story.asp?storyCode=3083469>
3. ACI Committee 116, Cement and Concrete Terminology, *ACI Manual of Concrete Practice, Part 1, Materials and General Properties of Concrete*, (American Concrete Institute: Farmington Hills, MI) Revised Annually.
4. Zuber, B., J. Marchand, A. Delagrave, and J. P. Bournazel, "Ice Formation Mechanisms in Normal and High-Performance Concrete Mixtures," *Journal of Materials in Civil Engineering, ASCE*, **12**, no. 1, 16-23, 2000.
5. Punkki J., O.E. Gjorv, and P. J. M. Monteiro, "Microstructure of High-Strength Lightweight Aggregate Concrete," in *4th International Symposium on Utilization of High-Strength/High-Performance Concrete*, F. de Larrard, and R. Lacroix (Eds.), (Presses de l'ecole nationale des ponts et chaussees: Laboratoire Central des Ponts et Chaussees), p 1281-87, 1996.
6. Nawy, E. G., Fundamentals of High-Performance Concrete, (John Wiley & Sons, Inc.: New York), 441 pages, 2001.
7. Khayat, K. H. , and P. C. Aitcin, "Silica Fume in Concrete: an Overview," *CANMET/ACI 4th International Conference on Fly Ash, Silica Fume, Slag and Natural Pozzolans in Concrete*, V.M. Malhotra (Ed.), (American Concrete Institute: Farmington Hills, Mich.), 835-72, 1992.
8. Li, V. C., and M. Maalej, "Toughening in Cement Based Composites. Part II: Fiber Reinforced Cementitious Composites," *Cement and Concrete Composites*, **18**, no. 4, 239-49, 1996.
9. Portland Cement Association, "High-strength concrete," *Concrete Technology Today*, (Portland Cement Association: Skokie, IL), **15**, no. 8, 1994.
10. American Society for Testing and Materials, "Designation C 230-98 - Standard Specification for Flow Table for Use in Tests of Hydraulic Cement," *Annual Book of ASTM Standards, 04.01 Cement; Lime; Gypsum*, (American Society for Testing and Materials: West Conshohocken, PA), Published annually.
11. Ray, I., A. K. Chakrabarty, and B. Sengupta, "High-Performance Concrete for Containment Structures," *Nuclear Engineering and Design*, **236**, no. 10, 1041-48, 2006.

12. Bhanja, S., and B. Sengupta, "Influence of Silica Fume on the Tensile Strength of Concrete," *Cement and Concrete Research*, **35**, no. 4, 743-47, 2005.
13. Diamond, S., S. Sahu, and N. Thaulow, "Reaction Products of Densified Silica Fume Agglomerates in Concrete: H. F. W. Taylor Commemorative Issue," *Cement and Concrete Research*, **34**, no. 9, 1625-32, 2004.
14. Toutanji, H. A., and Z. Bayasi, "Effect of Curing Procedures on Properties of Silica Fume Concrete," *Cement and Concrete Research*, **29**, no. 4, 497-501, 1999.
15. Wong, H. S., and H. Abdul Razak, "Efficiency of Calcined Kaolin and Silica Fume as Cement Replacement Material for Strength Performance," *Cement and Concrete Research*, **35**, no. 4, 696-702, 2005.
16. O'Neil, E. F., T. K. Cummins, B. P. Durst, P. G. Kinnebrew, R. N. Boone, and R. X. Torres, "Development of Very-High-Strength and High-Performance Concrete Materials for Improvement of Barriers Against Blast and Projectile Penetration," in *24th Army Science Conference*, Session F, (Assistant Secretary of the Army (ALT): Washington, D.C.), 2004.
17. Neville, A. M., Properties of Concrete, (John Wiley and Sons Inc.: New York), 1996.
18. Price, W. H., "Factors Influencing Concrete Strength," *Proceedings, Journal of the American Concrete Institute*, **47**, no. 6, 417-32, 1951.
19. Abulfaraj, W. H., and S. M. Kamal, "Evaluation of Ilmenite Serpentine Concrete and Ordinary Concrete as Nuclear Reactor Shielding," *Radiation Physics and Chemistry*, **44**, no. 1-2, 139-48, 1994.
20. Mahdy, M., P. R. S. Speare, and A. H. Abdel-Reheem, "Shielding Properties of Heavyweight, High Strength Concrete," *Proceedings, Annual Conference - Canadian Society for Civil Engineering*, (Canadian Society for Civil Engineering: Montreal, Canada) 925-34, 2002.
21. Narang, K. C., P. B. Rao, and A. Kumaraswamy, "Development of Oil Well Cements," *Cement Research Institute of India, (Research Bulletin)*, 1984.
22. ACI Committee 318, Structural Building Code, Building Code Requirements for Structural Concrete and Commentary, *ACI Manual of Concrete Practice, Part 3*, (American Concrete Institute: Farmington Hills, MI), Revised Annually.
23. Tasdemir, M. A., C. Tasdemir, S. Akyuz, A. D. Jefferson, F. D. Lydon, and B. I. G. Barr, "Evaluation of Strains at Peak Stresses in Concrete: A Three-Phase Composite Model Approach," *Cement and Concrete Composites*, **20**, no. 4, 301-18, 1998.

24. Mohamed, A. R., and W. Hansen, "Micromechanical Modeling of Concrete Response Under Static Loading - Part 1: Model Development and Validation," *ACI Materials Journal*, **96**, no. 2, 196-203, 1999.
25. ACI Committee 224, Cracking of Concrete Members in Direct Tension, *ACI Manual of Concrete Practice, Part 3*, (American Concrete Institute: Farmington Hills, MI), Revised Annually.
26. Conroy-Jones, G. A., and B. I. G. Barr, "Effect of Curing on the Tensile Strength of Medium to High Strength Concrete," *Magazine of Concrete Research*, **56**, no. 3, 151-58, 2004.
27. Marzouk, H., and Z. W. Chen, "Fracture Energy and Tension Properties of High-Strength Concrete," *Journal of Materials in Civil Engineering*, **7**, no. 2, 108-16, 1995.
28. Shah, S. P., S. E. Swartz, and C. Ouyang, Fracture Mechanics of Concrete: Applications of Fracture Mechanics to Concrete, Rock, and Other Quasi-Brittle Materials, (John Wiley & Sons, Inc.: New York, NY), 552 pp, 1995.
29. Li, V. C., and Mohamed Maalej, "Toughening in Cement Based Composites. Part I: Cement, Mortar, and Concrete," *Cement and Concrete Composites*, **18**, no. 4, 223-37, 1996.
30. Zhang, D., and K. Wu, "Fracture Process Zone of Notched Three-Point-Bending Concrete Beams," *Cement and Concrete Research*, **29**, no. 12, 1887-92, 1999.
31. Maji, A., and S. Shah, "Process Zone and Acoustic-Emission Measurements in Concrete," *Journal of Experimental Mechanics*, **28**, no. 1, 27-33, 1988.
32. Popovics, S., "Generalization of the Abram's Law - Prediction of Strength Development of Concrete from Cement Properties," *Journal of the American Concrete Institute*, **78**, no. 2, 123-29, 1981.
33. Farran, J., "Introduction: The Transition Zone - Discovery and Development," in *Interfacial Transition Zone in Concrete*, J. C. Maso (Ed.), (E & FN Spon: London, England), xiii-xv, 1995.
34. Kim, J-K, and Y-W Mai, Engineered Interfaces in Fiber Reinforced Composites, (Elsevier : New York, NY), 422 pp, 1998.
35. Bache, H. H., "Densified Cement/Ultrafine Particle Based Materials," *Aalborg Portland Cement and Concrete Laboratory Bulletin*, Report No. CBL-40 CONF.-8106349-1, 35 pp, 1981.

36. Sun, G. K., and J. F. Young, "Hydration Reactions in Autoclaved DSP Cements," *Advances in Cement Research*, **5**, no. 20, 163-69, 1993.
37. Powers, T. C., and T. L. Brownyard, "Studies of the Physical Properties of Hardened Portland Cement Paste," *Portland Cement Association Research Bulletin No.22*, 101-995, 1948.
38. Birchall, J. D., A. J. Howard, and K. Kendall, "Flexural Strengths and Porosity of Cements," *Nature*, **289**, 388-90, 1981.
39. St. John, D. A., L. C. McLeod, and N. B. Milestone, "An Investigation of the Mixing and Properties of DSP Mortars Made From New Zealand Cements and Aggregates," Report No. 40, Industrial Research Limited, 64 pp, 1993.
40. Chatterji, S. Letter to Birchall, et al, 2 July 1981.
41. Bailey, J. E., and D. D. Higgins. Letter to Birchall, et al, 2 July 1981.
42. Young, J. F., "Macro-Defect-Free Cement: A Review," in *Specialty Cements with Advanced Properties*, B. E. Scheets, A. G. Landers, I. Odler, and H Jennings (Eds.), (Materials Research Society: Pittsburg, PA), 101-21, 1991.
43. Richard, P., and Cheyrezy M. "Reactive Powder Concretes With High Ductility and 200-800 MPa Compressive Strength," P. K. Mehta (Ed.), (American Concrete Institute: Detroit, MI), 507-18, 1994.
44. U. S. Silica Company, "Min-U-Sil Ground Silica," 2008, <http://www.u-s-silica.com/mus.htm>
45. Gogotsi, G, "Fracture Toughness of Ceramics and Ceramic Composites," *Ceramics International*, **29**, 777-84, 2003.
46. Wittmann, F. H., "Crack Formation and Fracture Energy of Normal and High Strength Concrete," *Sadhana*, **27**, no. 4, 413-23, 2002.
47. Neeley, B. D., and D. M. Walley, "Very High-Strength Concrete," *The Military Engineer*, **87**, no. 572, 1995.
48. American Society for Testing and Materials, "Designation C 150-06 - Standard Specification for Portland Cement," *Annual Book of ASTM Standards, 04.01 Cement; Lime; Gypsum*, (American Society for Testing and Materials: West Conshohawken, PA), Published annually.

49. Grabowski, E., and J. E. Gillott, "Modification of Engineering Behavior of Thermal Cement Blends Containing Silica Fume and Silica Flour by Replacing Flour With Silica Sand," *Cement and Concrete Research*, **19**, no. 4, 449-508, 1989.
50. Grabowski, E., and J. E. Gillott, "Effect of Replacement of Silica Flour with Silica Fume on Engineering Properties of Oilwell Cements at Normal and Elevated Temperatures and Pressures," *Cement and Concrete Research*, **19**, no. 3, 333-44, 1989.
51. Alexander, M. G., "The Effects of Ageing on the Interface Zone in Concrete," in *Interfacial Transition Zone in Concrete*, J. C. Maso (Ed.), (E & FN Spon: London, England), 150-174, 1995.
52. Bentur, A, and M. D. Cohen, "Effect of Condensed Silica Fume on the Microstructure of the Interfacial Zone in Portland Cement Mortars," *Journal of the American Ceramic Society*, **70**, no. 10, 738-43, 1987.
53. Bentur, A., "The Role of the Interface in Controlling the Performance of High Quality Cement Composites," in *Advances in Cement Manufacturer and Use*, E. Gartner (Ed.), (Engineering Foundation: New York, NY), 227-37, 1989.
54. Darwin, D., "The Interface Transition Zone: "Direct" Evidence on Compressive Response," in *Microstructure of Cement-Based Systems/Bonding and Interfaces in Cementitious Materials*, S. Diamond, S. Mindess, F. P. Glasser, L. W. Roberts, J. P. Skalny, and L. D. Wakeley (Eds.), (Materials Research Society: Pittsburgh, Pennsylvania), 419-27, 1995.
55. Francois, R., and G. Arliguie, "Effect of the ITZ Damage on Durability of Reinforced Concretes in Chloride Environment," in *Microstructure of Cement-Based Systems/Bonding and Interfaces in Cementitious Materials*, S. Diamond, S. Mindess, F. P. Glasser, L. W. Roberts, J. P. Skalny, and L. D. Wakeley (Eds.), (Materials Research Society: Pittsburgh, Pennsylvania), 465-71, 1995.
56. Beaudoin, J. J., R. F. Feldman, and P J Tumidajski, "Pore Structure of Hardened Portland Cement Pastes and Its Influence on Properties," *Advanced Cement Based Materials*, no. 1, 224-36, 1994.
57. Ryshkewich, E, "Compression Strength of Porous Sintered Alumina and Zirconia," *Journal of the American Ceramic Society*, **36**, 66-68, 1953.
58. Beaudoin, J. J., and V. S. Ramachandran, "A New Perspective on the Hydration Characteristics of Cement Phases," *Cement and Concrete Research*, **22**, no. 4, 689-94, 1992.
59. Richard, P., and M. Cheyrezy, "Composition of Reactive Powder Concretes," *Cement and Concrete Research*, **25**, no. 7, 1501-11, 1995.

60. Haecker, C.-J., E. J. Garboczi, J. W. Bullard, R. B. Bohn, Z. Sun, S. P. Shah, and T. Voigt, "Modeling the linear elastic properties of portland cement paste," (SE Tylose GmbH & Co., NIST, Northwestern University), 2006, <http://ciks.cbt.nist.gov/~garbocz/paper148/index.html>
61. Hoek, E. and M. S. Diederichs, "Empirical estimation of rock mass modulus," 2006, <http://www.rocscience.com/library/rocnews/fall2005/RockMassModulus.pdf>
62. Kjellsen, K. O., O. H. Wallevik, and L. Fjallberg, "Microstructure and Microchemistry of the Paste-Aggregate Interfacial Transition Zone of High Performance Concrete," *Advances in Cement Research*, **Vol 10**, no. No 1, 33-40, 1998.
63. Zurz, A, and I. Odler, "XRD Studies of Portlandite Present in Hydrated Portland Cement Paste," *Advances in Cement Research*, **1**, no.1, 27-30, 1987.
64. Lutz, M. P., and P. J. M. Monteiro, "Effect of the Transition Zone on the Bulk Modulus of Concrete," *Proceedings of the 1994 MRS Fall Meeting, Nov 28-Dec 1 1994*, (Materials Research Society, Pittsburgh, PA, USA: Boston, MA, USA), 413-18, 1995.
65. Taylor, H. F. W., Cement Chemistry, (Thomas Telford: London, England), 459 pages, 1997.
66. Jennings, H. M., "A Model for the Microstructure of Calcium Silicate Hydrate in Cement Paste," *Cement and Concrete Research*, **30**, no. 1, 101-16, 2000.
67. Li, V. C., and J. Huang, "Relation of Concrete Fracture Toughness to its Internal Structure," *Engineering Fracture Mechanics*, **35**, no. 1/2/3, 39-46, 1990.
68. Mindess, S., F. V. Lawrence, and C. E. Kesler, "The J-Integral as a Fracture Criterion for Fiber Reinforced Concrete," *Cement and Concrete Research*, **7**, no. 6, 731-42, 1977.
69. Taylor, M. R., F. D. Lydon, and B. I. G. Barr, "Mix Proportions for High Strength Concrete," *Construction and Building Materials*, **10**, no. 6, 445-50, 1996.
70. Leung, C. K. Y, and V. C. Li, "Determination of Fracture Toughness Parameter of Quasi-Brittle Materials with Laboratory-Size Specimens," *Journal of Materials Science*, **24**, 854-62, 1989.
71. Nelson, P. K., Victor C. Li, and Toshiro Kamada, "Fracture Toughness of Microfiber Reinforced Cement Composites," *Journal of Materials in Civil Engineering*, **14**, no. 5, 384-91, 2002.

72. Low, N. M. P., and J. J. Beaudoin, "Flexural Strength and Microstructure of Cement Binders Reinforced with Wollastonite Micro-Fibres," *Cement and Concrete Research*, **23**, no. 4, 905-16, 1993.
73. ———, "The Flexural Toughness and Ductility of Portland Cement-Based Binders Reinforced With Wollastonite Micro-Fibres," *Cement and Concrete Research*, **24**, no. 2, 250-258, 1994.
74. ———, "Mechanical Properties of High Performance Cement Binders Reinforced With Wollastonite Micro-Fibres," *Cement and Concrete Research*, **22**, no. 5, 981-89, 1992.
75. American Society for Testing and Materials, "Designation C 305-94 - Standard Practice for Mechanical Mixing of Hydraulic Cement Pastes and Mortars of Plastic Consistency," *Annual Book of ASTM Standards, 04.01 Cement; Lime; Gypsum*, (American Society for Testing and Materials: West Conshohocken, PA), Published annually.
76. ———, "Designation C 109-99 - Standard Test Method for Compressive Strength of Hydraulic Cement Mortars (Using 50-Mm Cube Specimens)," *Annual Book of ASTM Standards, 04.01 Cement; Lime; Gypsum*, (American Society for Testing and Materials: West Conshohocken, PA), Published annually.
77. ———, "Designation C 39-96 - Standard Test Method for Compressive Strength of Cylindrical Concrete Specimens," *Annual Book of ASTM Standards, 04.02 Concrete and Aggregates*, (American Society for Testing and Materials: West Conshohocken, PA), Published annually.
78. Beaudoin, J. J., P. Gu, and W. Lin, "Flexural Behavior of Cement Systems Reinforced with High Aspect Ratio Aragonite Micro-Fibres," *Cement and Concrete Research*, **26**, no. 12, 1775-77, 1996.
79. Barbosa, M. T., and E. Sanchez, "Some Notes on Size Effect and Influence of Aggregate Roughness," *Proceedings of the International Conference on Cement Combinations for Durable Concrete*, (Thomas Telford Services Ltd: London, England), 351-56, 2005.
80. Applied Technology Services - Plastics, Omya International, "Physicochemical aspects of mineral components for plastics processors," 2007, http://www.omya.com/lit/kunststoff/e/OMYA_R1-02_E.pdf
81. Aiad, I., "Influence of Some Organic Admixtures on the Rheological and Mechanical Properties of Cement Pastes," *Advances in Cement Research*, **18**, no. 4, 171-77, 2006.
82. Puertas, F., H. Santos, M. Palacios, and S. Martinez-Ramirez, "Polycarboxylate Superplasticiser Admixtures: Effect on Hydration, Microstructure and Rheological Behaviour in Cement Pastes," *Advances in Cement Research*, **17**, no. 2, 77-89, 2005.

83. Uchikawa, H., D. Sawaki, and S. Hanehara, "Influence of Kind and Added Timing of Organic Admixture on the Composition, Structure and Property of Fresh Cement Paste," *Cement and Concrete Research*, **25**, no. 2, 353-64, 1995.
84. Yamada, K., T. Takahashi, S. Hanehara, and M. Matsuhisa, "Effects of the Chemical Structure on the Properties of Polycarboxylate-Type Superplasticizer," *Cement and Concrete Research*, **30**, no. 2, 197-207, 2000.
85. Stroband, J. , S. Poot, and J. Walraven, "The Effect of Mortar Joints Between Precast HSC Columns Loaded in Compression," *Fourth International Symposium on the Utilization of High Strength/High Performance Concrete*, F. de Larrard, and R. Lacroix (Eds.), (Presses de l'ecole nationale des ponts et chaussees: Paris, France), 817-33, 1996.
86. Fernandez-Altable, V., and I. Casanova, "Influence of Mixing Sequence and Superplasticiser Dosage on the Rheological Response of Cement Pastes at Different Temperatures," *Cement and Concrete Research*, **36**, no. 7, 1222-30, 2006.
87. Gagne, R., and P. C. Aitcin, "Superplasticizers for Durable Concrete." *Selected Papers on Superplasticizers* (Handy Chemicals LTD: Quebec, Canada), 249-65, 1993.
88. American Society for Testing and Materials, "Designation E 178-02 - Standard Practice for Dealing With Outlying Observations," *Annual Book of ASTM Standards, 14.02*, (American Society for Testing and Materials: West Conshohocken, PA), Published annually.
89. Cheyrezy, M., V. Maret, and L. Frouin, "Microstructural Analysis of RPC (Reactive Powder Concrete)," *Cement and Concrete Research*, **25**, no. 7, 1491-500, 1995.
90. Low, N. M. P., and J. J. Beaudoin, "Stability of Portland Cement-Based Binders Reinforced with Natural Wollastonite Micro-Fibers," *Cement and Concrete Research*, **24**, no. 5, 874-84, 1994.
91. Banthia, N., and J. Sheng, "Fracture Toughness of Micro-Fiber Reinforced Cement Composites," *Cement and Concrete Composites*, **18**, 251-69, 1986.
92. 3M Company, "3M Zeeospheres Ceramic Microspheres Gray Grades," 2007, <http://multimedia.3m.com/mws/mediawebserver?666666UuZjcFSLXTtlXMXOX&yEVuQEcuZgVs6EVs6E666666-->
93. American Society for Testing and Materials, "Designation C 593-99 - Standard Specification for Fly Ash and Other Pozzolans for Use With Lime," *Annual Book of ASTM Standards, 04.01 Cement; Lime; Gypsum*, (American Society for Testing and Materials: West Conshohocken, PA), Published annually.

94. ACI Committee 446, Fracture Mechanics of Concrete Concepts Models and Determination of Material Properties, *ACI Manual of Concrete Practice*, (American Concrete Institute: Farmington Hills, MI), Revised Annually.
95. Shah, S. P., and F. J. McGarry, "Griffith Fracture Criterion and Concrete," *Journal of the Engineering Mechanics Division, Proceedings of the American Society of Civil Engineers*, **97**, no. EM6, 1663-76, 1971.
96. Jacquot, P. , and P. K. Rastogi, "Speckle Metrology and Holographic Interferometry Applied to the Study of Cracks in Concrete.," *Developments in Civil Engineering*, 113-55, 1983.
97. Castro-Montero, A., S. P. Shah, and R. A. Miller, "Strain Field Measurement in Fracture Process Zone," *Journal of Engineering Mechanics*, **116**, no. 11, 2463-84, 1990.
98. Cedolin, L., S. D. Poli, and I. Iori, "Tensile Behavior Of Concrete," *Journal of Engineering Mechanics*, **113**, no. 3, 431-49, 1987.
99. Mihashi, H., and N. Nomura, "Correlation between Characteristics of Fracture Process Zone and Tension-Softening Properties of Concrete," *Nuclear Engineering and Design*, **165**, no. 3, 359-76, 1996.
100. Nomura, N., H. Mihashi, and M. Izumi, "Correlation of Fracture Process Zone and Tension Softening Behavior in Concrete," *Cement and Concrete Research*, **21**, 545-50, 1991.
101. Denarie, E., V. E. Saouma, A. Iocco, and D. Varelas, "Concrete Fracture Process Zone Characterization with Fiber Optics," *Journal of Engineering Mechanics, Proceedings of the American Society of Civil Engineers*, **127**, no. 5 , 494-502, 2001.
102. Faber, K. T., and A. G. Evans, "Crack Deflection Processes - 1 Theory.," *Acta Metallurgica*, **31**, no. 4, 565-76, 1983.
103. Timoshenko, S., and J. N. Goodier, Theory of Elasticity, (McGraw-Hill: New York, NY), 567 pages, 1970.
104. anonymous, "Fiber reinforced concrete," 2008, http://en.wikipedia.org/wiki/Fiber_reinforced_concrete
105. Jenq, Y. J., and S. P. Shah, "Two Parameter Fracture Model for Concrete," *ASCE Journal of Engineering Mechanics*, **111**, no. 10, 1227-41, 1985.
106. Navalurkar, R. K., C-T. T. Hsu, Kim. S.K., and M. Wecharatana, "True Fracture Energy If Concrete," *ACI Materials Journal*, **96**, no. 2, 213-25, 1999.

107. Karihaloo, B. L., Fracture Mechanics and Structural Concrete, (John Wiley & Sons, Inc.: New York), 330 pp, 1995.
108. Barr, B., R. Gettu, S. Al-Oraimi, and L. Bryars, "Toughness Measurement - the Need to Think Again," *Cement and Concrete Composites*, **18**, 281-97, 1996.
109. Nataraja, M. C., N. Dhang, and A. P. Gupta, "Toughness Characterization of Steel Fiber-Reinforced Concrete by JSCE Approach," *Cement and Concrete Research*, **30**, 593-97, 2000.
110. ACI Committee 544, "Measurement of Properties of Concrete," *ACI Materials Journal*, **85**, 583-93, 1988.
111. American Society for Testing and Materials, "Designation C 1018-92 - Standard Test Method for Flexural Toughness and First-Crack Strength of Fiber-Reinforced Concrete (Using Beam with Third-Point Loading)," *Annual Book of ASTM Standards*, 04.02, (American Society for Testing and Materials: West Conshohawken, PA), Published Annually.
112. Mindess, S., L. Chen, and D. R. Morgan, "Determination of the First-Crack Strength and Flexural Toughness of Steel Fiber-Reinforced Concrete," *Advanced Cement Based Materials*, **1**, no. 5, 201-8, 1994.
113. Song, P. S., and S. Hwang, "Mechanical Properties of High-Strength Steel Fiber-Reinforced Concrete," *Construction and Building Materials*, **18**, no. 9, 669-73, 2004.
114. Jeng, F., M-L Lin, and S-C Yuan, "Performance of Toughness Indices for Steel Fiber Reinforced Shotcrete," *Tunnelling and Underground Space Technology*, **17**, no. 1, 69-82, 2002.
115. Jennings, H., and J. Thomas, unpublished contract report to U. S. Army Corps of Engineers.
116. Cincotto, M. A., A. A. Melo, and W. L. Repette, "Effect of Different Activators Type and Dosages and Relation to Autogenous Shrinkage of Activated Blast Furnace Slag Cement," *Proceedings of the 11th International Congress on the Chemistry of Cement, Cement's Contribution to the Development in the 21st Century*, G. Grieve, and G. Owens (Eds.) Document Transformation Technologies, 1878-87, 2003.
117. Ghafoori, N., and S. Dutta, "Building and Nonpavement Applications of No-Fines Concrete," *Journal of Materials in Civil Engineering, American Society of Civil Engineers*, **7**, no. 4, 286-89, 1995.
118. U. S. Army Corps of Engineers Protective Design Center, "ConWep - Conventional Weapons Effects," 2007, <https://pdc.usace.army.mil/software/conwep/>

119. Mindess, S., and J. F. Young, Concrete, (Prentice-Hall, Inc.: Englewood Cliffs, NJ), 671 pages, 1981.
120. Popovics, S, Strength and Related Properties of Concrete a Quantitative Approach, (John Wiley & Sons, Inc.: New York), 538 pages, 1998.
121. Bentz, D. P., P. V. Coveney, E. J. Garboczi, M. F. Kleyn, and P. E. Stutzman. "Cellular Automaton Simulations of Cement Hydration and Microstructure Development." Web page, [accessed May 2008-30 June 2008]. Available at <http://ciks.cbt.nist.gov/garbocz/cell1994/cellauto.htm>.
122. Michaux, M. , E. B. Nelson, and B. Vidick, "Chemistry and Characterization of Portland Cement," Oil Well Cements, Schlumberger Dowell.
123. Cyr, M., P. Lawrence, and E. Ringot, "Efficiency of Mineral Admixtures in Mortars: Quantification of the Physical and Chemical Effects of Fine Admixtures in Relation With Compressive Strength," *Cement and Concrete Research*, **36**, 264-77, 2006.

APPENDIX A: MASS STUDY OF THE HYDRATION PRODUCTS OF VHSC

A.1 Background and assumptions

Describing the relationships of VHSC requires a description of the chemical reactions that occur when cement, silica fume, and water are combined. The processes that take place when these materials are combined are very complex and not fully understood. To be able to represent these relationships, the chemical reactions that occur must be modeled; however, full agreement on the chemical relationships that govern the reactions has not been reached. This is due, in part, to the variable chemistry of the calcium-silicate-hydrate reaction. Calcium silicate hydrate is described as an amorphous solid without an accurately defined molecular composition. The two major cement phases responsible for the production of calcium silicate hydrate are tricalcium silicate (C_3S) and dicalcium silicate (C_2S) but how they react to form calcium silicate hydrate is strongly influenced by the impurities in the two compounds. Most texts covering the subject of cement chemistry have placed the C/S ratio of the reaction somewhere between 1.5 and 2 [17, 65, 120, 121] but this range allows for many variations on the molecular formula. As a result, the product is represented without subscript in the chemical shorthand as C-S-H to reflect the uncertainty of its composition.

Further complicating the relationships are the facts that most research to describe the reactions has been conducted on pure compounds of the cement phases that lack the impurities of the hybrid phases (different proportions of silicates, ferrites, and aluminates) [121]; and particularly in the case of VHSC, the chemistry of oil well cement (VHSC uses class H oil well cement) is also on the fringe of the understood reactions.

For purposes of calculations in this appendix, the densities and molar volumes in Table A.1 and the cement chemistry reactions in Table A.2 reported by both Bentz et al. [121] and Mindess and Young [119] are used. While the densities and molar volumes reported are accurate, the cement reactions are still regarded as approximations.

Compound Name	Chemical Formula	Density, (g cm ⁻³)	Molar Volume, (cm ⁻³ mol ⁻¹)
Tricalcium Silicate	C ₃ S	3.21	71
Dicalcium Silicate	C ₂ S	3.28	52.4
Tricalcium Aluminate	C ₃ A	3.03	89.1
Tetracalcium Aluminoferrite	C ₄ AF	3.73	128
Calcium Silicate Hydrate	C _{1.7} SH ₄	1.85	124
Pozzolan C-S-H	C _{1.1} SH _{2.1}	1.97	81
Calcium Hydroxide	CH	2.24	33.1
Ettringite	C ₆ A ₃ H ₃₂	1.75	715
Monosulfate	C ₄ A ₃ H ₁₂	1.99	313
Hydrogarnet	C ₃ AH ₆	2.52	150
Iron Hydroxide	FH ₃	2.2	95.2

Silicate Reactions		
$C_3S + 5.3H \rightarrow C_{1.7}SH_4 + 1.3CH$		(A.1)
$C_2S + 4.3H \rightarrow C_{1.7}SH_4 + 0.3CH$		(A.2)
$1.1CH + S + H \rightarrow C_{1.1}SH_{2.1}$		(A.3)
Aluminate and Ferrite Reactions		
$C_3A + 6H \rightarrow C_3AH_6$		(A.4)
$C_3A + 3C_2SH_2 + 26H \rightarrow C_6A_3H_{32}$		(A.5)
$2C_3A + C_6A_3H_{32} + 4H \rightarrow 3C_4A_3H_{12}$		(A.6)
$C_4AF + 3C_2SH_2 + 30H \rightarrow C_6A_3H_{32} + CH + FH_3$		(A.7)
$3C_4AF + C_6A_3H_{32} + 19H \rightarrow 3C_4A_3H_{12} + 6CH + 3FH_3$		(A.8)
$C_4AF + 10H \rightarrow C_3AH_6 + CH + FH_3$		(A.9)

Note: The molar masses of equation A.8 have been modified from what appears in the source web page to balance the equation.

A.2 Component materials

The baseline VHSC consists of the materials listed in Table A.3 with the mass proportion of cement set as 1 and the remaining materials being decimal fractions of the mass of the cement. Also given in this table are pertinent data for the source of the component materials. The data from the mill test report for the Lafarge class H cement, Joppa plant used are given in Table A.4.

Component	Mass Ratio	Comments
Cement	1	Class H from Lafarge, Joppa Plant
Sand	0.97	Chert sand, 6.4 mm msa, Prescott, AR
Silica Flour	0.28	Crushed quartz, ~5 μ m, U.S. Silica
Silica Fume	0.39	Elkem ES 900 W
HRWRA	0.03	Powder DISAL™, Handy Chemical
Water	0.22	w/cm = 0.158

Composition	%
C ₃ S	62.00
C ₂ S	15.15
C ₃ A	0.20
C ₄ AF	13.39
SiO ₂	21.60
Al ₂ O ₃	2.90
Fe ₂ O ₃	4.40
CaO	63.70
MgO	3.10
SO ₃	2.60
Loss on Ignition	0.98
Insoluble Res.	0.25
Free Lime	0.37
Total Alkali	0.22

For the exercise conducted in this appendix, the following five assumptions were made.

- 1) The mass proportions of the mixture were based on 100 grams of cement.
- 2) The silica flour and sand in the mixture are inert fillers and did not enter into any chemical reactions.
- 3)

Although VHSC is cured in ambient temperature water from 24-hrs age until the end of 7-days

age, it is so dense that very little outside water is absorbed into its microstructure and it behaves more like a sealed system, obtaining its level of hydration from the original mixing water. 4) The available mass of original material for any reaction was based on the calculation of percentage of cement converted to hydration products before self-desiccation occurred and any further reaction ceased when that percentage was reached. 5) Hydration of all phases in the cement occurs simultaneously, although not necessarily at the same rate of reaction; and the reactions of pure phase compounds are different from those of portland cement phases due to impurities in the manufactured cement.

A.3 Calculation of percent hydration under very-low w/c conditions

When insufficient water is available to hydrate all the available cement, the reaction self-desiccates and will stop at some percentage of full hydration, leaving part of the cement as unreacted clinker. When this happens the masses of the original phases consumed and the reaction products formed will be based on the percentage of hydration. Such is the case with VHSC. The w/c used with VHSC is 0.22, a ratio that is far short of the 0.38 – 0.40 calculated to produce full hydration. The chore in such a case is to calculate the percentage of clinker that will hydrate before the reaction stops. Pioneering work by Powers and Brownyard [37] established the volumetric relationships that make such a calculation possible. The following exercise to calculate percent hydration is based on the work of Powers and Brownyard as described by Neville [17] and modified in this dissertation to include the hydration effects of silica fume on the outcome of the reactions.

To establish the mass of cement that will hydrate with a 0.22 w/c (starting with 100g of cement, 39g of silica fume, and 22g of water), let x represent the mass of cement that will

hydrate. The absolute volume of x grams of unhydrated cement is:

$$xg / 3.15g \text{ cm}^{-3} = 0.318x \text{ cm}^3 \quad (\text{A.10})$$

The volume of non-evaporable water produced, based on the averaging assumption that 23% of the mass of cement will be non-evaporable water [17], is:

$$xg * 0.23 * 1 \text{ cm}^3 \text{ g}^{-1} = 0.23x \text{ cm}^3 \quad (\text{A.11})$$

As given by Neville, the specific gravities of the solid products of hydration are less than those of unhydrated cement; consequently the solid products of hydration occupy a larger volume than the dry cement. This has been estimated to be approximately equal to the sum of the volumes of the dry cement and non-evaporable water, less approximately 25% of the volume of the non-evaporable water. In equation form this is:

$$0.318x + 0.23x * (1 - 0.254) = 0.489x \text{ cm}^3 \quad (\text{A.12})$$

The reaction products produced during the hydration of VHSC include pozzolanic C-S-H created from the combination of CH, S, and H in the original mixture (see mass calculations later in this appendix). This must be factored into the solid products of hydration since it produces additional C-S-H and affects the water available for original cement hydration. The mass of the pozzolanic C-S-H created in a preliminary set of mass calculations was 23 g based on a calculation of 52% hydration before desiccation. This realized a volume of $23 \text{ g} / 1.97 \text{ g cm}^{-3} = 11.7 \text{ cm}^3$. Adding this volume of pozzolanic C-S-H into the current volume calculations presents a recursive situation that requires a number of iterations to resolve errors. It is understood that this is just an approximation to the increase in volume, and for the present exercise this first iteration will be used.

With the above data, the mass of hydrated cement, x , can be determined as follows: The volume of the total water is equal to the volumes of the non-evaporable water, the volume of the

gel water, and the volume of capillary water. With a w/c of 0.22, it is reasonable to assume that the volume of capillary water will be zero leaving the equation for volume of total water as:

$$0.23x + \omega_g v_g = 22 \text{ g/1 g cm}^{-3} \quad (\text{A.13})$$

in which ω_g is the mass of gel water and v_g is the specific volume of water, $1 \text{ cm}^3 \text{ g}^{-1}$. Since the characteristic porosity of the hydrated cement is approximately 28% [17], it can be expressed as the volume of gel water divided by the sum of the volumes of the solid products of hydration (including the pozzolanic C-S-H) plus the volume of gel water or:

$$\frac{\omega_g v_g}{0.489x + 11.7 + \omega_g v_g} = 0.28 \quad (\text{A.14})$$

and equations A.13 and A.14 can be solved for x yielding 41.53 g or 41.53% hydration. This percentage will be used beginning in paragraph A.4 to estimate the masses of original component phases that will be consumed before hydration ceases.

Knowing the mass of cement that will hydrate with a w/c = 0.22, equation A.13 can be solved for the mass of gel water as:

$$\omega_g = \frac{22 - 0.23x}{v_g} \quad (\text{A.15})$$

Solving A.15 yields the mass of gel water as 12.49 g.

A.4 Mass calculations of reactants and products for the VHSC model

The remaining tables in this appendix represent calculations of the compounds consumed and products produced from the chemical reactions (equations A.1 through A.9) in Table A.2.

With the point at which hydration will cease being established at 41.53%, Table A.5 shows the mass of reactants that will be available to enter into the model. Twenty-two grams of water and 39 grams of silica fume will be available to react with these compounds.

Table A.5 Masses of reacted compounds

Compound	Total Mass, g	Mass reacted at 41.53% hydration, g
C ₃ S	62.00	25.7
C ₂ S	15.15	6.29
C ₃ A	0.20	0.08
C ₄ AF	13.39	5.56

A.5 Chemical reactions

The chemical reactions associated with equations A.1 to A.9 will be presented in table form as shown in the example given in Table A.6. An explanation of the calculations presented in this table is given for clarity. The table cell to the right of the cell labeled chemical reaction gives the reaction under consideration from Table A.2. This cell may contain two variations of the same reaction. The top reaction is identical to the equation of interest in Table A.2, while the reaction directly beneath it is the same, only with the molar quantities proportioned to give 1 mole to the compound controlling the reaction. The column headed “moles in reaction” has been

Table A.6 Example table of consumed and produced compounds using equation A.8

Phase	C ₄ AF						
Chemical Reaction	$3C_4AF + C_6S_3H_{32} + 19H \rightarrow 3C_4ASH_{12} + 6CH + 3FH_3$						
Compounds consumed							
Compound	g/mole	moles in reaction	grams in reaction	grams available	moles available	moles consumed	grams consumed
C ₄ AF	485.98	3.0	1457.94	5.983	0.01231	0.00624	3.034
C ₆ S ₃ H ₃₂	1153.19	1.0	1153.190	2.400	0.00208	0.00208	2.400
H	18.016	19.0	342.304	22.00	1.221	0.03954	0.712
Sum of grams consumed							6.147
Compounds produced							
Compound	g/mole	moles in reaction	grams in reaction	grams available	moles available	moles produced	grams produced
C ₄ ASH ₁₂	622.538	3.0	1867.614	na	na	0.00624	3.887
CH	74.096	6.0	444.576	na	na	0.01249	0.925
FH ₃	213.748	3.0	641.244	na	na	0.00624	1.335
Sum of grams produced							6.147

set to match the moles in the chemical reaction used. “Grams in reaction” is grams per mole multiplied by moles in reaction. “Grams available” represents the available mass of the compound being consumed. This column is only relevant in the compounds consumed section of the table. In the compounds produced section an “na” will appear in this cell. The column headed “moles available” is obtained by dividing “grams available” by “g/mole”. Like the “grams available” column, this column is only relevant in the compounds consumed section of the table. The column headed by “moles consumed” in the compounds consumed section and “moles produced” in the compounds produced section is obtained by multiplying the “moles available” by the “moles in reaction”. In this calculation the value of the “moles available” for the controlling compound (where moles in reaction = 1.0) in the compounds consumed section of the table is used for all calculations of the compounds consumed and produced since the moles consumed or produced will be dependent on the moles available from the controlling compound. Finally the column for the “grams consumed” or the “grams produced” is obtained by multiplying the “moles consumed” or “moles produced” by the “g/mole”. As a check of the stoichiometry, the grams consumed must equal the grams produced.

A.6 Tricalcium aluminate phase

In this exercise, the reactions will be discussed in the order of fastest to slowest reaction. The C_3A is the most reactive phase at short hydration times. It reacts so fast that a phenomenon known as flash set occurs within a number of minutes of the addition of water if gypsum is not added to the unhydrated cement to slow down this rapid onset of setting. Flash setting is particularly debilitating in oil well cements that have to maintain fluidity for the length of time it takes the cement to be pumped into the annular space between the well hole and the pipe, often having to be pumped to depths of 4880 m under very high temperatures [122]. C_3A in the cement

is also undesirable because it contributes very little strength to the mixture and consumes more water than the silicates. It usually consists of a small proportion of the compounds in the unhydrated cement. In VHSC, when made using class H oil well cement, its presence is very small, constituting only 0.20% of the compounds present (see Table A.4) for the reasons discussed above.

Table A.4 shows that the sulfates in the cement amount to approximately 2.6% or 2.6 g per each 100 g of cement. Were all the sulfates to come from the gypsum in the cement it would account for 5.6 g of available gypsum to react with the C_3A .

Of the reaction equations available to describe the aluminates (equations A.4 through A.6), equation A.4 will not take place because there is gypsum present. Equation A.5 can occur because there is sufficient aluminate, gypsum, and water to react. While it is true that all reactions occur simultaneously, for simplicity sake it will be assumed that this reaction goes to completion consuming what little available C_3A there is and preventing reaction A.6 for lack of C_3A . Under this assumption, all the aluminate is consumed in equation A.5 along with 0.159 g of gypsum and 0.144 g of water producing 0.386 g of ettringite as shown in Table A.7. The ettringite will remain stable and not convert to monosulfoaluminate because of the excess sulfate.

A.7 The silicate phases

The reaction of the silicates, C_3S and C_2S , accounts for the greatest portion of the reactions in the model producing nearly all of the C-S-H and CH. Tricalcium silicate reacts faster than dicalcium silicate and is available in much larger quantity than the C_2S . The C_3S consume about four times as much water and more than twice as much CH as does C_2S . While the reactions take place simultaneously, for this exercise, the reaction equation A.1 is given first in

Table A.7 Consumed and produced compounds of the C₃A phase using equation A.5							
Phase	C ₃ A						
Chemical Reaction	C ₃ A + 3C ₂ S _H ₂ + 26H → C ₆ A ₃ H ₃₂						
Compounds consumed							
Compound	g/mole	moles in reaction	grams in reaction	grams available	moles available	moles consumed	grams consumed
C ₃ A	270.2	1.0	270.200	0.083	0.00031	0.00031	0.083
C ₂ S _H ₂	172.178	3.0	516.534	5.60	0.03250	0.00092	0.159
H	18.016	26.0	468.416	22.00	1.221	0.00799	0.144
Sum of grams consumed							0.386
Compounds produced							
Compound	g/mole	moles in reaction	grams in reaction	grams available	moles available	moles produced	grams produced
C ₆ A ₃ H ₃₂	1255.15	1.0	1255.150	na	na	0.00031	0.386
Sum of grams produced							0.386

Table A.8 and reaction A.2 is given in Table A.9. They both deplete their respective phases, collectively consuming 13.6 g of water, and producing 33.96 g of C-S-H and 11.67 g of CH.

Table A.8 Consumed and produced compounds of the C₃S phase using equation A.1							
Phase	C ₃ S						
Chemical Reaction	C ₃ S + 5.3H → C _{1.7} S _H ₄ + 1.3CH						
Compounds consumed							
Compound	g/mole	Moles in reaction	grams in reaction	grams available	moles available	moles consumed	grams consumed
C ₃ S	228.33	1.0	228.330	25.75	0.113	0.113	25.75
H	18.016	5.3	95.485	21.86	1.213	0.598	10.77
Sum of grams consumed							36.52
Compounds produced							
Compound	g/mole	Moles in reaction	grams in reaction	grams available	moles available	moles produced	grams produced
C _{1.7} S _H ₄	227.49	1.0	227.490	na	na	0.113	25.65
CH	74.096	1.3	96.325	na	na	0.147	10.86
Sum of grams produced							36.52

Table A.9 Consumed and produced compounds of the C₂S phase using equation A.2

Phase	C ₂ S						
Chemical Reaction	C ₂ S + 4.3H → C _{1.7} SH ₄ + 0.3CH						
Compounds consumed							
Compound	g/mole	Moles in reaction	grams in reaction	grams available	moles available	moles consumed	grams consumed
C ₂ S	172.25	1.0	172.250	6.29	0.037	0.037	6.29
H	18.016	4.3	77.469	11.09	0.615	0.157	2.83
Sum of grams consumed							9.12
Compounds produced							
Compound	g/mole	Moles in reaction	grams in reaction	grams available	moles available	moles produced	grams produced
C _{1.7} SH ₄	227.49	1.0	227.490	na	na	0.037	8.31
CH	74.096	0.3	22.229	na	na	0.011	0.81
Sum of grams produced							9.12

A.8 The effect of silica fume

Silica fume in the mixture serves two major purposes. It consumes the detrimental CH in the mixture, producing a pozzolanic version of C-S-H in the process and acts as a very tiny filler to occupy void space between larger particles in the microstructure. There is a massive over abundance of silica fume in VHSC. Where most researchers recommend using up to 12 percent by mass of cement, VHSC uses 39 percent. This most certainly assures full consumption of the CH with a large surplus of material to act as excellent filler material. Table A.10 shows the consumption and production of compounds resulting from the addition of silica fume to the mixture. The silicate phases produced 11.67 g of CH which, as shown in Table A.10, is completely consumed by 4.02 g of the 39 g of silica fume used in the mixture. The contribution of the remaining 34.98 g of silica fume is a question that has not been fully answered by the research community. Two possibilities for additional physical effects were proposed by Cyr et al.

Table A.10 Consumed and produced compounds of the S reaction using equation A.3

Phase	S							
Chemical Reaction	$1.1\text{CH} + \text{S} + \text{H} \rightarrow \text{C}_{1.1}\text{SH}_{2.1}$							
	$1\text{CH} + 0.909\text{S} + 0.909\text{H} \rightarrow 0.909\text{C}_{1.1}\text{SH}_{2.1}$							
Compounds consumed								
Compound	g/mole	moles in reaction	grams in reaction	grams available	moles available	moles consumed	grams consumed	
CH	74.096	1.0	74.096	11.67	0.158	0.158	11.67	
S	28.09	0.909	25.537	39.00	1.388	0.143	4.02	
H	18.016	0.909	16.378	8.26	0.458	0.143	2.58	
Sum of grams consumed								18.28
Compounds produced								
Compound	g/mole	moles in reaction	grams in reaction	grams available	moles available	moles produced	grams produced	
$\text{C}_{1.1}\text{SH}_{2.1}$	127.61	0.909	116.010	na	na	0.143	18.28	
Sum of grams produced								18.28

[123]: as filler material altering the porosity and density of the mixture and as sites of heterogeneous nucleation leading to chemical activation of the hydration of cement. Further pozzolanic reaction beyond the conversion of the CH into C-S-H is a matter of speculation and beyond the scope of this exercise. It can be stated with confidence that the excess silica fume fills in space between larger particles, improves the integrity of the paste aggregate interface, and acts as a spherical-particle lubricant in the bulk paste. Because silica fume is a very expensive pozzolan, replacing some of the silica fume with a less expensive material of the same fineness would reduce the cost and maintain the density of the mixture.

A.9 The tetracalcium aluminoferrite phase

The ferrite phase is the least well understood of the four cement phases. It is said to react slowly and only contribute to the long-term strength of the cement [121]. In the model followed here it behaves much like the aluminate phase, consuming gypsum and water and producing ettringite, monosulfate, portlandite, and iron (III) hydroxide. The C_4AF reaction with gypsum

may also help accelerate the hydration of the silicates [17]. The bulk A/F ratio of this phase has a strong effect on the thickening of oil well cements. In Table A.11, it is assumed that reaction equation A.7 consumes all the remaining water and that water controls the reaction. The reaction produces ettringite and a small amount of CH and FH₃. It is assumed the ettringite will remain stable because of the small remnant of remaining sulfate. Because there is excess S in the mixture the additional 0.778 g of CH produced here should be converted to C-S-H, but because all the water was depleted in the reaction of equation A.7 this conversion was ignored.

Table A.11 Consumed and produced compounds of the C₄AF phase using equation A.7

Phase	C ₄ AF						
Chemical Reaction	C ₄ AF + 3C _S H ₂ + 30H → C ₆ A _S ₃ H ₃₂ + CH + FH ₃ 0.033C ₄ AF + 0.1C _S H ₂ + H → 0.033C ₆ A _S ₃ H ₃₂ + 0.033CH + 0.033FH ₃						
Compounds consumed							
Compound	g/mole	moles in reaction	grams in reaction	grams available	moles available	moles consumed	grams consumed
C ₄ AF	485.98	0.033	16.183	5.561	0.01144	0.01051	5.105
C _S H ₂	172.178	0.100	17.218	5.431	0.03154	0.03152	5.426
H	18.016	1.000	18.016	5.678	0.315	0.31516	5.678
Sum of grams consumed							16.210
Compounds produced							
Compound	g/mole	moles in reaction	grams in reaction	grams available	moles available	moles produced	grams produced
C ₆ A _S ₃ H ₃₂	1255.15	0.033	41.796	na	na	0.01051	13.186
CH	74.096	0.033	2.467	na	na	0.01051	0.778
FH ₃	213.748	0.033	7.118	na	na	0.01051	2.246
Sum of grams produced							16.210

A10. Summary of reactions

It has been seen through this hydration exercise that the limited amount of water available with a 0.22 w/c results in self-desiccation of the hydration reaction which stops at approximately 41.5% completion. This limits the amount of conventional C-S-H formed to approximately 41.5% of the amount that would be formed if 100% hydration occurred.

The original compounds consumed and hydration products produced in the above exercise are summarized in Table A.12. All the original compounds were consumed except for 0.45 g of C_4AF , 0.005 g of C_2SH_2 and 34.98 g of S. The compounds produced from these reactions were 33.96 g of $C_{1.7}SH_4$, 18.28 g of pozzolanic $C_{1.1}SH_{2.1}$, 13.57 g of ettringite, 2.25 g of iron hydroxide, and 0.78 g of CH. Of high interest in this exercise is the amount of pozzolanic C-S-H formed at the consumption of a small amount of silica fume. Roughly 54% additional C-S-H is produced over that produced by the silicates. While the combined total of normal plus pozzolanic C-S-H is less than the amount of normal C-S-H that would be formed under full hydration it represents a large amount of additional C-S-H and nearly complete removal of the unwanted CH.

**APPENDIX B:
DESCRIPTION OF THE PHYSICAL TRANSFORMATION OF DRY
CEMENTITIOUS POWDER COMPONENTS INTO FRESH VHSC PASTE
WHEN WETTED WITH WATER AND HIGH-RANGE WATER-
REDUCING ADMIXTURES**

B.1 Introduction and time-line format

While nothing more spectacular than high-range, water-reducing admixtures (HRWRAs) and water are added to cementitious and inert powders to produce VHSC, the transformation from wetted powders to fully-mixed mortar is strikingly removed from the ordinary experience in making concrete. This difference is primarily due to three conditions. First, the size and proportional volumes of the particles, sand, cement, silica flour, and silica fume, are concentrated on the small end of the particle size range and the ratio of cementitious material to sand is much higher than ordinary concrete. Consequently, the surface area of the dry particles is very high and affects the distribution of water in the mixture. Secondly, the mass of water used to hydrate these powders is very small. A typical w/cm for VHSC is on the order of 0.16 whereas the w/cm for normal and high-strength concretes is on the order of 0.35 to 0.4. Lastly the reliance on HRWRAs to supplement the rheology of the mixture calls for high dosages of the chemicals to make the otherwise stiff paste workable.

Depending on the proportions of the materials used in the mixing the VHSC, the time it takes to make a paste (time-to-paste) (ttp) can be as much as 60 minutes. This is an extreme time-line and never tolerated under normal circumstances, but has been seen in the mixing rheology research conducted in the development of VHSC. Fifteen minutes is a more plausible ttp figure and very rapid ttp figures have been as short as 5 minutes. The length of time depends highly on the proportions of dry and wet materials, the amount of HRWRA used, and the amount

of energy put into the mixing process. In this appendix, fractional portions of the ttp will be used as descriptors rather than actual times to describe the process in a more general fashion.

B.2 Appearance of the wetted powders during mixing

Not only is the time line different from conventional mixing, but also the physical transformation of wetted powder to paste is unique. Adding water and admixtures to conventional concrete produces wetted materials almost immediately and fully mixed concrete in a matter of minutes. The transformation is rapid and nothing out of the ordinary is normally expected.

Mixing the dry powders in VHSC is the same as in conventional dry ingredient mixing, although the smaller diameter particles (those ranging from 0.1 to 100 μm) are added to the mixer first and capped over with the larger diameter particles (those ranging from 100 μm to 6 mm) to prevent losing fine-particle material when the mixer is engaged. Dry mixing time generally is from 5 to 10 minutes under research conditions and is not part of the ttp time line.

Time-to-paste is the unit time figure mentioned above and typical times to physical changes in appearance will be described as percentage parts of this unit. If the HRWRA is a powder it generally is added at the time of dry component blending. However, if it is a liquid it is added to the mixing water and the mass of mixing water is reduced by the mass of water that is part of the HRWRA to maintain the low w/cm of the proportioning. When the liquids are added to the blended dry materials, the mixer is already engaged and the liquids gradually added over a 30 second period to spread the liquid over the powders as evenly as possible. If ttp is being recorded, it is started with the first addition of liquid. After addition of the liquids nothing changes for about 10% of the ttp; the dry powders look much the same only they appear to be damp. As the damp powders continue to be mixed, the originally cement colored powders begin

to gradually darken, first to a light-gray at about 15% ttp and to a deep-gray color at about 70% ttp. This color change comes about as the HRWRA is beginning the deflocculating process on the cement so the water can come in contact with the cement. The dark-gray color is similar to the color one would see on mixing cement and water to a paste.

The dampened material is still powder grains at this point, but they are bigger (perhaps 150 μm in diameter at this point) and getting bigger as time progresses. At about 85% of ttp the powders begin to exhibit a sheen on their surface and they begin to come together as shiny gray balls about 500 μm in diameter. The small shiny balls continue to form larger balls about 1 to 3 mm in diameter at about 95% ttp. Finally, the now large balls of wet cement form together into a very stiff, dough-like paste at 100% ttp.

At this point, the paste is not fully mixed nor has it achieved the full change in rheological properties it will have when properly mixed. Post-ttp mixing is continued for 10 minutes under research conditions during which time the dough-like paste will become much more fluid-like before being considered fully mixed. The mixed mortar will now have a consistency anywhere between thick oatmeal and viscous honey^{B1} depending on the component ingredients used, and the mass of water and HRWRA employed. Although the slump-cone test has not been used in VHSC research, the slump can range from no-slump to self-leveling.

^{B1} Please pardon the non-technical rheological descriptors.

APPENDIX C: SAMPLE CALCULATIONS USED FOR FRACTURE TOUGHNESS IN CHAPTER 6

C.1 Background and assumptions

The following example presents the detail calculations made for the experiments involving fracture toughness, K_{Ic} of the unreinforced VHSC described in the paragraphs under section 6.2.1 of chapter 6. These procedures and equations were used for all fracture toughness measurements and calculations from chapter 6 unless discussed differently in the body of the chapter. The example here is for beam 1 of the unreinforced VHSC mixture.

C.2 Set-up of experiment and dimension calculations

The test set up for the fracture toughness beam experiments is shown in Figure C.1. Beam dimensions L , B , and W were measured three times at top, and bottom or left, mid, and

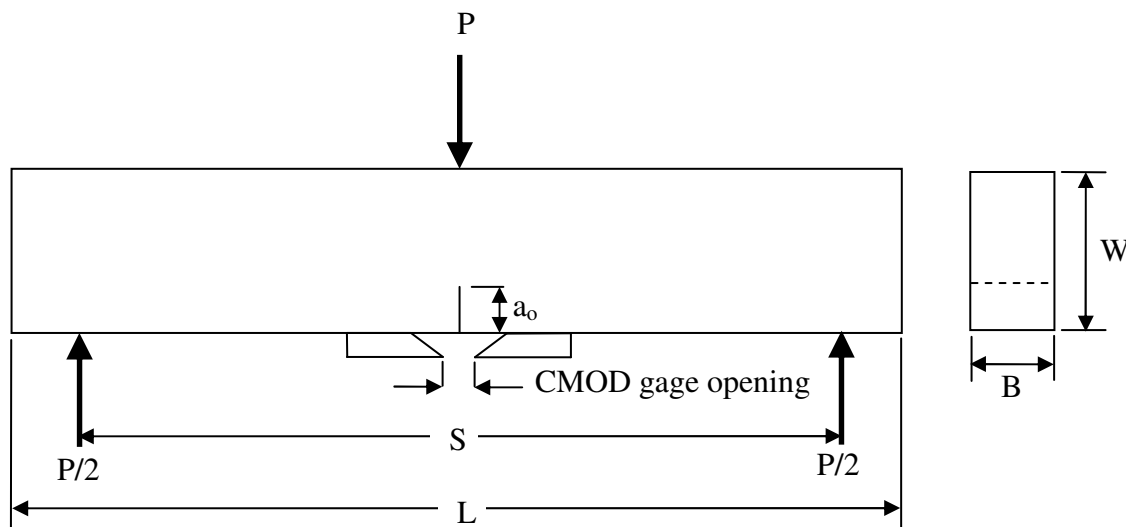
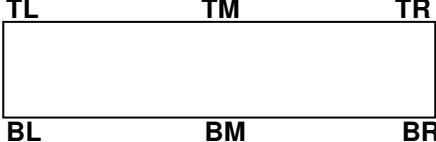


Figure C.1 Beam dimensions and test set up

right and the measurements averaged as shown in Table C.1 below. The CMOD clip-gage had a full measurement span of 6.35 mm and was connected to the hydraulic actuator as feedback to a

displacement controlled loading algorithm in the test system. The loading supports were steel cylinders, 12.7 mm in diameter and 101.2 mm long.

Table C.1 Beam measurements

Table C.1 Beam measurements							
							
		Beam mass, g	2619.70	Beam density, g/cm³	2.37		
Beam Thickness, B, at top, mm							
Reading	TL		TM		TR		
1	38.20		38.81		39.60	Thickness	
2	38.20		38.76		39.60	Top avg.	
3	38.07		38.81		39.55	38.85	
Average	38.16		38.79		39.58		Thickness Grand avg. 38.98
Beam Thickness, B, at bottom, mm							
Reading	BL		BM		BR		
1	38.46		39.55		39.32	Thickness	
2	38.48		39.52		39.32	Bottom avg.	
3	38.58		39.57		39.27	39.12	
Average	38.51		39.55		39.30		
Beam Depth, W, mm							
Reading	Left		Middle		Right		
1	80.04		79.93		79.91	Depth	
2	80.04		79.71		79.91	Grand avg.	
3	80.01		79.65		79.93	79.90	
Average	80.03		79.76		79.92		
Beam Length, L, mm							
Reading	Top	Bottom		Notch Depth, a₀, mm			
1	355.60	354.01	Length	Front	Back		
2	354.01	355.60	Grand avg.	26.21	26.48		
Average	354.81	354.81	354.81	Average 26.35			

C.3 Analysis of fracture toughness data

C.3.1 Models

The model used to calculate fracture toughness was the Two Parameter Fracture Model (TPFM) of Jenq and Shah [105]. This model requires a load-CMOD test with an unloading-to-zero-an-reloading segment taken at a point on the strain-softening side of the curve within 95% of the maximum load to obtain the two parameters, K_{Ic} , and $CMOD_c$. This was not possible in

the ERDC laboratory tests because of software problems that hampered the functioning of the unloading-reloading segment of the loading algorithm. The alternative solution was to test the beams in simple load-CMOD format and to calculate the unloading compliance, C_u , using a mathematical technique presented by Navalurkar et al. [106]. In their paper the authors presented load-deflection and load-CMOD test results for concrete specimens of various geometries and strengths in both direct tension and flexural bending and developed relationships that would allow the calculation of fracture energy from load-CMOD rather than load-deflection curves. Their reasoning for this approach was to eliminate deflection errors caused by crushing of concrete under supports. Their technique involved calculating fracture energy from the area under the plastic deformation portion of the load-CMOD curve and applying correlation constants to allow the use of load-CMOD rather than load-deformation curves. The technique also provides for a mathematical calculation of the unloading stiffness at any point along the load-CMOD curve based on the assumption that the stiffness of the beam will decrease as the crack propagates and that it decreases linearly with increasing displacement of the specimen. To obtain the unloading compliance needed to calculate K_{Ic} , and $CMOD_c$ in the TPFM, this technique was employed.

C.3.2 Fracture toughness calculations

Following the approach of Navalurkar, the beam was tested in load – CMOD mode. The load applied to the specimen varied to keep the rate of crack mouth opening equal to 0.08 mm/min. Testing was run until beam broke or CMOD gage hit its limit. Output data from the closed-loop hydraulic test system included Time, sec; CMOD, mm; and Load, kg. Approximately 700 to 800 data points were collected for each test. The resulting graph is shown in Figure C.2.

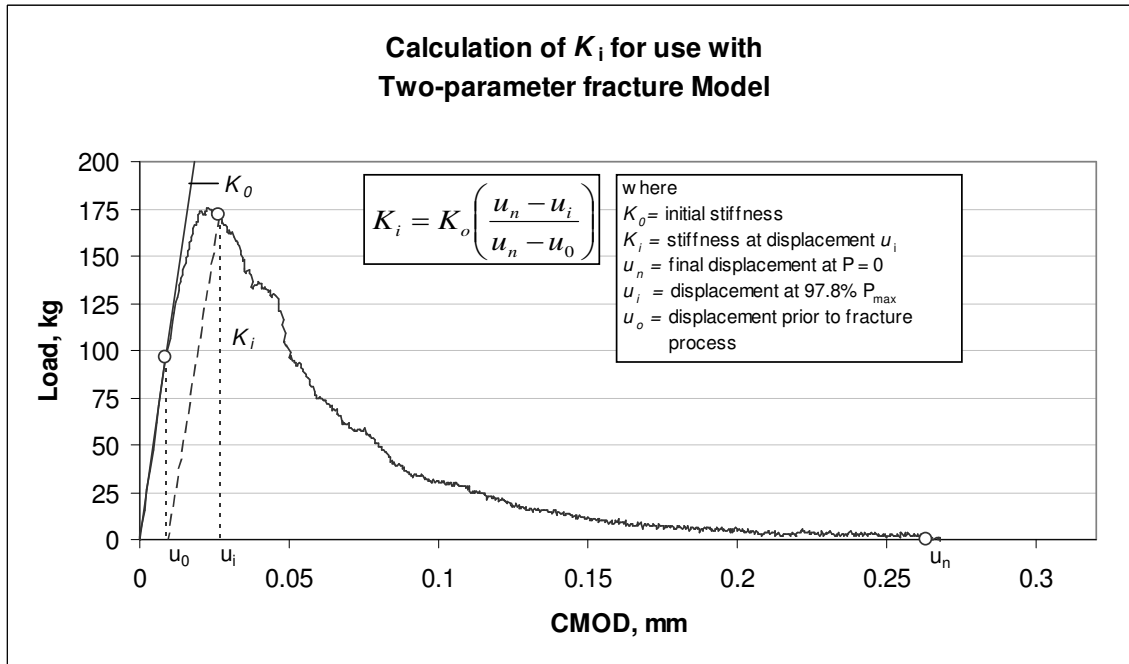


Figure C.2 Load-CMOD curve for beam 1 of unreinforced baseline VHSC

This test does not provide enough information to calculate the fracture toughness, K_{Ic} . The load-CMOD curve will identify the initial stiffness, the peak load, and will allow calculation of the work of fracture. The initial stiffness was determined by superimposing a straight line (with origin at the intersection of the Load and CMOD axes) over the lower-half of the rising portion of the curve and determining the initial stiffness as:

$$K_0 = \Delta P_e / \Delta CMOD_e = 95.94 \text{ kg} / 0.0089 \text{ mm} = 10791.50 \text{ kg/mm} \quad (C.1)$$

where ΔP_e and $\Delta CMOD_e$ are the increment of load and CMOD at the estimated elastic limit at $0.55 P_{max}$. The initial compliance, C_i , is the inverse of K_0 which is $9.267E-05 \text{ mm/kg}$. In the TPFM the effective-elastic critical crack length, a_c , is calculated from:

$$a_c = a_0 \frac{C_u g_2(\alpha_0)}{C_i g_2(\alpha_c)} \quad (C.2)$$

where a_0 is the initial crack length, C_i and C_u are the initial and unloading compliances respectively, and $g_2(\alpha_0)$ and $g_2(\alpha_c)$ are geometric functions tied to the initial and effective-elastic critical crack length. Because the unloading-reloading cycle of the load-CMOD curve could not be made, C_u was calculated as follows. Referring to equation (9) in Navalurkar et al. [106] (reproduced here as equation C.3) the stiffness of the cracked beam at any point along the load-CMOD curve can be calculated as:

$$K_i = K_o \left(\frac{u_n - u_i}{u_n - u_o} \right) \quad (C.3)$$

where K_i is the stiffness at the desired load level, P; K_o is the initial stiffness; and u_i , u_o , and u_n represent the CMOD displacement at the desired load level P, the elastic CMOD displacement prior to start of the fracture process, and the final CMOD displacement (at P = 0) respectively. These CMOD displacements are marked in Figure C.2.

Using equation C.3 with $K_o = 10791.50$ kg/mm, $u_i = 0.026162$ mm, $u_o = 0.00889$ mm, and $u_n = 0.26822$ mm yields stiffness factor K_i (at P = 171.96 kg or 97.5% of P_{\max}) = 10072.8 kg/mm which can be inverted to get the unloading compliance $C_u = 9.9278E-05$ mm/kg.

Before the effective-elastic critical crack length can be calculated the geometry factors $g_2(\alpha_0)$ and $g_2(\alpha_c)$ must be resolved. Shah et al. [28] use the equation:

$$g_2(\alpha_o) = 0.76 - 2.28\alpha_o + 3.87\alpha_o^2 - 2.04\alpha_o^3 + \frac{0.66}{(1 - \alpha_o)^2}, \alpha_o = \frac{a_o + \Delta h}{W + \Delta h} \quad (C.4)$$

where Δh is the distance below the bottom of the test beam where the CMOD gage is actually attached (in these calculations $\Delta h = 9.53$ mm).

To calculate $g_2(\alpha_c)$, $\alpha_c = (a_c + \Delta h)/(W + \Delta h)$ should be substituted into C.4. The original crack length, $a_o = 26.35$ mm is known. $g_2(\alpha_c)$ can be expressed in terms of a_c as

$$g_2(\alpha_c) = 0.76 - 2.28\alpha_c + 3.87\alpha_c^2 - 2.04\alpha_c^3 + \frac{0.66}{(1-\alpha_c)^2}, \alpha_c = \frac{a_c + \Delta h}{W + \Delta h} \quad (C.5)$$

The effective-elastic critical crack length a_c can be calculated by using the equations used by Shah et al. [28] to calculate the modulus of elasticity, E :

$$E = \frac{6Sa_o g_2(\alpha_o)}{C_i W^2 B} \quad \text{and} \quad E = \frac{6Sa_c g_2(\alpha_c)}{C_u W^2 B} \quad (C.6)$$

where S , W , and B are as defined in Table C.1. Substituting $a_o = 26.35$ mm into the first equation in equation pair C.6 yields the value of $E = 4549.75$ kg/mm² or 44.62 GPa. Substituting the value of E into the second equation in equation pair C.6 and solving for a_c yields a value for the effective-elastic critical crack length of 27.36 mm.

With these data calculated, K_{Ic} and $CTOD_c$ can be calculated using the equations.

$$K_{Ic}^S = 3(P_{\max} + 0.5W_h) \frac{S\sqrt{\pi a_c} g_1(a_c/W)}{2W^2 B} \quad (C.7)$$

and

$$CTOD_c = \frac{6(P_{\max} + 0.5W_h)Sa_c g_2(a_c/W)}{EW^2 B} \left[(1 - \beta_o)^2 + (1.081 - 1.149 \frac{a_c}{W})(\beta_o - \beta_o^2) \right]^{1/2} \quad (C.8)$$

where in equations C.7 and C.8 P_{\max} = peak load, $W_h = W_{ho}$ (S/L), W_{ho} = beam self-weight, and

$$g_1\left(\frac{a_c}{W}\right) = \frac{1.99 - (a_c/W)(1 - a_c/W)(2.15 - 3.93a_c/W + 2.70(a_c/W)^2)}{\sqrt{\pi}(1 + 2a_c/W)(1 - a_c/W)^{3/2}} \quad (C.9)$$

and $\beta_o = a_o/a_c$, and $g_2(a_c/W)$ is based on equation C.4 with α_o replaced with a_c/W .

Thus for K_{Ic}^S :

$$\frac{a_c}{W} = \frac{27.36}{79.9} = 0.342 \quad (C.10)$$

$$g_1\left(\frac{a_c}{W}\right) = \frac{1.99 - 0.342(1 - 0.342)(2.15 - 3.93(0.342) + 2.70(0.342)^2)}{\sqrt{\pi}(1 + 2(0.342))(1 - 0.342)^{3/2}} = 1.091 \quad (\text{C.11})$$

$$W_h = W_{ho} (304.8/354.8) = 2.62(304.8/354.8) = 2.25 \text{ kg} \quad (\text{C.12})$$

$$K_{Ic}^S = 3(175.8 + 0.5(2.25)) \frac{304.8 \sqrt{\pi(0.0274)}(1.091)}{2(79.9)^2(38.98)} = 0.104 \frac{\text{kg} \sqrt{\text{m}}}{\text{mm}^2} = 1.02 \text{ MPa} \sqrt{\text{m}} \quad (\text{C.13})$$

and for $CTOD_c$ where $\beta_o = a_o/a_c = 26.35/27.36 = 0.963$ and equation C.5 $g_2(a_c/W) = 1.877$

$$CTOD_c = \frac{6(175.8 + 0.5(2.25))(304.8(27.36)(1.877))}{(4549.75)(79.9)^2(38.98)} [Y] = 0.0024 \text{ mm}$$

where (C.14)

$$Y = \left[(1 - 0.9632)^2 + (1.081 - 1.149(27.36/79.9))(0.9632 - 0.9632^2) \right]^{1/2}$$

C.3.3 Fracture energy

To calculate the fracture energy, G_f , it was necessary to calculate the work of fracture which is the area under the load-CMOD curve. A Reimann sum was used to approximate the area as:

$$\int_0^{\delta} P d\delta = \sum_0^n \left(\left(\frac{P_n + P_{n+1}}{2} \right) (\delta_{n+1} - \delta_n) \right) \quad (\text{C.10})$$

where P is the incremental load, δ is the incremental displacement, and n is the number of data points in the graph. The work of fracture was 4.96 kg-mm or 0.0486 N-m. This work was applied over the area of the ligament of the beam which from Table C.1 was 38.98 mm thick by 79.90 – 26.35 = 53.55 mm in depth giving an area of 2.09 E-03 m² and a fracture energy of 23.31 N/m.